九州大学学術情報リポジトリ
Kyushu University Institutional Repository

Chemical-Thermodynamic Explorations on the Dissolution of Water in Magma: Breaking of the Ideal Mixing Model and Estimations of Temperature Change with Decompression-Induced Vesiculation

西脇, 瑞紀

https://hdl.handle.net/2324/6787423

出版情報：Kyushu University, 2022, 博士（理学）, 課程博士
バージョン：
権利関係：

KYUSHU UNIVERSITY

Chemical-Thermodynamic Explorations on the Dissolution of Water in Magma: Breaking of the Ideal Mixing Model and Estimations of Temperature Change with Decompression-Induced Vesiculation

March 2023

Doctoral Dissertation

Mizuki Nishiwaki

Department of Earth and Planetary Sciences,
Graduate School of Science, Kyushu University

Contents

Abstract **3**

Introduction **5**
-1.1 Importance of water solubility in silicate melts 5
-1.2 A paradox of the partial molar volume of water in silicate melt 7
-1.3 How to solve the paradox: Reconsidering the ideal mixing model 9
-1.4 Effects of latent heat generated by vesiculation and crystallization on temperature changes of ascending magma 10
-1.5 Experimental and theoretical determination of latent heat generated by crystallization and water exsolution of silicate melts 12
-1.6 Chemical-thermodynamic estimations of temperature change of magma with decompressed-induced vesiculation 13
-1.7 Flow of this paper 14

0 Preparation **15**
0.1 Dissolution process of water in silicate melt 15
0.2 Derivation of the equation for water solubility in silicate melts 19

I Pressure Dependence of Water Solubility in Silicate Melt **23**

1 A paradox of the partial molar volume of water in silicate melt and its solution **24**
1.1 Studies before Stolper's method 24
1.2 Estimation of the partial molar volume of H_2O_m by Stolper's method 25
1.3 A paradox of the partial molar volume of water in silicate melt 29
1.4 Resolving the paradox: Breaking of the ideal mixing model 33

2 Three-component asymmetric regular solution model **38**
2.1 Regular solution approximation 38
2.2 Three-component asymmetric regular solution 39
2.3 Calculations of interaction parameters and activity coefficients by the steepest descent method 41

II Temperature Dependence of Water Solubility in Silicate Melt **46**

3 Estimation of the heat of dissolution of water in rhyolitic melt **47**
3.1 Previous studies 47

3.2 Calculation methods 50
3.3 Calculation results 52
3.4 Comparison of "Regular solution model" with "Ideal solution model" 56
3.5 Comparison with Liu et al. (2005) 57

4 Numerical calculations of temperature change of magma with decompression-induced vesiculation **58**
4.1 Assumptions and formulation 58
4.2 Calculation methods 61
4.3 Calculation results 63
4.4 Comparison with Sahagian and Proussevitch (1996) 66
4.5 Implications for natural systems 68

Conclusions **69**

Acknowledgments **71**

References **74**

Abstract

Since water solubility in magmas (silicate melts) is a very fundamental and important piece of information in volcanology, it has been investigated extensively from both experimental and theoretical perspectives. Nevertheless, there has been no consensus on the consistency between experimentally determined water solubility values and those estimated through a chemical thermodynamics-based theoretical equation. In this study, I explicitly revisit this traditional problem and consider how the consistency should be established between experimental and theoretical values for the partial molar volume and heat of dissolution of water, which characterize the pressure- and temperature-dependence of water solubility, respectively.

The partial molar volume of water in silicate melt has been often estimated through an indirect way in which an experimentally determined water solubility in silicate melt is substituted into a theoretical equation derived from chemical thermodynamics. However, it has been also often reported that the values estimated in such a way significantly deviated from the value estimated through a direct method such as density measurement of quenched glass. In this study, I attributed this paradox to the assumption of the ideal mixing of bridging oxygen (O) of silicate and water (molecular water H_2O_m and hydroxyl groups OH), i.e., neglecting non-ideality, in the theoretical equation of water solubility used in the past. Therefore, I showed that the assumption of the ideal mixing is broken by a simple calculation, and by applying the asymmetric regular solution model for the three components mentioned above, I found that strong positive non-ideality appears when H_2O_m enters an environment with high O content.

Next, by using the above results to describe the equilibrium constant for the first dissolution reaction of water into melt (r1: H_2O_m (vapor) $\leftrightarrow$ H_2O_m (in melt)) and substituting it into the theoretical equation, I calculated the enthalpy change (i.e., the heat of dissolution of water into melt) for r1 in a wide range of temperatures and pressures. As a result, the heat of dissolution for r1 is about -20 kJ/mol regardless of the temperature and pressure, indicating that it is an exothermic reaction. By adding the heat of dissolution for the second reaction (r2: H_2O_m (in melt) + Si$-$O$-$Si $\leftrightarrow$ 2 Si$-$OH, endothermic), the heat of dissolution for the entire dissolution reaction can also be calculated over a wide temperature and pressure range. The results show a shift toward endothermic at higher temperatures and toward exothermic at

lower temperatures and higher pressures, but the magnitude of the shift is highly dependent on the previously estimated value of the heat of dissolution for r2, which varies depending on the method of measurement of the speciation of H_2O_m and OH.

Furthermore, based on these values, I numerically calculated the temperature change of hydrous rhyolitic melt with decompression-induced water vesiculation ascending a volcanic conduit, assuming it is the equilibrium degassing in a closed system. The results showed that the effects of the heat of exsolution of water from melt and the mechanical work of bubble expansion contributed to warming and cooling the system, respectively, and the sum of them resulted in slight cooling due to the relation of their magnitudes.

In the future, by combining the results of this study with the effect of latent heat of crystallization of magma and solving them simultaneously, it may be possible to construct a new conduit flow model with an enhanced material science aspect that incorporates temperature changes due to vesiculation and crystallization in magma.

Introduction

-1.1 Importance of water solubility in silicate melts

The driving force of volcanic eruptions is thought to be the vesiculation of the volatile components (e.g. H_2O, CO_2, SO_4) dissolved in magma (e.g. Sparks, 1978; Mangan et al., 1993; Klug and Cashman, 1996; Navon and Lyakhovsky, 1998; Cashman and Sparks, 2013; Gonnermann, 2015; Toramaru, 1989; 1995; 2022). The explosion intensity (from effusive to explosive) of an eruption is strongly controlled by the amount of volatile components originally dissolved in the magma and the amount of those components that precipitate with decompression or temperature increase. In particular, water accounts for a large proportion of the silicic compositions that are prone to explosive and giant eruptions. (e.g. Woods and Koyaguchi, 1994; Eichelberger, 1995; Gonnermann and Manga, 2007; Cassidy et al., 2018) In other words, quantitative study of water solubility in silicate melt (hereinafter, melt) is of great importance in volcanology.

Water solubility in melt has been extensively investigated since Goranson (1931) through high temperature and pressure experiments at various temperatures and pressures and for various melt compositions. Burnham and Davis (1974) and Burnham (1975, 1979) proposed the first chemical thermodynamic model to explain the experimental results in an albite-H_2O system. However, Burnham's model assumed that all the water is dissolved as hydroxyl groups OH. Later, with the development of analytical techniques, such as infrared spectroscopy (IR) and nuclear magnetic resonance (NMR), it is found that water exists as two molecular species (speciation), i.e., molecular water, H_2O_m, and OH, by analyzing hydrous glasses (including those quenched in high-temperature and high-pressure experiments) (Orlova, 1962; Ostrovskiy et al., 1964; Ernsberger, 1977; Bartholomew et al., 1980; Wu, 1980; Takata et al., 1981; Stolper, 1982a, 1982b). Stolper (1982a, 1982b) and Silver and Stolper (1985) proposed the following new chemical thermodynamic model to explain this experimental data. For the highly polimerized silicate melts, such as silica, albite, and rhyolite, where the ratio NBO/T is almost zero, ideal mixing (ideal solution approximation) is realized when the hydrous melt is regarded as a mixture of three components, namely, H_2O_m, OH, and O (all oxygen in the oxides except water is

regarded as bridging oxygen). This simple theoretical model has been trusted and widely used since its inception. One such example is the Excel macro VolatileCalc provided by Newman and Lowenstern (2002), a publicly available program that can calculate the solubility of H_2O in the magma for a wide range of temperature and pressure.

-1.2 A paradox of the partial molar volume of water in silicate melt

Stolper's equation has also been used to estimate the partial molar volume of water in melts by keeping the temperature fixed and varying the pressure term (Silver et al., 1990; Blank et al., 1993; Lange, 1994; Holloway and Blank, 1994; Dixon et al., 1995; Holtz et al., 1995; Mysen and Acton, 1999; Zhang, 1999a, Mysen and Wheeler, 2000; Mysen and Cody, 2004; Mysen, 2007; Lesne et al., 2011). The partial molar volume of water in melt is an essential parameter for calculating the density of hydrous melts, which is fundamental for discussing the gravitational stability and migration of the magma in the interior of the Earth and planets. However, due to experimental difficulties, direct measurements have only been made in two cases by Burnham and Davis (1971) and Ochs and Lange (1997, 1999). In those experimental studies, the partial molar volume of water in melt was reported to be about 20 cm^3/mol at the temperatures and pressures of a typical shallow magma. In contrast, the partial molar volume of water in melt estimated from Stolper's equation ranges very widely from large positive values well above 20 cm^3/mol to negative values, which are significantly different from the experimentally derived one. Although this paradox has been mentioned in various papers, and a number of views have been presented, no satisfied resolution has yet been reached. In other words, in recent years, there has been no attempt in this field to deepen our chemical-thermodynamic understanding by revisiting the fundamental theoretical equations. This is because convenient empirical models compiled from large data sets have become the predominant tool for calculating water solubility in melts (Papale, 1997, 1999; Moore et al., 1998; Liu et al., 2005; Papale et al., 2006; Moore, 2008; Iacono-Marziano et al., 2012; Duan, 2014; Shishkina et al., 2014; Ghiorso and Gualda, 2015; Burgisser et al., 2015; Iacovino et al., 2021; Wieser et al., 2021, including papers focused on H_2O-CO_2 solubility), and the urgency to improve Stolper's equations has diminished.

However, the large variation in previous estimates of the partial molar volume of water in melt not only brings significant uncertainty to density calculations for hydrous melts (Lange, 1994; Kuritani, 2007), but also to our understanding of nucleation processes of supersaturated volatiles in magma, the first stage of decompression-induced vesiculation of magma, especially estimation calculations of surface tension between critical bubble nuclei and the surrounding melt based on observations of the micro-scale textures of experimental products from laboratory decompression experiments and on classical nucleation theory (CNT) (Mangan and Sisson, 2000, 2005; Mangan et al., 2004; Mourtada-Bonnefoi and Laporte, 2002, 2004; Cluzel et al., 2008; Hamada et al., 2010; Gardner and Ketcham, 2011; Gardner, 2012; Gonnermann and Gardner, 2013; Gardner et al., 2013, 2018). Therefore, resolving this paradox, which has

remained unresolved for about 30 years, to provide strong constraints on the choice of estimated values for the partial molar volume of water in melts is of great significance because it will lead to a deeper understanding of the fundamental physical properties necessary for future research in various fields of earth and planetary sciences.

-1.3 How to solve the paradox: Reconsidering the ideal mixing model

For the above-mentioned paradox, this study takes the position of questioning the ideal solution approximation assumed in Stolper's model. Ideal mixing is defined as "there are no volume change and no heat generation during the mixing" (Uchida, 2012), whereas in reality it is experimentally confirmed that there is volume change (Ochs and Lange, 1997, 1999) and heat generation (Richet et al., 2006) due to water dissolution into silicate melt. In addition, if silicate-water mixture is ideally mixed, a miscibility gap would not appear, but in reality there is a large miscibility gap below the second critical point (Kennedy et al., 1962; Ostrovsky, 1966; Shen and Keppler, 1997; Bureau and Keppler, 1999). In other words, it is necessary to reexamine whether the ideal solution approximation is really adequate in explaining the silicate-water mutual dissolution system in a solution model based on chemical thermodynamics. Assuming ideal mixing means ignoring non-ideality, so the paradox described above may arise as a result of the neglected non-ideality being imposed on the partial molar volume. Specifically, the non-ideality refers to an interaction parameter that acts between each component of a mixture system and describes whether the energy state of the system will change to a stable or unstable state due to intermolecular forces or other factors when a particle of one component enters into a group of particles of another component on a lattice arrangement. This study relies on Ochs and Lange's measurements (1997, 1999) of the partial molar volume of water in melts to reveal the neglected non-ideality and applies an asymmetric regular solution model by Kakuda et al. (1991, 1994) to quantitatively determine, for the first time, the magnitude of the interaction parameter between the three components H_2O_m, OH, and O. In future, the results of this study may be integrated with experimental measurements (e.g., X-ray diffraction and spectroscopic techniques) and computer simulations (e.g., molecular dynamics) of the microstructure of hydrous melts to provide more insight into the chemical behavior of water in silicate melts at high temperatures and pressures.

-1.4 Effects of latent heat generated by vesiculation and crystallization on temperature changes of ascending magma

While until now the pressure dependence of the water solubility in melt has focused with fixed temperature, in contrast, if pressure is fixed and the temperature dependence of the equilibrium constants for the chemical reactions of dissolution is focused, the latent heat of dissolution of water in melt (the enthalpy change during mixing) can be estimated from a chemical thermodynamic perspective. Since the opposite sign of the heat of exsolution of water from melt has the same numerical value as the heat of dissolution, estimating it in detail enables to estimate its effect on the magma temperature as the magma dehydrates in a volcanic eruption. It is important to comprehend the temperature-pressure path of magma during a volcanic eruption to elucidate the conduit processes leading to the various eruptive phenomena observed on the ground surface. Temperature change of magma has a significant impact on flow dynamics in the conduit through rheological shift by the formation of bubbles and crystals, as their formation processes are kinetically controlled by temperature-pressure condition on the basis of equilibrium phase diagram. Simultaneously, pressure changes through the shift of flow dynamics. Thus, temperature change has the primary significance on the entire history of temperature and pressure of ascending magmas in the conduit. There are several causes of temperature change of ascending magma in the conduit: cooling by the surrounding host rock or hydrothermal system, viscous heating, temperature change by latent heat of volatile exsolution, cooling by the work of volatile bubble expansion, and heating by latent heat of condensation of crystals (Costa et al., 2007b).

However, most conduit flow models have assumed that the magma in the volcanic conduit is isothermal from the magma chamber to the crater (e.g., Wilson et al., 1980; Giberti and Wilson, 1990; Dobran, 1992; Jaupart, 1996; Melnik and Sparks, 1999; Yoshida and Koyaguchi, 1999; Legros and Kelfoun, 2000; Massol et al., 2001; Papale, 2001; Sahagian and Proussevitch, 2005; Tanaka and Hashimoto, 2013; Kozono, 2021). Even though some models calculate temperature changes assuming adiabatic changes in the system (Buresti and Casarosa, 1989; Mastin and Ghiorso, 2001; Mastin, 2002; Mitchell, 2005), so far only Costa et al. (2007a) and Proussevitch and Sahagian (1998) have considered in their models the temperature changes due to the heat of solidification released during crystallization and the heat of exsolution generated during vesiculation, respectively. However, the former did not refer to any publication on which the value of the heat of solidification used is based, and the latter used the values of the heat of exsolution obtained by the theoretical approach in Sahagian and Proussevitch (1996) where

several logical flaws were contained (Zhang, 1999b). Thus, the incorporation of latent heat effects from magma vesiculation and crystallization in the conduit flow model is still in a nascent stage, leaving ample room to take advantage of the latent heat values estimated by various experiments and theories.

-1.5 Experimental and theoretical determination of latent heat generated by crystallization and water exsolution of silicate melts

The value of the heat of fusion of crystals, which has the opposite sign of the heat of solidification, has been measured in great detail through various experimental techniques, such as direct measurement by transposed-temperature-drop calorimetry and indirect measurement by solution calorimetry and differential scanning calorimetry (Lange et al., 1994; Kojitani and Akaogi, 1997; Sugawara and Akaogi, 2003; Sugawara, 2005; Kolzenburg et al., 2016; Whittington and Sehlke, 2021). In contrast, the measurement of the heat of exsolution of water is difficult and has only been attempted in two previous studies by Clemens and Navrotsky (1987) and Richet et al. (2006). Clemens and Navrotsky (1987) combined drop-solution calorimetry at ambient pressure and relative-enthalpy measurements at high pressure for hydrous albite melt. Richet et al. (2006) applied HF solution calorimetry to hydrous phonolite and albite melts.

In the meantime, a small number of studies have also been conducted that theoretically estimated the heat of exsolution of water using chemical thermodynamics (Sahagian and Proussevitch, 1996; Zhang, 1999b). Sahagian and Proussevitch (1996) estimated the heat of exsolution of water over a wide range of temperatures and pressures using a chemical thermodynamic method "Entropy method" based on data on water solubility in the albite melt (Burnham and Davis, 1974). In particular, they assumed that all water dissolved in melt exists as hydroxyl (OH) groups, while water exists as both molecules H_2O_m and OH in reality. Thus, the assumption is unreliable in the low-temperature and high-pressure regions, where H_2O_m is dominant (Zhang, 1999b). Zhang (1999b) appropriately considered these problems and reconstructed an equation for the exsolution enthalpy of water from rhyolitic melt and proposed the procedure to determine the standard enthalpy change for the first reaction of dissolution (H_2O_m (vapor) $\leftrightarrow$ H_2O_m (in melt)). Unfortunately, he only succeeded in calculating the values only at very low pressure ($\leq$ 10 MPa) because in those days the reliable experimental data of the equilibrium constant K_{r2} for the second reaction of dissolution (H_2O_m (in melt) + Si$-$O$-$Si $\leftrightarrow$ 2 Si$-$OH) were not available for higher total water content than 2.4 wt%. In addition, the data were obtained by measuring quenched glass/melt at relatively low temperatures of 400-600°C (Zhang et al., 1991, 1995, 1997; Ihinger et al., 1999).

-1.6 Chemical-thermodynamic estimations of temperature change of magma with decompressed-induced vesiculation

Subsequently, progress has been made in collecting infrared spectroscopic data on H_2O_m and OH species at higher water contents and higher temperatures (Sowerby and Keppler, 1999, 2000; Nowak and Behrens, 2001; Behrensand Nowak, 2003), which should make it possible to apply the calculation method of Zhang (1999b) to a wider range of temperatures and pressures. In addition, Zhang (1999b) constructed his argument assuming the ideal mixing of silicate and water species, but if the information on non-ideality obtained by solving the above-mentioned problem, "the paradox of the partial molar volume of water in silicate melts," the heat of dissolution (heat of exsolution) can be determined much more accurately than when assuming the ideal mixing. Furthermore, the temperature change in the magma due to decompression-induced vesiculation of water in the magma ascendng in a volcanic conduit (the sum of the effects of the heat of exsolution and mechanical work due to bubble expansion), which was first calculated by Sahagian and Proussevitch (1996), can be estimated more accurately. In the future, it is expected that these attempts tried in this study will contribute to the calculation and estimation of more detailed temperature and pressure paths of the magma in the volcanic conduit during eruptions by integrating them with various factors that cause temperature changes.

-1.7 Flow of this paper

In this paper, first, Chapter 0 describes the water dissolution process in melt, and an equation for water solubility in melt is derived. From then on, based on the equation, Part I and Part II focus on the pressure dependence of water solubility and the temperature dependence of the equilibrium constant of the first dissolution reaction K_{r1}, respectively. In Part I, Chapter 1 describes the paradox of the partial molar volume of water in melt and shows by simple calculations that the ideal mixing model, which was thought to be valid for silicate (O) and water (H_2O_m and OH) since Stolper (1982a, 1982b), fails. In the following Chapter 2, the three-component asymmetric regular solution model (Kakuda et al., 1991, 1994) is applied to this system to reveal the magnitude of the interaction parameters between the components to show the non-ideality of H_2O_m is especially high. In Part II, in Chapter 3, the enthalpy change, or the heat of dissolution for the first dissolution reaction r1 is calculated using Zhang's (1999b) method: the Gibbs-Helmholtz equation, taking into account the non-ideality of mixing clarified in Part I, and the heat of dissolution for the entire dissolution reaction is determined for a wide range of temperatures and pressures. The obtained results are compared with those of Sahagian and Proussevitch (1996) and Liu et al. (2005). In Chapter 4, the equation for the temperature change of magma with decompression-induced vesiculation derived by Sahagian and Proussevitch (1996) is improved, and the two effects of the heat of exsolution and mechanical work of bubble expansion are numerically calculated using the values of the heat of dissolution obtained in Chapter 3. The obtained results are compared with those of Sahagian and Proussevitch (1996) and finally implications for natural systems are considered.

Chapter 0

Preparation

0.1 Dissolution process of water in silicate melt

It is known based on analytical data with infrared (IR) or near-infrared (NIR) spectroscopy, and nuclear magnetic resonance (NMR) that water dissolved in silicate melt exists as two molecular species, i.e., molecular water, H_2O_m, and hydroxyl group, OH (Orlova, 1962; Ostrovskiy et al., 1964; Ernsberger, 1977; Bartholomew et al., 1980; Wu, 1980; Takata et al., 1981; Stolper, 1982a, 1982b). The dissolution process is explained by breaking it down into two chemical reactions as follows. Reaction 1 (r1) is a physical change in which vapor H_2O_m undergoes a phase transition and is incorporated into melt in the molecular state. Reaction 2 (r2) is a chemical reaction in which a portion of dissolved H_2O_m hydrolyzes the bridging oxygen between Si to form two OHs.

$$\begin{cases} \text{reaction 1 (r1)} : H_2O_m \text{ (vapor)} \leftrightarrow H_2O_m \text{ (in melt)}, & (1) \\ \text{reaction 2 (r2)} : H_2O_m \text{ (in melt)} + \text{Si}-\text{O}-\text{Si} \leftrightarrow 2\ \text{Si}-\text{OH}. & (2) \end{cases}$$

Fig. 0.1 shows the chemical structure of water dissolved in silicate melt. Schaller and Sebald (1995) reported that ^{1}H magic-angle spinning nuclear magnetic resonance (^{1}H MAS NMR) analyses indicated that H_2O_m may exist in the gaps of the silicate melt network as clusters. In reality, in addition to SiO_2, there exists other oxides, such as P_2O_5 as a network former; TiO_2, Al_2O_3, and Fe_2O_3 as intermediates; and FeO, MnO, MgO, CaO, Na_2O, and K_2O as network modifiers (Sun, 1947; Taniguchi, 2001), but only SiO_2 and H_2O are focused on in the drawing.

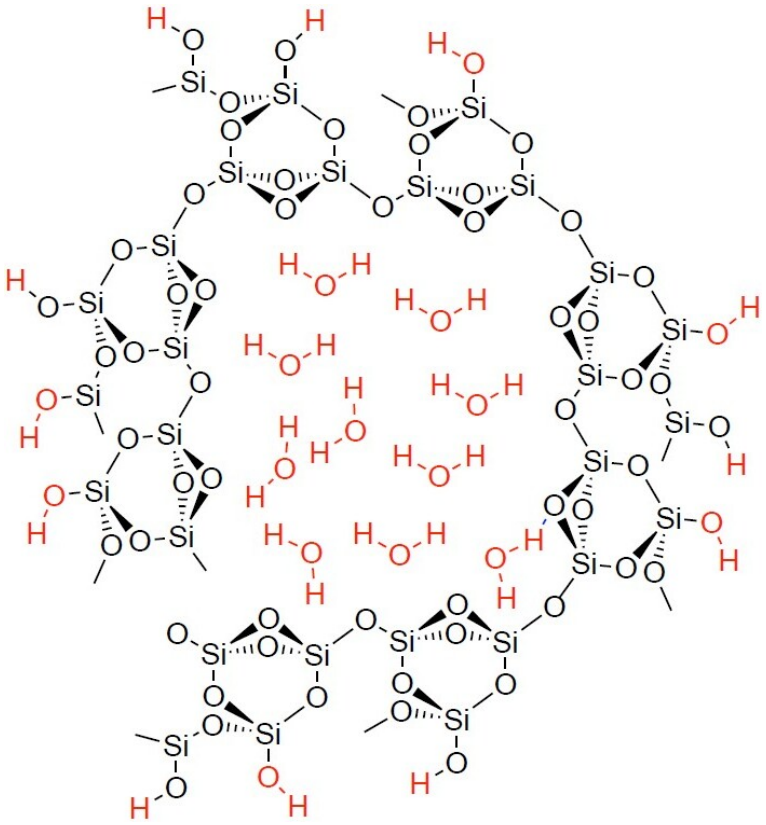

[Figure 0.1] A schematic diagram of silicate melt in which water is dissolved. Oxides other than SiO_2 and H_2O are omitted. Disslved water species are shown as red characters. H_2O_m is present as a cluster in the gap of the silicate network, and some of the bridging oxygen are hydrolyzed to OH.

Stolper (1982a, 1982b) and Silver and Stolper (1985) assumed that for highly polimerized melts among the silicate melts, such as silica, albite, and rhyolite, where NBO/T is close to zero, the ideal mixing (ideal solution approximation) is realized when the hydrous melt is regarded as a mixture of three components, H_2O_m, OH, and O (all oxygen in the oxides except water is regarded as bridging oxygen and represented as such). The rationale is that if the sum of the mole fractions of each molecular species in melt was assumed to be 1:

$$X_{H_2O_m} + X_{OH} + X_O = 1 \tag{3}$$

and if the ideal mixing:

$$\begin{cases} a_{H_2O_m} = X_{H_2O_m} \\ a_{OH} = X_{OH} \\ a_O = X_O \end{cases} \tag{4}$$

held for each of them, when the values of the "apparent" equilibrium constant of the second reaction Q_{r2}:

$$Q_{\mathrm{r2}} \equiv \frac{X_{\mathrm{OH}}^2}{X_{\mathrm{H_2O_m}} \cdot X_{\mathrm{O}}} \tag{5}$$

were given appropriately, it was possible to fit the approximation well to each mole fraction of $\mathrm{H_2O_m}$ and OH, respectively, obtained from the total water content and speciation data by IR spectroscopy at low pressure. The detail calculation method of $X_{\mathrm{H_2O_m}}$ is shown at the end of this section. Here a_i and X_i ($i = \mathrm{H_2O_m}$, OH, and O) represent the activity and mole fraction (calculated with one oxygen basis) of component i, respectively, and are represented by the following relation via the activity coefficient γ_i, where the ideal mixture is equivalent to $\gamma_i = 1$.

$$a_i = \gamma_i X_i. \tag{6}$$

The reason why Q_{r2} is expressed as the "apparent" equilibrium constant is that Q_{r2} is calculable because the total water content and speciation measurements for hydrous quenched glass prepared over a wide range of temperature and pressure have already been obtained for melts of various chemical compositions, whereas K_{r2} is not calculable because the "exact" equilibrium constant K_{r2} is defined as

$$K_{\mathrm{r2}} \equiv \frac{a_{\mathrm{OH}}^2}{a_{\mathrm{H_2O_m}} \cdot a_{\mathrm{O}}} = \frac{\gamma_{\mathrm{OH}}^2}{\gamma_{\mathrm{H_2O_m}} \cdot \gamma_{\mathrm{O}}} \cdot \frac{X_{\mathrm{OH}}^2}{X_{\mathrm{H_2O_m}} \cdot X_{\mathrm{O}}} \tag{7}$$

and because how each γ_i behaves with respect to temperature, pressure, and melt composition has not been investigated in detail in the past. Assuming ideal mixing, $\gamma_{\mathrm{H_2O_m}} = \gamma_{\mathrm{OH}} = \gamma_{\mathrm{O}} = 1$, i.e., $\dfrac{\gamma_{\mathrm{OH}}^2}{\gamma_{\mathrm{H_2O_m}} \cdot \gamma_{\mathrm{O}}} = 1$, from $K_{\mathrm{r2}} = Q_{\mathrm{r2}}$.

Essentially, however, the ideal mixing is defined as follows (Uchida, 2012):

1. No internal energy change upon mixing: $\Delta U^{\mathrm{mix}} = 0$.
2. No volume change upon mixing: $\Delta V^{\mathrm{mix}} = 0$.
3. No heat generation upon mixing: $\Delta H^{\mathrm{mix}} = 0$ (this is derived from 1 and 2 according to the relation, $\Delta H^{\mathrm{mix}} = \Delta U^{\mathrm{mix}} + P\Delta V^{\mathrm{mix}}$).
4. The mixing entropy is the ideal mixing entropy: for a three-component system consisting of A, B, and C: $\Delta S^{\mathrm{mix}}_{\mathrm{ABC}} = -nR(x_{\mathrm{A}} \ln x_{\mathrm{A}} + x_{\mathrm{B}} \ln x_{\mathrm{B}} + x_{\mathrm{C}} \ln x_{\mathrm{C}})$ (derived by applying Stirling's formula to Boltzmann's entropy formula in statistical mechanics).

In the 1980s, since there were few reliable quantitative measured data on volume change and heat generation upon mixing of the silicate melt and water, Stolper (1982b) provided no experimental facts to support the claim that Definitions 2. and 3. (which automatically encompass Definition 1.) were satisfied. In addition, Definition 4. can also be read as "A, B, and

C are interchangeable on a lattice site, and the interaction energy of any pair is zero (Guggenheim, 1952)." Stolper (1982b) assumed this and constructed the ideal mixing model, but a thermodynamic corollary based on experimental measurement data was still not presented.

Calculation method of $X_{H_2O_m}$

The mole fraction of total water $X_{\text{total } H_2O}$ is calculated as below:

$$X_{\text{total } H_2O} = X_{H_2O_m} + \frac{1}{2} X_{OH}. \tag{8}$$

Using eqs. (3) and (5), eq. (8) can be written as the function of $X_{H_2O_m}$ and K_{r2} as below (the same as equation (9) in Silver and Stolper, 1985):

$$X_{\text{total } H_2O} = X_{H_2O_m} + \frac{1}{4}\left[-K_{r2} X_{H_2O_m} + \left\{(K_{r2}^2 - 4K_{r2}) X_{H_2O_m}^2 + 4K_{r2} X_{H_2O_m}\right\}^{\frac{1}{2}}\right]. \tag{9}$$

This equation indicates that the pressure dependence of the total water content approaches linearity when H_2O_m is abundant (at low temperature or at high pressure) and conversely approaches parabolic when OH is abundant (at high temperature or at low pressure).
By solving eq. (9) by $X_{H_2O_m}$, the following equation is obtained:

$$X_{H_2O_m} = X_{\text{total } H_2O} - \frac{\frac{1}{2} - \left\{\frac{1}{4} - \left(1 - \frac{4}{K_{r2}}\right)\left(X_{\text{total } H_2O} - X_{\text{total } H_2O}^2\right)\right\}^{\frac{1}{2}}}{1 - \frac{4}{K_{r2}}}. \tag{10}$$

0.2 Derivation of the equation for water solubility in silicate melts

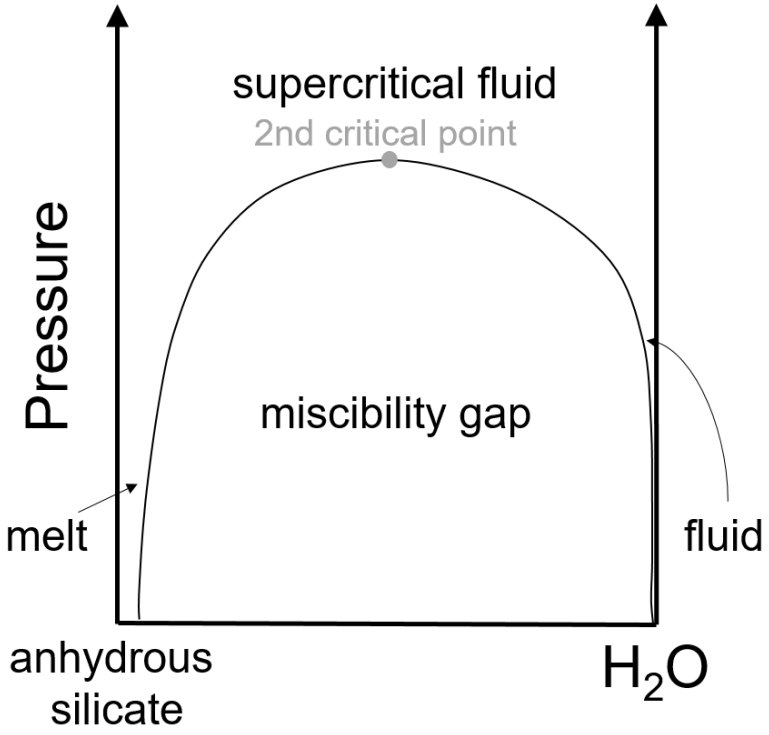

[Figure 0.2] The phase diagram of a two-component mixture of anhydrous silicate and water at some temperature below the second critical point. The miscibility gap is formed at pressures below the second critical point. The anhydrous silicate side of the region outside the miscibility gap is called "melt," and the pure water side is called "fluid." The fluid is generally equated with pure water vapor.

Silicate and water are mutually soluble and have the miscibility gap at somewhat higher temperatures below the second critical point (Fig. 0.2). Experimentally, it was elucidated in detail by the results of Kennedy et al. (1962) and Ostrovsky (1966) for the SiO_2-water system, Paillat et al. (1992), Shen and Keppler (1997), Stalder et al. (2000) and Makhluf et al. (2020) for the albite-water system, and Bureau and Keppler (1999) for the haplogranite-water system. The composition on the left side of the miscibility gap is called "melt," and the composition on the right side is called "fluid." Melt can be viewed as a substance in which water is dissolved in silicate, and the fluid as a substance in which silicate is dissolved in water. When divided at a certain pressure, the boundary between melt and the miscibility gap represents melt saturated with water, while the boundary between the fluid and the miscibility gap represents the fluid saturated with silicate. Note that the melt region is generally much larger than the fluid region,

i.e., water solubility in silicate is much larger than the solubility of silicate in water (Gerya et al., 2005); therefore, the fluid can be regarded as almost the same as pure water vapor.

The equation for the first reaction of dissolution represents the coexistence of pure water vapor and H_2O_m dissolved in melt. That is, when melt is saturated with water, the chemical equilibria between water in melt and vapor at an arbitrary state $(T, P, a_{H_2O_m})$ and a reference state $(T_0, P_0, a_{H_2O_m,0})$ hold:

$$\begin{cases} \mu^{\text{melt}}_{H_2O_m}(T, P, a_{H_2O_m}) = \mu^{\text{vapor}}_{H_2O_m}(T, P), & (11) \\ \mu^{\text{melt}}_{H_2O_m}(T_0, P_0, a_{H_2O_m,0}) = \mu^{\text{vapor}}_{H_2O_m}(T_0, P_0), & (12) \end{cases}$$

where μ (J/mol) is the chemical potential. T (K) and P (bar) are arbitrary temperature and pressure. "0" in the subscript means the reference state. $a_{H_2O_m}$ is the relative activity of H_2O_m.

From above two equations, the following formula is written:

$$\mu^{\text{melt}}_{H_2O_m}(T, P, a_{H_2O_m}) - \mu^{\text{melt}}_{H_2O_m}(T_0, P_0, a_{H_2O_m,0}) = \mu^{\text{vapor}}_{H_2O_m}(T, P) - \mu^{\text{vapor}}_{H_2O_m}(T_0, P_0). \quad (13)$$

The left hand side (LHS) and the right hand side (RHS) of this formula are expanded as follows:

$$\begin{aligned} \text{LHS} &= \mu^{\text{melt}}_{H_2O_m}(T, P, a_{H_2O_m}) - \mu^{\text{melt}}_{H_2O_m}(T, P, a_{H_2O_m,0}) + \mu^{\text{melt}}_{H_2O_m}(T, P, a_{H_2O_m,0}) - \mu^{\text{melt}}_{H_2O_m}(T_0, P_0, a_{H_2O_m,0}) \\ &= \mu^{\text{melt}}_{H_2O_m}(T, P, a_{H_2O_m}) - \mu^{\text{melt}}_{H_2O_m}(T, P, a_{H_2O_m,0}) + \mu^{\text{melt}}_{H_2O_m}(T, P_0, a_{H_2O_m,0}) - \mu^{\text{melt}}_{H_2O_m}(T_0, P_0, a_{H_2O_m,0}) \\ &\quad + \mu^{\text{melt}}_{H_2O_m}(T, P, a_{H_2O_m,0}) - \mu^{\text{melt}}_{H_2O_m}(T, P_0, a_{H_2O_m,0}) \\ &= \int_{a_{H_2O_m,0}}^{a_{H_2O_m}} \left(\frac{\partial \mu^{\text{melt}}_{H_2O_m}}{\partial a'_{H_2O_m}}\right)_{T,P} da'_{H_2O_m} + \int_{T_0}^{T} \left(\frac{\partial \mu^{\text{melt}}_{H_2O_m}}{\partial T'}\right)_{P_0, a_{H_2O_m,0}} dT' + \int_{P_0}^{P} \left(\frac{\partial \mu^{\text{melt}}_{H_2O_m}}{\partial P'}\right)_{T, a_{H_2O_m,0}} dP' \\ &= RT \ln\left(\frac{a_{H_2O_m}}{a_{H_2O_m,0}}\right) + \int_{T_0}^{T} -\overline{S}^{\text{melt}}_{H_2O_m}(T', P_0, a_{H_2O_m,0}) dT' + \int_{P_0}^{P} \overline{V}^{\text{melt}}_{H_2O_m}(T, P', a_{H_2O_m,0}) dP', \end{aligned} \quad (14)$$

$$\begin{aligned} \text{RHS} &= \mu^{\text{vapor}}_{H_2O_m}(T, P) - \mu^{\text{vapor}}_{H_2O_m}(T, P_0) + \mu^{\text{vapor}}_{H_2O_m}(T, P_0) - \mu^{\text{vapor}}_{H_2O_m}(T_0, P_0) \\ &= \mu^{\text{vapor}}_{H_2O_m}(T, P_0) - \mu^{\text{vapor}}_{H_2O_m}(T_0, P_0) + \mu^{\text{vapor}}_{H_2O_m}(T, P) - \mu^{\text{vapor}}_{H_2O_m}(T, P_0) \\ &= \int_{T_0}^{T} \left(\frac{\partial \mu^{\text{vapor}}_{H_2O_m}}{\partial T'}\right)_{P_0} dT' + \int_{P_0}^{P} \left(\frac{\partial \mu^{\text{vapor}}_{H_2O_m}}{\partial P'}\right)_{T} dP' \\ &= \int_{T_0}^{T} -\overline{S}^{\text{vapor}}_{H_2O_m}(T', P_0) dT' + RT \ln\left(\frac{f_{H_2O}(T, P)}{f_{H_2O}(T, P_0)}\right). \end{aligned} \quad (15)$$

Here R is the universal gas constant (83.14 $cm^3 \cdot$ bar/(mol $\cdot$ K)). $a'_{H_2O_m}, T'$, and P' are the dummy variables of $a_{H_2O_m}, T$, and P. $\overline{S}^{\text{melt}}_{H_2O_m}$ and $\overline{S}^{\text{vapor}}_{H_2O_m}$ (J/(K $\cdot$ mol)) are the partial molar entropy of H_2O_m in melt and the molar entropy of H_2O_m in vapor, respectively. $\overline{V}^{\text{melt}}_{H_2O_m}(T, P)$

(cm^3/mol) is the partial molar volume of H_2O_m in melt. $f_{H_2O}(T,P)$ (bar) is the fugacity of pure water vapor.

From the relation LHS = RHS, the following formula is given:

$$RT\left\{\ln\left(\frac{a_{H_2O_m}}{a_{H_2O_m,0}}\right)-\ln\left(\frac{f_{H_2O}(T,P)}{f_{H_2O}(T,P_0)}\right)\right\}=\int_{T_0}^{T}\Delta\overline{S}^{\circ}_{r1}(T',P_0)dT'-\int_{P_0}^{P}\overline{V}^{melt}_{H_2O_m}(T,P')dP', \quad (16)$$

where $\Delta\overline{S}^{\circ}_{r1}(T',P_0) \equiv \overline{S}^{melt}_{H_2O_m}(T',P_0,a_{H_2O_m,0}) - \overline{S}^{vapor}_{H_2O_m}(T',P_0)$ is the molar entropy change through the first dissolution reaction. The superscript $\circ$ means the standard state. Here we neglect the dependence of $\overline{V}^{melt}_{H_2O_m}$ on the chemical composition of melt and water content for a reason discussed in Chapter 1.

This equation can be modified as below:

$$\frac{a_{H_2O_m}}{a_{H_2O_m,0}}=\frac{f_{H_2O}(T,P)}{f_{H_2O}(T,P_0)}\exp\left(\frac{\displaystyle\int_{T_0}^{T}\Delta\overline{S}^{\circ}_{r1}(T',P_0)dT'}{RT}-\frac{\displaystyle\int_{P_0}^{P}\overline{V}^{melt}_{H_2O_m}(T,P')dP'}{RT}\right). \quad (17)$$

In general, since the activity a_i and the mole fraction X_i of component i are expressed via the activity coefficient γ_i as eq. (6), if a_i, γ_i, and X_i, obtained by expanding eq. (17) according to the above relation, each is assumed to be temperature and pressure-dependent, the following can be derived.

$$\begin{aligned}\frac{a_{H_2O_m}(T,P)}{a_{H_2O_m}(T_0,P_0)}&=\frac{\gamma_{H_2O_m}(T,P)}{\gamma_{H_2O_m}(T_0,P_0)}\cdot\frac{X_{H_2O_m}(T,P)}{X_{H_2O_m}(T_0,P_0)}\\&=\frac{f_{H_2O}(T,P)}{f_{H_2O}(T,P_0)}\exp\left(\frac{\displaystyle\int_{T_0}^{T}\Delta\overline{S}^{\circ}_{r1}(T',P_0)dT'}{RT}-\frac{\displaystyle\int_{P_0}^{P}\overline{V}^{melt}_{H_2O_m}(T,P')dP'}{RT}\right).\end{aligned} \quad (18)$$

The first of the exponential term in this equation represents the temperature dependence of solubility, and the second term represents the pressure dependence. The above derivation process is almost identical to that presented in Silver and Stolper (1985), with a few differences in detail:

1. As mentioned in section 0.1, since it was argued by Stolper (1982a, 1982b) that the mixing of the silicate and two species of water (H_2O_m and OH) can be approximated to the ideal mixing in general, the activity coefficients of these three components, γ_i ($i = H_2O_m$, OH, and O), were all approximated to 1.

2. The fugacity term before the exponential term is the result of the integration in the pressure direction of the partial molar volume of vapor at a given temperature T. In other words, the temperatures of the denominator and numerator arguments must be aligned at T.

In Silver and Stolper (1985), this was exactly how it was expressed, but in Silver and Stolper (1989) and Silver et al. (1990), it changed to the incorrect expression $f_{H_2O}(T,P)/f_{H_2O}(T_0,P_0)$. This expression is also used in studies on solubility of other volatile species (e.g., CO_2, H_2S) in magmas (Papale et al., 2022).

3. In Silver and Stolper (1989), Silver et al. (1990), and Yamashita (1999), the enthalpy change of the first reaction at the standard state, $\Delta\overline{H}^{\circ}_{r1}(T,P_0)$ (J/mol), was defined as $\Delta\overline{H}^{\circ}_{r1}(T,P_0) \equiv T\Delta\overline{S}^{\circ}_{r1}(T,P_0)$, and the equation was modified. However, this modification is incorrect because in general the Gibbs free energy change in the standard state is non-zero ($\Delta\overline{G}^{\circ}$ (J/mol) $\neq 0$). Also this expression is used in studies on solubility of other volatile species in magmas (Papale et al., 2022), so a close examination of the correctness of mathematical expressions is needed. Therefore, $\Delta\overline{H}^{\circ}_{r1}(T,P)$ cannot be obtained from eq. (18), and another method is needed. The anothor method (the Gibbs-Helmholtz equation) is described in detail in Part II.

Part I

Pressure Dependence of Water Solubility in Silicate Melt

Chapter 1

A paradox of the partial molar volume of water in silicate melt and its solution

1.1 Studies before Stolper's method

Burnham and Davis (1971) prepared hydrous albite glasses at a wide range of temperatures and pressures (up to 950°C and 8.5 kbar with total water contents up to 10.9 wt%) and precisely measured their densities to obtain the partial molar volumes of water $\overline{V}^{\text{melt}}_{\text{total H}_2\text{O}}$ in the albite melts, which were approximated polynomially as a function of temperature and pressure:

$$\begin{aligned}\overline{V}^{\text{melt}}_{\text{total H}_2\text{O}} = {} & 10.98 + 0.962T + 0.1005T^2 - 0.00199T^3 - (0.530 + 0.2031T + 0.00158T^2)P \\ & + (0.0780 + 0.01144T)P^2 - 0.00396P^3, \end{aligned} \tag{1.1}$$

where P is in kbar and T is in hundreds of °C. The function is designed to be consistent with the data on the partial molar volume of water in the hydrous albite glass at around 20°C (Orlova, 1962; Burnham and Davis, 1971). Before them, Goranson (1938), Wasserburg (1957), Khitarov et al. (1963), Shaw (1964), and Ostrovskii and Orlova (1966) also tried to estimate $\overline{V}^{\text{melt}}_{\text{total H}_2\text{O}}$ in the hydrous albite melt from water solubility data. However, none of them could ignore the imprecision of the experimental data or the ambiguity of the theoretical assumptions, and the differences between the values of $\overline{V}^{\text{melt}}_{\text{total H}_2\text{O}}$ published in their respective literatures were very large (See Fig. 16 in Burnham and Davis, 1971). Therefore, the empirical eq. (1.1) obtained as a result of employing the most direct experimental measurement (density measurement) can be considered as the first reliable result on this topic.

1.2 Estimation of the partial molar volume of H_2O_m by Stolper's method

In this part, only the pressure dependence of the solubility equation is discussed, assuming a constant temperature. This is equivalent to setting $T = T_0$ in eq. (18) and can be written as follows, omitting the temperature argument:

$$\begin{aligned}\frac{a_{H_2O_m}(P)}{a_{H_2O_m}(P_0)} &= \frac{\gamma_{H_2O_m}(P)}{\gamma_{H_2O_m}(P_0)} \cdot \frac{X_{H_2O_m}(P)}{X_{H_2O_m}(P_0)} \\ &= \frac{f_{H_2O}(P)}{f_{H_2O}(P_0)} \exp\left(-\frac{\int_{P_0}^{P} \overline{V}^{melt}_{H_2O_m}(P')dP'}{RT} \right). \end{aligned} \tag{1.2}$$

Since Stolper (1982a, 1982b) considered that the mixing of silicate and two water species (H_2O_m and OH) can be roughly approximated to the ideal mixing, the approximation $\gamma_{H_2O_m} = 1$ was used in his subsequent derivation of the theoretical equation for water solubility in silicate melts (Silver and Stolper, 1985). That is, eq. (1.2) was simplified as follows:

$$\frac{X_{H_2O_m}(P)}{X_{H_2O_m}(P_0)} = \frac{f_{H_2O}(P)}{f_{H_2O}(P_0)} \exp\left(-\frac{\int_{P_0}^{P} \overline{V}^{melt}_{H_2O_m}(P')dP'}{RT} \right). \tag{1.3}$$

When melt is saturated with water, the mole fraction $X_{H_2O_m}$ of H_2O_m can be calculated based on the experimentally measured water solubility, the chemical composition of melt, and the speciation data of H_2O_m and OH obtained from the IR spectroscopy. In addition, the fugacity of vapor f_{H_2O} can be calculated with great accuracy from the equation of state of water as a real gas (Burnham et al., 1969; Holloway, 1977; Haar et al., 1984; Wagner and Pruß, 2002; Wagner and Kretzschmar, 2007).

However, the partial molar volume of H_2O_m in melt, $\overline{V}^{melt}_{H_2O_m}$, is not guaranteed to be equal to $\overline{V}^{melt}_{\text{total } H_2O}$, and it was an unknown value. Therefore, many attempts have been made to estimate the unknown $\overline{V}^{melt}_{H_2O_m}$ from the known $X_{H_2O_m}$ and f_{H_2O} through eq. (1.3) (Silver et al., 1990; Blank et al., 1993; Lange, 1994; Holloway and Blank, 1994; Dixon et al., 1995; Holtz et al., 1995; Mysen and Acton, 1999; Zhang, 1999a, Mysen and Wheeler, 2000; Mysen and Cody, 2004; Mysen, 2007; Lesne et al., 2011).

In particular, Silver et al. (1990) took a limit in eq. (1.3) that brings an arbitrary pressure P close to the reference pressure P_0, and the concept is introduced below.

Calculation procedure of $\overline{V}^{\mathrm{melt}}_{\mathrm{H_2O_m}}$ in Silver et al. (1990)

At typical magma temperatures, the magnitude of RT is approximately $\simeq 10^5$ bar $\cdot$ cm^3. In contrast, when P is taken in a neighborhood of P_0, $\int_{P_0}^{P} \overline{V}^{\mathrm{melt}}_{\mathrm{H_2O_m}}(P')dP'$ can be sufficiently small, and the exponential term in eq. (1.2) approaches 1. That is, when $P \to P_0$, it can be regarded as:

$$a_{\mathrm{H_2O_m}} \propto f_{\mathrm{H_2O}}. \tag{1.4}$$

In addition, since the plot of $X_{\mathrm{H_2O_m}}$ vs. $f_{\mathrm{H_2O}}$ in the low pressure region $P \lesssim 1$ kbar shows good linearity, it can be expressed as:

$$X_{\mathrm{H_2O_m}} \propto f_{\mathrm{H_2O}}. \tag{1.5}$$

Therefore, Henry's law holds in the low pressure region as follows. This also means that $\gamma_{\mathrm{H_2O_m}}$ is independent of pressure.

$$a_{\mathrm{H_2O_m}} \propto X_{\mathrm{H_2O_m}}. \tag{1.6}$$

From the above, the unknown $\overline{V}_{\mathrm{H_2O_m}}(P)$ can be obtained using the known $X_{\mathrm{H_2O_m}}(P)$ and $f_{\mathrm{H_2O}}(P)$:

$$\begin{aligned}
\overline{V}^{\mathrm{melt}}_{\mathrm{H_2O_m}}(P_0) &= -RT \lim_{P\to P_0} \frac{\ln \dfrac{X_{\mathrm{H_2O_m}}(P)}{X_{\mathrm{H_2O_m}}(P_0)} - \ln \dfrac{f_{\mathrm{H_2O}}(P)}{f_{\mathrm{H_2O}}(P_0)}}{P - P_0} \\
&= -RT \lim_{P\to P_0} \frac{\ln \dfrac{X_{\mathrm{H_2O_m}}(P)}{f_{\mathrm{H_2O}}(P)} - \ln \dfrac{X_{\mathrm{H_2O_m}}(P_0)}{f_{\mathrm{H_2O}}(P_0)}}{P - P_0} \\
&= -RT \left. \frac{\partial \ln \dfrac{X_{\mathrm{H_2O_m}}(P)}{f_{\mathrm{H_2O}}(P)}}{\partial P} \right|_{P=P_0}.
\end{aligned} \tag{1.7}$$

However, in the above idea, even if taking the limit $P \to P_0$, simply $\dfrac{a_{\mathrm{H_2O_m}}(P)}{f_{\mathrm{H_2O}}(P)} = \dfrac{a_{\mathrm{H_2O_m}}(P_0)}{f_{\mathrm{H_2O}}(P_0)}$ holds, so deriving eq. (1.4) is clearly wrong.

In an exceptional case, Silver and Stolper (1989) implicitly assumed that $\overline{V}^{\mathrm{melt}}_{\mathrm{total\ H_2O}} = \overline{V}^{\mathrm{melt}}_{\mathrm{H_2O_m}}$, and substituted the empirical equation (eq. (1.1)) of Burnham and Davis (1971) into the theoretical solubility equation to obtain various thermodynamic parameters. This is discussed later in Chapter 2.

The values of $\overline{V}^{\mathrm{melt}}_{\mathrm{H_2O_m}}$ obtained in this way varied greatly from positive to negative depending on melt temperature, pressure and composition as shown in Table 1.1 below.

Table 1.1: Values of $\overline{V}^{\text{melt}}_{\text{H}_2\text{O}_\text{m}}$ estimated through the theoretical expression for $\text{H}_2\text{O}_\text{m}$ solubility in silicate melts (eq. (1.3)).

Source	Composition	T (°C)	P (bars)	$\overline{V}^{\text{melt}}_{\text{H}_2\text{O}_\text{m}}$ (cm^3/mol)
Silver et al. (1990)	rhyolite	850	1	-3.3 ± 2.8
	rhyolite	n.d.	up to 7 k	12.0
	E2	1180	1	16.2
	CAS-E2	1200–1450	15 k–20 k	13.8
	albite	850	1	20.9 ± 0.6
	albite	1000	1	22.4
	albite	800–1000	800	22–25
	albite	1200–1450	15 k–20 k	14.3
	albite	n.d.	up to 7 k	11.6
	orthoclase	850	1	25.1
	orthoclase	1200–1450	15 k–20 k	15.1
	Na, Zn-rich silicate	n.d.	up to 7 k	12
	$\text{Na}_2\text{Si}_3\text{O}_7$	n.d.	up to 7 k	13
Blank et al. (1993)	rhyolite	850, 1200	49–983	-2.5 ± 3.0
Lange (1994)	albite	850	486–546	-4.0 ± 4.7
Dixon et al. (1995)	tholeiitic basalt	1100–1200	180–8 k	12 ± 1
Holtz et al. (1995)	haplogranite (AOQ)	900	1 k–8 k	10–12
Mysen and Acton (1999)	haploandesite join	700–1300	8 k–20 k	6–14
Zhang (1999a)	haplogranite (AOQ)	550–1321	1–5 k	$32.8 - 0.02057T$ (K)
Mysen and Wheeler (2000)	haploandesite join	1000–1300	8 k–20 k	7.8–12.8
Mysen and Cody (2004)	Na_2O-SiO_2 join	1000–1300	8 k–20 k	10–14
Mysen (2007)	$\text{Na}_2\text{O}{\cdot}4\text{TO}_2$	1100	8 k–20 k	8.9–12.5
Lesne et al. (2011)	alkali basalt	1200	163–3848	$26.9, -15.9, -48$

· T (°C) and P (bars) represent the temperature and pressure of experimental determinations of water solubility in silicate melts.

· $\overline{V}^{\text{melt}}_{\text{H}_2\text{O}_\text{m}}$ (cm^3/mol) represents the partial molar volume of $\text{H}_2\text{O}_\text{m}$ in silicate melts.

· rhyolite = 77.5 wt% SiO_2 + 12.5 wt% Al_2O_3 + 0.5 wt% CaO + 1.0 wt% FeO + 3.6 wt% Na_2O + 4.8 wt% K_2O. · E2 = 63.7 wt% SiO_2 + 14.3 wt% Al_2O_3 + 22.0 wt% CaO.

· CAS = 62.8 wt% SiO_2 + 14.3 wt% Al_2O_3 + 22.9 wt% CaO (almost the same as E2).

· albite = $\text{NaAlSi}_3\text{O}_8$.

· orthoclase = KAlSi_3O_8.

· Na, Zn-rich silicate = 72.9 wt% SiO_2 + 2.1 wt% Al_2O_3 + 10.6 wt% Na_2O + 4.5 wt% K_2O + 10.0 wt% ZnO.

· tholeiitic basalt = 50.8 wt% SiO_2 + 13.7 wt% Al_2O_3 + 1.84 wt% TiO_2 + 12.4 wt% FeO + 0.22 wt% MnO + 6.67 wt% MgO + 11.5 wt% CaO + 2.68 wt% Na_2O + 0.15 wt% K_2O + 0.19 wt% P_2O_5 + 0.15 wt% S.

· haplogranite (AOQ) = 76.14 wt% SiO_2 + 13.53 wt% Al_2O_3 + 4.65 wt% Na_2O + 5.68 wt% K_2O ($\text{Ab}_{38}\text{Or}_{34}\text{Qz}_{28}$, almost the same as rhyolite).

· haploandesite join = $\text{K}_2\text{Si}_4\text{O}_9$-$\text{K}_2(\text{KAl})_4\text{O}_9$ with 0, 3 and 6 mol% Al_2O_3 added as $\text{K}_2(\text{KAl})_4\text{O}_9$ component.

· alkali basalt = 47.59-49.40 wt% SiO_2 + 14.52-17.19 wt% Al_2O_3 + 0.80-1.66 wt% TiO_2 + 7.51-10.15 wt% FeO + 0.14-0.20 wt% MnO + 5.72-8.00 wt% MgO + 10.85-12.77 wt% CaO + 1.80-3.42 wt% Na_2O + 1.90-5.55 wt% K_2O + 0.40-0.65 wt% P_2O_5.

· Na_2O-SiO_2 join = NSx (x = 2, 2 2/3, 4, and 8), where x represents the number of moles of SiO_2 relative to 1 Na_2O.

· $\text{Na}_2\text{O}{\cdot}4\text{TO}_2$ = the join between tetrasilicate (T = Si) and tetra-alminate (T = NaAl).

1.3 A paradox of the partial molar volume of water in silicate melt

Subsequently, like Burnham and Davis (1971), Ochs and Lange (1997) measured the density of the quenched hydrous albite glasses with various water contents synthesized at high temperature and high pressure. In addition, by combining the measured thermal expansion coefficients of glass and melt near the glass transition point, the density of the hydrous albite melt was precisely estimated, and $\overline{V}^{\mathrm{melt}}_{\mathrm{total\ H_2O}}$ was calculated. Subsequently, Ochs and Lange (1999) performed density measurements for the first time on two compositions of hydrous melts other than albite (rhyolite and KCS, KCS = 59.51 wt% SiO_2 + 30.51 wt% CaO + 9.97 wt% K_2O) to investigate the melt composition dependence of $\overline{V}^{\mathrm{melt}}_{\mathrm{total\ H_2O}}$. Albite and rhyolite are fully polymerized liquids (NBO/T = 0), whereas KCS is a depolymerized melt (NBO/T = 1.9). The results of these experiments showed that $\overline{V}^{\mathrm{melt}}_{\mathrm{total\ H_2O}}$ satisfied the following empirical equation in the range of 298-1500 K and 0.1 MPa-1.0 GPa, independent of the chemical composition of melt, total water content, and water speciation:

$$\overline{V}^{\mathrm{melt}}_{\mathrm{total\ H_2O}}(1000^{\circ}\mathrm{C}, 1\ \mathrm{bar}) = 22.89 \pm 0.55\ \mathrm{cm}^3/\mathrm{mol}, \tag{1.8}$$

$$\frac{\partial \overline{V}^{\mathrm{melt}}_{\mathrm{total\ H_2O}}}{\partial T} = (9.46 \pm 0.83) \times 10^{-3}\ \mathrm{cm}^3/(\mathrm{mol}\cdot\mathrm{K}), \tag{1.9}$$

$$\frac{\partial \overline{V}^{\mathrm{melt}}_{\mathrm{total\ H_2O}}}{\partial P} = (-3.15 \pm 0.61) \times 10^{-4}\ \mathrm{cm}^3/(\mathrm{mol}\cdot\mathrm{bar}). \tag{1.10}$$

The values of $\overline{V}^{\mathrm{melt}}_{\mathrm{total\ H_2O}}$ obtained by this empirical expression were in general agreement with those estimated from the empirical equation (eq. (1.1)) of Burnham and Davis (1971), with a maximum deviation of a few cm^3/mol (See Fig. 4.1 in Ochs and Lange, 1997). Moreover, Bouhifd et al.'s (2001) experiments with phonolite melt, similar to those of Ochs and Lange (1997), also supported the above empirical equations. The fact that $\overline{V}^{\mathrm{melt}}_{\mathrm{total\ H_2O}}$ is independent of water speciation means that the following equation holds:

$$\overline{V}^{\mathrm{melt}}_{\mathrm{total\ H_2O}} = \overline{V}^{\mathrm{melt}}_{\mathrm{H_2O_m}} = \overline{V}^{\mathrm{melt}}_{\mathrm{OH}}, \tag{1.11}$$

where $\overline{V}^{\mathrm{melt}}_{\mathrm{OH}}$ means one cluster of two OH groups minus one oxygen, i.e., one H_2O molecule dissolved in the form of OH groups. Thus, the subscripts of $\overline{V}^{\mathrm{melt}}$ in eq. (1.8), eq. (1.9) and eq. (1.10) can be read as H_2O_m.

In other words, Stolper's method presented in section 1.2 calculates values far removed from $\overline{V}^{\mathrm{melt}}_{\mathrm{H_2O_m}}$ obtained from the empirical equations experimentally determined by Burnham and Davis (1971) and Ochs and Lange (1997, 1999). That is, the theoretical solubility equation,

eq. (1.3), used to estimate $\overline{V}^{\rm melt}_{\rm H_2O_m}$ is not internally consistent. This paradox has been pointed out in a number of publications (Silver et al., 1990; Lange, 1994; Holloway and Blank, 1994; Dixon et al., 1995; Zhang, 1999b; Lesne et al., 2011), however, there have been no studies to date that have explicitly addressed its causes.

Zhang (1999b) offered two ideas as to the cause of this inconsistency.
(1) Assuming that both the values of $\overline{V}^{\rm melt}_{\rm H_2O_m}$ obtained via the theoretical solubility equation and the experimentally determined values of $\overline{V}^{\rm melt}_{\rm total\ H_2O}$ are correct, $\overline{V}^{\rm melt}_{\rm H_2O_m} \neq \overline{V}^{\rm melt}_{\rm OH}$ is required to satisfy both. In other words, he pointed out that the partial molar volume may differ between H_2O_m and OH when water is dissolved into melt. However, this idea contradicts the above equation (1.11) suggested by the experimental results of Ochs and Lange (1997, 1999). In addition, since the ionic radius of the O atom is relatively large among the atoms constituting melt, and a packing structure of O atoms can be assumed, it is unlikely that there is a large difference between $\overline{V}^{\rm melt}_{\rm H_2O_m}$ and $\overline{V}^{\rm melt}_{\rm OH}$; therefore, this idea does not seem to be appropriate that includes the case where positive and negative values of $\overline{V}^{\rm melt}_{\rm H_2O_m}$ and $\overline{V}^{\rm melt}_{\rm OH}$ may be inverted.
(2) At that time, since equilibrium constants for the second reaction of dissolution had only been determined for glasses and melts at 400-600°C with the water content of $\leq$ 2.4 wt% for the rhyolite compositions (Zhang et al., 1997; Ihinger et al., 1999), he pointed out that applying the equilibrium constants extrapolated to general magma temperatures and water contents may have led to inaccurate estimations of $X_{\rm H_2O_m}$ and $\overline{V}^{\rm melt}_{\rm H_2O_m}$. However, the equilibrium constants at higher temperatures or higher water contents later obtained experimentally by Nowak and Behrens (2001), Behrens and Nowak (2003), and others are not so different from the extrapolated value of the equilibrium constant in Zhang et al. (1997) or Ihinger et al. (1999), and thus it is unlikely to be the root cause of the paradox described above.

The Excel macro VolatileCalc, provided by Newman and Lowenstern (2002), a widely used publicly available program, can calculate the solubility of H_2O and CO_2 in basaltic and rhyolitic melts. The program to calculate the H_2O solubility (especially H_2O_m) is incorporated based on the theoretical equation of Silver and Stolper (1985): eq. (1.3). In their calculation algorithm for water solubility in rhyolitic melt, they arbitrarily set $\overline{V}_{\rm H_2O_m} = 5$ cm^3/mol independent of temperature and pressure, which is far from the value of Ochs and Lange (1997, 1999), with no evidence so that water solubility obtained from eq. (1.3) roughly matched the previous experimental data. Fig. 1.1 shows water solubilities in rhyolitic melts at 850°C and below 500 MPa: previous experimental data (circles), calculated values using an empirical model compiled from these data (the light blue curve, Liu et al., 2005), and calculated values using VolatileCalc (the gray curve). The equation for the empirical model of Liu et al. (2005) is as follows:

$$Liu(T, P') = \frac{(354.94P'^{0.5} + 9.623P' - 1.5223P'^{1.5})}{T} + 0.0012439P'^{1.5}, \qquad (1.12)$$

where $Liu(T, P')$ is total dissolved H_2O content in wt%, T is temperature in K, and P' is pressure in MPa. The applicable range of this equation is 700-1200°C and 1-5000 bars. Although the figure shows that the curve of VolatileCalc seems to reproduce the data measured in previous experiments, it has an upward convex at pressures higher than 200 MPa and total water content higher than 6.0 wt%, while the curve of the empirical model has a downward convex. Therefore, it is preferable to use eq. (1.12) rather than VolatileCalc for determining water solubility in rhyolitic melts at 200-500 MPa.

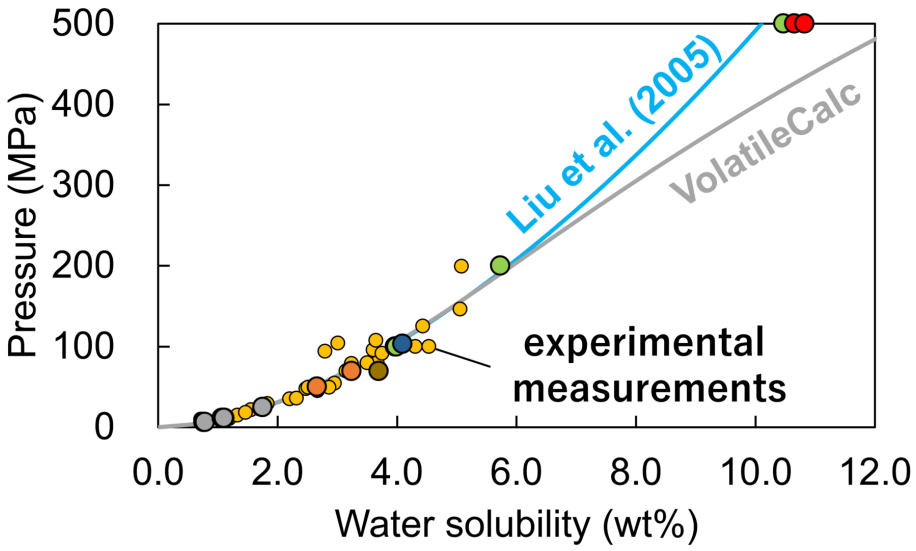

[Figure 1.1] Water solubility in 850°C rhyolitic melt or haplogranite (AOQ) melt. Circles are experimental measurements in previous studies: dark blue - Burnham and Jahns (1962); brown - Shaw (1974); small yellow - Silver et al. (1990); yellowish green - Holtz et al. (1992, 1995); orange - Yamashita (1999); red - Wilke et al. (2002); gray - Liu et al. (2005). The light blue curve shows an empirical model derived from a compilation of some of the above by Liu et al. (2005). The gray curve shows the calculated values by an open program VolatileCalc provided by Newman and Lowenstern (2002).

The question of which value of $\overline{V}^{\mathrm{melt}}_{\mathrm{H_2O_m}}$ should be chosen, the one obtained via the theoretical solubility equation or the one determined by experiment, is also important in experimental studies of bubble nucleation, the initial stage of vesiculation of magma induced by decompression that is the driving force for volcanic eruptions. Specifically, in experiments to reproduce the decompression-induced vesiculation of magma in a laboratory system with controlled initial pressure and decompression rate, the uncertainty in the value of $\overline{V}^{\mathrm{melt}}_{\mathrm{H_2O_m}}$ greatly affects the estimation of surface tension between melt and bubble nucleus by substituting the nucleation rate estimated from the bubble number density (BND) of the experimental product into the

classical nucleation theory (CNT, e.g., Hirth et al., 1970; Blander and Katz, 1975), (Mangan and Sisson, 2000; 2005; Mangan et al., 2004; Mourtada-Bonnefoi and Laporte, 2002; 2004; Cluzel et al., 2008; Hamada et al., 2010; Gardner and Ketcham, 2011; Gardner, 2012; Gonnermann and Gardner, 2013; Gardner et al., 2013; Gardner et al., 2018). Surface tension is the strongest parameter governing bubble nucleation, but it is difficult to measure directly and has only a few precedents (Epel'baum, 1973; Khitarov et al., 1979; Bagdassarov et al., 2000), so it is mostly estimated indirectly through these laboratory decompression experiments. This estimate impacts the question of whether homogeneous or heterogeneous nucleation predominates in natural magma (Shea, 2017), and is also relevant to attempts to estimate the decompression rate of magma from observations of bubble textures in pyroclastic fall deposits, such as pumice, scoria and volcanic ash (Toramaru, 1989; 1995; 2006, Nishiwaki and Toramaru, 2019), so the problem of the uncertainty of $\overline{V}^{\mathrm{melt}}_{\mathrm{H_2O_m}}$ should be resolved as soon as possible.

1.4 Resolving the paradox: Breaking of the ideal mixing model

As noted in section 0.1, Stolper (1982a, 1982b) explained that the mutually soluble system of silicate and water can be regarded as the ideal mixing. In addition, as discussed in section 1.2, for the subsequent approximately 40 years, the ideal solution approximation (eq. (1.3)) was used for the theoretical expression of water solubility in silicate melts. However, in reality, the mixture of silicate and water has a miscibility gap as shown in Fig 0.2 and involves volume change and heat generation during mixing. This behavior is clearly at odds with Definitions of the ideal solution 2. and 3. given in section 0.1.

In other words, to solve the above paradox, the silicate-water mixture should not be approximated as the ideal solution, but as in eq. (1.2), the term $\gamma_{H_2O_m}(P)/\gamma_{H_2O_m}(P_0)$ must be properly taken into account. In this study, the partial molar volume of H_2O_m in melt, $\overline{V}_{H_2O_m}$, is considered as known (eq. (1.8), eq. (1.9), and eq. (1.10)), and the unknown term $\gamma_{H_2O_m}(P)/\gamma_{H_2O_m}(P_0)$ is evaluated through eq. (1.2). This idea is contrary to previous studies (see section 1.3) that tried to find "unknown" $\overline{V}_{H_2O_m}$ by trusting the theoretical equation.

If a reference pressure $P_0 = 1$ bar is assumed in eq. (1.2), the theoretical expression for the solubility of H_2O_m in melt is written as below:

$$\frac{\gamma_{H_2O_m}(P)}{\gamma_{H_2O_m}(1)} \cdot \frac{X_{H_2O_m}(P)}{X_{H_2O_m}(1)} = \frac{f_{H_2O}(P)}{f_{H_2O}(1)} \exp\left(-\frac{\int_1^P \overline{V}^{melt}_{H_2O_m}(P')dP'}{RT} \right). \tag{1.13}$$

$X_{H_2O_m}$ was obtained from eq. (10) by determining $X_{\text{total } H_2O}$ and the "apparent" equilibrium constant Q_{r2} (defined as eq. (2.15), later explained in section 2.3) in haplogranite (AOQ) melt (Behrens and Nowak, 2003), which is close in composition to rhyolitic melt. For the representative chemical composition of anhydrous rhyolitic melt, that of obsidian glass from Wada Pass, Nagano Prefecture, Japan (Yoshimura and Nakamura, 2010) was used. It is needed for converting the value of water solubility *Liu* (wt%, eq. (1.12)) to $X_{\text{total } H_2O}$ (mol). The conversion equation is expressed as below:

$$X_{\text{total } H_2O} = \frac{32.24 \cdot \dfrac{Liu}{100}}{18.02 + 14.22 \cdot \dfrac{Liu}{100}}. \tag{1.14}$$

f_{H_2O} can be calculated from the equation of state of a real gas by "IAPWS-95" (Wagner and Kretzschmar, 2007). That equation for lower than 1000°C is extrapolated directly to the range of 1000-1200°C. The extrapolation result agrees well with the result obtained from the modified Redlich-Kwong eqation (calculated with VolatileCalc provided by Newman and Lowenstern, 2002) within 1.58 % error.

If eq. (1.5) of the method by Silver et al. (1990) is correct, the relation

$$\frac{X_{\mathrm{H_2O_m}}(P)}{f_{\mathrm{H_2O}}(P)} \Big/ \frac{X_{\mathrm{H_2O_m}}(1)}{f_{\mathrm{H_2O}}(1)} = 1 \tag{1.15}$$

should hold in the low pressure region, however, the quantity of the LHS at 700-1200°C can be drawn as Fig. 1.2. Around 1000°C, eq. (1.15) seems to be a good approximation over a wide pressure range, but at other temperatures it deviates from unity significantly, thus eq. (1.5) is not valid.

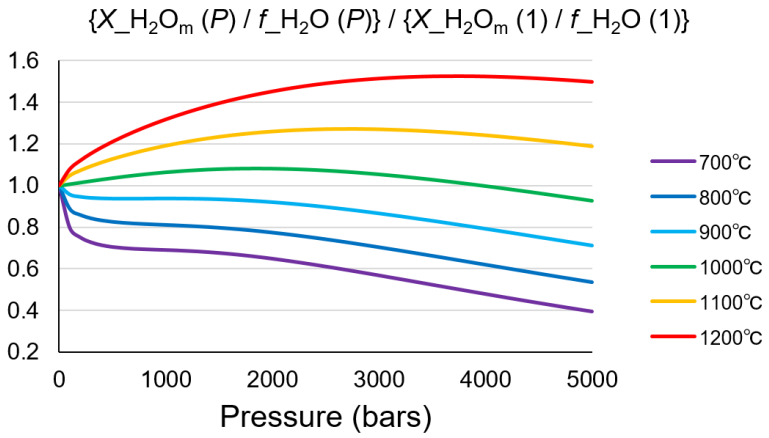

[Figure 1.2] $\{X_{\mathrm{H_2O_m}}(P)/f_{\mathrm{H_2O}}(P)\}/\{X_{\mathrm{H_2O_m}}(1)/f_{\mathrm{H_2O}}(1)\}$. $X_{\mathrm{H_2O_m}}(P)$ is the mole fraction of $\mathrm{H_2O_m}$ in rhyolitic melt at P bars, obtained by the empirical model of water solubility in rhyolitic melt (Liu et al., 2005, eq. (1.12)) and the apparent equilibrium constant of the second dissolution reaction of water (r2, eq. (2)) in haplogranite melt Q_{r2} (Behrens and Nowak, 2003, defined as eq. (5)). $f_{\mathrm{H_2O}}(P)$ is the pure water vapor fugacity at P bars.

The unknown term $\gamma_{\mathrm{H_2O_m}}(P)/\gamma_{\mathrm{H_2O_m}}(1)$ for the same temperature and pressure range can be drawn as Fig. 1.3. In the ideal mixing assumed in Stolper (1982a, 1982b) and Silver and Stolper (1985), $\gamma_{\mathrm{H_2O_m}}(P)/\gamma_{\mathrm{H_2O_m}}(1) = 1$. However, Fig. 1.3 shows that $\gamma_{\mathrm{H_2O_m}}(P)/\gamma_{\mathrm{H_2O_m}}(1) \neq 1$ in most temperature and pressure regions. This means that Henry's law (eq. (1.6)) of Silver et al.'s (1990) method and the ideal mixing model are broken. It immediately follows that eq. (1.7) of Silver et al.'s (1990) method is also inappropriate.

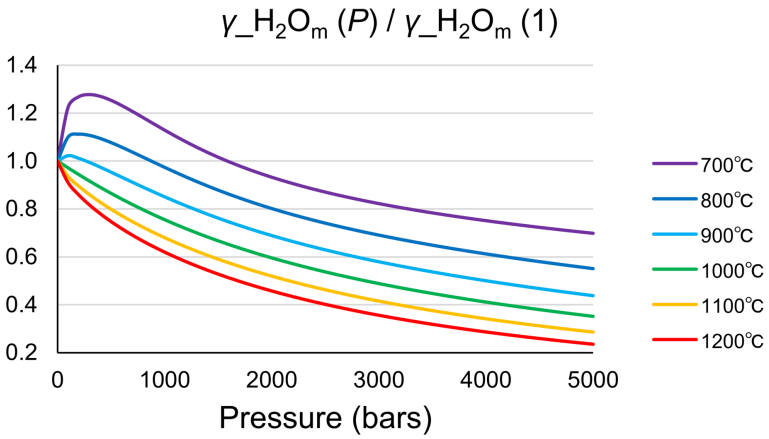

[Figure 1.3] The ratio of the activity coefficient of H_2O_m in melt $\gamma_{H_2O_m}(P)/\gamma_{H_2O_m}(1)$, calculated when $X_{H_2O_m}(P)$, $f_{H_2O}(P)$, and the partial molar volume of H_2O_m in melt $\overline{V}^{melt}_{H_2O_m}(P')$ in eq. (1.13) are assumed to be known.

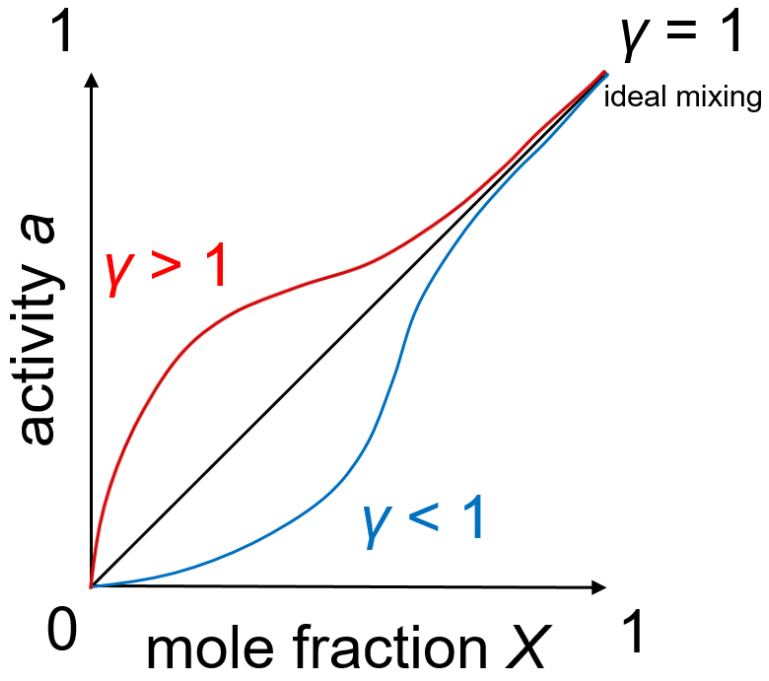

[Figure 1.4] A conceptual diagram of the relation between the mole fraction X and the activity a of a solute in a solution. The straight line $a = X$ denotes the ideal mixing case. When the activity coefficient $\gamma = a/X$ is greater than unity, the mixing of solute and solvent molecules is energetically unstable compared to the mixing of only solute or only solvent molecules. In contrast, when γ is less than unity, the mixing of solute and solvent molecules is energetically more stable than the mixing of only solute or only solvent molecules.

Figure 1.4 shows a conceptual diagram of the relation between the mole fraction X and the activity a of a solute in a solution. The activity coefficient γ (see eq. (6)) is the ratio of a and X. Since solubility generally increases with increasing pressure, the horizontal axis corresponds to the direction of increasing pressure. If X is small enough ($X \ll 1$), γ decreases monotonically with increasing pressure when the mixing of solute and solvent molecules is energetically unstable ($\gamma > 1$, the red curve) compared to the mixing of only solute or only solvent molecules. Conversely, if the mixing of solute and solvent molecules is energetically stable ($\gamma < 1$, the blue curve) compared to the mixing of only solute or only solvent molecules, γ increases monotonically with increasing pressure. In the system discussed here, since O is overwhelmingly more abundant than H_2O_m, O corresponds to the solvent and H_2O_m to the solute. Even in the case of the highest solubility of H_2O_m in the temperature and pressure range treated in this study (700°C, 5000 bars), at most $X_{H_2O_m} < 0.1$. The ratio $\gamma_{H_2O_m}(P)/\gamma_{H_2O_m}(1)$ plotted in Fig. 1.3 is smaller than unity in most temperature and pressure regions and decreases monotonically with increasing pressure; therefore, $\gamma_{H_2O_m}(P)$ is a monotonically decreasing function. This corresponds to the red curve, indicating that the mixing of O and H_2O_m is more unstable than the mixing of O alone. In contrast, the ratio $\gamma_{H_2O_m}(P)/\gamma_{H_2O_m}(1)$ is greater than unity in the temperature and pressure regions of (700°C, $\lesssim$ 1600 bars), (800°C, $\lesssim$ 900 bars), and (900°C, $\lesssim$ 300 bars), and all of them increase with increasing pressure at very low pressures. The reason for this is unknown and still under consideration.

In the following, the reason why the estimated value of $\overline{V}_{H_2O_m}$ was extremely unstable when assuming the ideal mixing (i.e., $\gamma_{H_2O_m} = 1$, see Table 1.1), is examined by comparing the magnitude of the two terms $\gamma_{H_2O_m}$ and $X_{H_2O_m}/f_{H_2O}$.

According to Ochs and Lange (1999), since the pressure dependence of $\overline{V}^{melt}_{H_2O_m}$ is expressed as eq. (1.10), $\overline{V}_{H_2O_m}$ at 1000°C varies at most only 1.6 cm^3/mol in the range of 1-5000 bars. Therefore, ignoring the pressure dependence of $\overline{V}_{H_2O_m}$, the equation for estimating $\overline{V}_{H_2O_m}$ can be approximated in a form of difference rather than in the differential form as eq. (1.7) in the method by Silver et al. (1990):

$$\overline{V}_{H_2O_m} \simeq -RT \frac{\ln \dfrac{a_{H_2O_m}(P)}{a_{H_2O_m}(P_0)} - \ln \dfrac{f_{H_2O}(P)}{f_{H_2O}(P_0)}}{P - P_0}. \tag{1.16}$$

When $P_0 = 1$ bar, the RHS of eq. (1.16) can be transformed as follows:

Table 1.2: $\ln \dfrac{\gamma_{\mathrm{H_2O_m}}(P)}{\gamma_{\mathrm{H_2O_m}}(1)}$ vs. $\ln \left(\dfrac{X_{\mathrm{H_2O_m}}(P)}{X_{\mathrm{H_2O_m}}(1)} \Big/ \dfrac{f_{\mathrm{H_2O}}(P)}{f_{\mathrm{H_2O}}(1)} \right)$

T/P	1000 bars	3000 bars	5000 bars
800°C	$(-0.0263, -0.210)$	$(-0.369, -0.352)$	$(-0.595, 0.625)$
1000°C	$(-0.281, 0.0632)$	$(-0.716, 0.0540)$	$(-1.04, -0.0742)$
1200°C	$(-0.479, 0.275)$	$(-1.03, 0.414)$	$(-1.45, 0.404)$

Values of the first and second terms in the numerator of eq. (1.17) at specific temperatures and pressures.

Table 1.3: Estimated values of $\overline{V}_{\mathrm{H_2O_m}}$ ($\mathrm{cm^3/mol}$): assuming Henry's law vs. Ochs and Lange's (1999) equation

T/P	1000 bars	3000 bars	5000 bars
800°C	$(18.8, 20.7)$	$(10.5, 20.0)$	$(11.2, 19.4)$
1000°C	$(-6.70, 22.6)$	$(-1.90, 21.9)$	$(1.57, 21.3)$
1200°C	$(-33.7, 24.5)$	$(-16.9, 23.8)$	$(-9.89, 23.2)$

Values calculated when the first term of the numerator in eq. (1.17) is set to 0 vs. from eq. (1.8), eq. (1.9), and eq. (1.10) derived from the density measurement experiments by Ochs and Lange (1999).

$$
\begin{aligned}
&= -RT \frac{\ln \dfrac{a_{\mathrm{H_2O_m}}(P)}{a_{\mathrm{H_2O_m}}(1)} - \ln \dfrac{f_{\mathrm{H_2O}}(P)}{f_{\mathrm{H_2O}}(1)}}{P-1} \\
&= -RT \frac{\ln \dfrac{\gamma_{\mathrm{H_2O_m}}(P)}{\gamma_{\mathrm{H_2O_m}}(1)} + \ln \dfrac{X_{\mathrm{H_2O_m}}(P)}{X_{\mathrm{H_2O_m}}(1)} - \ln \dfrac{f_{\mathrm{H_2O}}(P)}{f_{\mathrm{H_2O}}(1)}}{P-1} \\
&= -RT \frac{\ln \dfrac{\gamma_{\mathrm{H_2O_m}}(P)}{\gamma_{\mathrm{H_2O_m}}(1)} + \ln \left(\dfrac{X_{\mathrm{H_2O_m}}(P)}{X_{\mathrm{H_2O_m}}(1)} \Big/ \dfrac{f_{\mathrm{H_2O}}(P)}{f_{\mathrm{H_2O}}(1)} \right)}{P-1}.
\end{aligned} \tag{1.17}
$$

When the temperature is fixed to one of 800, 1000, or 1200°C, and the pressure is varied to 1000, 3000, or 5000 bars, the pairs of values of the two logarithmic terms in the numerator of eq. (1.17) $\left\{ \ln \dfrac{\gamma_{\mathrm{H_2O_m}}(P)}{\gamma_{\mathrm{H_2O_m}}(1)}, \ln \left(\dfrac{X_{\mathrm{H_2O_m}}(P)}{X_{\mathrm{H_2O_m}}(1)} \Big/ \dfrac{f_{\mathrm{H_2O}}(P)}{f_{\mathrm{H_2O}}(1)} \right) \right\}$ are shown as Table 1.2. At any temperature, the term $\gamma_{\mathrm{H_2O_m}}$ is non-negligible compared to the term $X_{\mathrm{H_2O_m}}/f_{\mathrm{H_2O}}$.

Moreover, the pairs of the values of $\overline{V}_{\mathrm{H_2O_m}}$: when Henry's law $\dfrac{\gamma_{\mathrm{H_2O_m}}(P)}{\gamma_{\mathrm{H_2O_m}}(1)} = 1$ i.e. $\ln \dfrac{\gamma_{\mathrm{H_2O_m}}(P)}{\gamma_{\mathrm{H_2O_m}}(1)} = 0$ is applied in eq. (1.17) (the conventional method) vs. obtained by Ochs and Lange (1999)'s equations (1.8), (1.9), and (1.10) are listed in Table 1.3. Since the term $\gamma_{\mathrm{H_2O_m}}$ sensitively changes with temperature and pressure, it can be concluded that neglecting this term have led to the previous estimations of extremely unstable $\overline{V}_{\mathrm{H_2O_m}}$ values.

Chapter 2

Three-component asymmetric regular solution model

2.1 Regular solution approximation

In Chapter 1, it was shown that the ideal solution approximation for the three-component mixture of silicate and water (H_2O_m + OH) breaks down, and the values of $\gamma_{H_2O_m}(P)/\gamma_{H_2O_m}(P_0)$ were obtained over a wide temperature and pressure range for a reference pressure $P_0 = 1$ bar. However, this is only the ratio of $\gamma_{H_2O_m}$ at arbitrary and reference pressures. Therefore, in this chapter, it is attempted to find the specific value of $\gamma_{H_2O_m}$.

If the deviation from an ideal solution in a real solution is expressed as "ex" (excess), the excess mixing enthalpy ΔH^{ex} and the excess mixing entropy ΔS^{ex} of the ideal solution are

$$\begin{cases} \Delta H^{ex} = 0, & (2.1) \\ \Delta S^{ex} = 0, & (2.2) \end{cases}$$

whereas those of the real solution are

$$\begin{cases} \Delta H^{ex} \neq 0, & (2.3) \\ \Delta S^{ex} \neq 0. & (2.4) \end{cases}$$

Note that an inorganic solid solution is generally treated as a regular solution, where ΔS^{ex} is assumed to be minute (Uchida, 2012):

$$\begin{cases} \Delta H^{ex} \neq 0, & (2.5) \\ \Delta S^{ex} = 0. & (2.6) \end{cases}$$

This study also attempts to approximate the regular solution for the three-component mixture of silicate and water (H_2O_m + OH). In this chapter, the three components are denoted by A, B, and C, where A = H_2O_m, B = OH, and C = O (bridging oxygen), to avoid complicated subscripts.

2.2 Three-component asymmetric regular solution

In general, the curve of the excess Gibbs energy ΔG^{ex} of mixing for a multicomponent solid solution is asymmetric between components. Kakuda et al. (1991, 1994) extended the Bragg-Williams approximation in the two-component system to the three-component (A, B, and C) system and derived an equation for $\Delta G^{\mathrm{ex}}_{\mathrm{ABC}}$ for a three-component asymmetric regular solution.

$$G_{\mathrm{ABC}} = G^{\circ}_{\mathrm{ABC}} + \Delta G^{\mathrm{mix}}_{\mathrm{ABC}} + \Delta G^{\mathrm{ex}}_{\mathrm{ABC}}. \tag{2.7}$$

In addition, each term is expanded as follows:

$$G^{\circ}_{\mathrm{ABC}} = n_{\mathrm{A}}\mu^{\circ}_{\mathrm{A}} + n_{\mathrm{B}}\mu^{\circ}_{\mathrm{B}} + n_{\mathrm{C}}\mu^{\circ}_{\mathrm{C}}, \tag{2.8}$$

$$\Delta G^{\mathrm{mix}}_{\mathrm{ABC}} = RT\left(n_{\mathrm{A}}\ln\frac{n_{\mathrm{A}}}{n_{\mathrm{A}}+n_{\mathrm{B}}+n_{\mathrm{C}}} + n_{\mathrm{B}}\ln\frac{n_{\mathrm{B}}}{n_{\mathrm{A}}+n_{\mathrm{B}}+n_{\mathrm{C}}} + n_{\mathrm{C}}\ln\frac{n_{\mathrm{C}}}{n_{\mathrm{A}}+n_{\mathrm{B}}+n_{\mathrm{C}}}\right), \tag{2.9}$$

$$\begin{aligned}\Delta G^{\mathrm{ex}}_{\mathrm{ABC}} = \frac{1}{(n_{\mathrm{A}}+n_{\mathrm{B}}+n_{\mathrm{C}})^2} \\ \{&n_{\mathrm{A}}n_{\mathrm{B}}(n_{\mathrm{A}}w_{\mathrm{AAB}} + n_{\mathrm{B}}w_{\mathrm{ABB}}) \\ &+ n_{\mathrm{B}}n_{\mathrm{C}}(n_{\mathrm{B}}w_{\mathrm{BBC}} + n_{\mathrm{C}}w_{\mathrm{BCC}}) \\ &+ n_{\mathrm{C}}n_{\mathrm{A}}(n_{\mathrm{C}}w_{\mathrm{CCA}} + n_{\mathrm{A}}w_{\mathrm{CAA}}) \\ &+ 2n_{\mathrm{A}}n_{\mathrm{B}}n_{\mathrm{C}}w_{\mathrm{ABC}}\},\end{aligned} \tag{2.10}$$

where μ°_{i} ($i = \mathrm{A}, \mathrm{B}$, and C) are chemical potentials of the pure components, respectively. w_{ijk} ($i = \mathrm{A}, \mathrm{B}$, and C) are interaction parameters that represent the magnitude of the interaction energy acting among three nearest neighbor particles (triplet). For example, "iij" represents the interaction when one particle of j enters an i-rich environment, and "ijj" represents the interaction when one particle of i enters a j-rich environment. This can be interpreted as reflecting the fact that the two-body interaction between i and j changes under the influence of the surrounding environment. $w_{\mathrm{iij}} > 0$ means that the i-only state is more energetically stable than the state in which one particle of j enters. Conversely, $w_{\mathrm{iij}} < 0$ means that the state in which one j particle enters is more energetically stable than the i-only state.

$\Delta G^{\mathrm{ex}}_{\mathrm{ABC}}$ and γ_{A}, the activity coefficient of the component A, are connected by the following relation, expanded from eq. (2.10):

$$\begin{aligned}\mu_{\mathrm{A}}^{\mathrm{ex}} = RT\ln\gamma_{\mathrm{A}} &= \frac{\partial \Delta G_{\mathrm{ABC}}^{\mathrm{ex}}}{\partial n_{\mathrm{A}}} \\ &= w_{\mathrm{AAB}}(-2x_{\mathrm{A}}^2x_{\mathrm{B}} + 2x_{\mathrm{A}}x_{\mathrm{B}}) \\ &+ w_{\mathrm{ABB}}(-2x_{\mathrm{A}}x_{\mathrm{B}}^2 + x_{\mathrm{B}}^2) \\ &+ w_{\mathrm{BBC}}(-2x_{\mathrm{B}}^2x_{\mathrm{C}}) \\ &+ w_{\mathrm{BCC}}(-2x_{\mathrm{B}}x_{\mathrm{C}}^2) \\ &+ w_{\mathrm{CCA}}(-2x_{\mathrm{A}}x_{\mathrm{C}}^2 + x_{\mathrm{C}}^2) \\ &+ w_{\mathrm{CAA}}(-2x_{\mathrm{C}}x_{\mathrm{A}}^2 + 2x_{\mathrm{C}}x_{\mathrm{A}}) \\ &+ w_{\mathrm{ABC}}(-4x_{\mathrm{A}}x_{\mathrm{B}}x_{\mathrm{C}} + 2x_{\mathrm{B}}x_{\mathrm{C}}),\end{aligned} \tag{2.11}$$

where $\mu_{\mathrm{A}}^{\mathrm{ex}}$ is the excess chemical potential of the component A, and $x_{\mathrm{A}} = \dfrac{n_{\mathrm{A}}}{n_{\mathrm{A}} + n_{\mathrm{B}} + n_{\mathrm{C}}}$, $x_{\mathrm{B}} = \dfrac{n_{\mathrm{B}}}{n_{\mathrm{A}} + n_{\mathrm{B}} + n_{\mathrm{C}}}$, $x_{\mathrm{C}} = \dfrac{n_{\mathrm{C}}}{n_{\mathrm{A}} + n_{\mathrm{B}} + n_{\mathrm{C}}}$. The identical equations can be expanded for the components B and C as follows:

$$\begin{aligned}\mu_{\mathrm{B}}^{\mathrm{ex}} = RT\ln\gamma_{\mathrm{B}} &= \frac{\partial \Delta G_{\mathrm{ABC}}^{\mathrm{ex}}}{\partial n_{\mathrm{B}}} \\ &= w_{\mathrm{AAB}}(-2x_{\mathrm{B}}x_{\mathrm{A}}^2 + x_{\mathrm{A}}^2) \\ &+ w_{\mathrm{ABB}}(-2x_{\mathrm{A}}x_{\mathrm{B}}^2 + 2x_{\mathrm{A}}x_{\mathrm{B}}) \\ &+ w_{\mathrm{BBC}}(-2x_{\mathrm{B}}^2x_{\mathrm{C}} + 2x_{\mathrm{B}}x_{\mathrm{C}}) \\ &+ w_{\mathrm{BCC}}(-2x_{\mathrm{C}}x_{\mathrm{A}}^2 + x_{\mathrm{A}}^2) \\ &+ w_{\mathrm{CCA}}(-2x_{\mathrm{C}}^2x_{\mathrm{A}}) \\ &+ w_{\mathrm{CAA}}(-2x_{\mathrm{C}}x_{\mathrm{A}}^2) \\ &+ w_{\mathrm{ABC}}(-4x_{\mathrm{A}}x_{\mathrm{B}}x_{\mathrm{C}} + 2x_{\mathrm{C}}x_{\mathrm{A}}),\end{aligned} \tag{2.12}$$

$$\begin{aligned}\mu_{\mathrm{C}}^{\mathrm{ex}} = RT\ln\gamma_{\mathrm{C}} &= \frac{\partial \Delta G_{\mathrm{ABC}}^{\mathrm{ex}}}{\partial n_{\mathrm{C}}} \\ &= w_{\mathrm{AAB}}(-2x_{\mathrm{A}}^2x_{\mathrm{B}}) \\ &+ w_{\mathrm{ABB}}(-2x_{\mathrm{A}}x_{\mathrm{B}}^2) \\ &+ w_{\mathrm{BBC}}(-2x_{\mathrm{C}}x_{\mathrm{B}}^2 + x_{\mathrm{B}}^2) \\ &+ w_{\mathrm{BCC}}(-2x_{\mathrm{B}}x_{\mathrm{C}}^2 + 2x_{\mathrm{B}}x_{\mathrm{C}}) \\ &+ w_{\mathrm{CCA}}(-2x_{\mathrm{C}}^2x_{\mathrm{A}} + 2x_{\mathrm{C}}x_{\mathrm{A}}) \\ &+ w_{\mathrm{CAA}}(-2x_{\mathrm{A}}x_{\mathrm{B}}^2 + x_{\mathrm{B}}^2) \\ &+ w_{\mathrm{ABC}}(-4x_{\mathrm{A}}x_{\mathrm{B}}x_{\mathrm{C}} + 2x_{\mathrm{A}}x_{\mathrm{B}}).\end{aligned} \tag{2.13}$$

2.3 Calculations of interaction parameters and activity coefficients by the steepest descent method

After fixing the temperature to one of 700, 800, 900, 1000, 1100, or 1200°C, the pressure range 4999.00-5000.00 bars was divided into 100 parts. The values of x_A, x_B, and x_C at each pressure were substituted into eq. (2.11). In addition, the ratio $\gamma_{H_2O_m}(P)/\gamma_{H_2O_m}(5000)$ was also calculated for each pressure, and then the values of the seven interaction parameters of eq. (2.11) at 5000 bars were calculated by the steepest descent method based on those 100 equations (Table 2.1). The steepest descent method is an algorithm that searches for the minimum value of a function when viewed as a potential surface, based on the slope of the function (the first-order derivative) and an arbitrarily given initial value. The step size and the number of step were set to a value as large as possible that allows the calculated value to converge without divergence and 100,000 times, respectively, to confirm that the calculated value converges sufficiently. The reason why P_0 was not set at 1 bar was that the values of x_A and x_B around 1 bar were about 10^{-5}, very small compared to x_C which was about unity, and that the difference in magnitude among the coefficient terms of each w_{ijk} was by a factor of 10^{15} at most, making the calculation of the steepest descent method very unstable. For $P_0 = 5000$ bars, approximately x_A was 0.071-0.089, x_B was 0.138-0.221, and x_C was 0.708-0.772, i.e., the coefficient terms for each w_{ijk} differed only by a factor of 30 at most, allowing the steepest descent method to be computed without any problems.

Table 2.1 shows that w_{CCA} is by far the largest when compared with the absolute values of each of the seven interaction parameters. This is consistent with the prediction described in section 1.4 that the mixture of O and H_2O_m is more energetically unstable than the mixture of only O. In addition, every parameter depends on temperature, and their absolute values are larger at higher temperatures. This is consistent with the fact that the miscibility gap between silicate and water widens at higher temperatures (Mysen and Acton, 1999).

Silver and Stolper (1989) applied the data of water solubility in albite melt to two theoretical models: the ideal mixing model and the symmetric regular solution model. In the symmetric regular solution model, only three interaction parameters, $W_{H_2O_m-O}$, W_{O-OH}, and $W_{H_2O_m-OH}$, were used because energy symmetry was assumed for H_2O_m, OH, and O. They used the theoretical equation of Burnham and Davis (1971) for $\overline{V}_{H_2O_m}(T, P)$ (eq. (1.1)) to obtain those three interaction parameters to explain the results of speciation measurements by IR spectroscopy. The parameters obtained were then used to calculate, for example, the heat of dissolution for r1. However, they made two arbitrary assumptions: the three interaction parameters were constants independent on temperature and pressure; and $W_{H_2O_m-O} = 0$. The

Table 2.1: Interaction parameters at 5000 bars (J/mol) calculated by the steepest descent method

T (°C)	w_{AAB}	w_{ABB}	w_{BBC}	w_{BCC}	w_{CCA}	w_{CAA}	w_{ABC}
700	−125	−40	78	19	1233	-379	2
800	−195	−75	138	5	1704	-501	5
900	−256	−116	203	−20	2046	-576	6
1000	−315	−166	273	−53	2348	-634	4
1100	−371	−222	348	−92	2633	-684	1
1200	−427	−286	429	−137	2913	-728	-3

Value of the interaction parameter at 5000 bars. The subscript A, B and C represent H_2O_m, OH, and O, respectively. w_{iij} represents the interaction energy for a single particle of j entering an i-rich environment. When it is positive, the i-only state is more energetically stable than the state in which one particle of j enters. Conversely, when it is negative, the state in which one j particle enters is more energetically stable than the i-only state. These were obtained by the steepest descent method by combining eq. (2.11) at 5000 bars and at different pressures close to that.

results of the above calculations with the asymmetric regular solution model adopted in this study were in sharp contradiction with their assumptions, suggesting that their assumptions were not valid.

In addition, $\gamma_{\mathrm{H_2O_m}}(5000)$, i.e., γ_{A} at $P = 5000$ bars was calculated by re-substituting the seven interaction parameter values to eq. (2.11). Similarly, the steepest descent method was applied to eq. (2.12) and eq. (2.13) to obtain the values of $\gamma_{\mathrm{OH}}(5000)$ and $\gamma_{\mathrm{O}}(5000)$ (Table 2.2). The value of $\gamma_{\mathrm{OH}}(5000)$ is slightly less than unity, which corresponds to the blue curve in Fig. 1.4, indicating that the mixing of O and OH is more unstable than the mixing of O alone. This is the opposite behavior of H_2O_m, but I still have no idea why, specifically the geometric arrangement of each molecule and how the intermolecular forces (electrostatic forces) between them interact.

Furthermore, $\gamma_{\mathrm{OH}}^2/(\gamma_{\mathrm{H_2O_m}} \cdot \gamma_{\mathrm{O}})$ at 5000 bars were calculated based on the above, and they were smaller than unity (Table 2.2). As mentioned in section 0.1, the equilibrium constant K_{r2} for the second reaction of dissolution (defined as eq. (7)) has been considered equal to the "apparent" equilibrium constant Q_{r2} (defined as eq. (5)). The speciation of H_2O_m and OH in hydrous silicate melts at high temperatures and high pressures has been measured by various experimental techniques including "heat and quench" and in situ IR (Shen and Keppler, 1995; Nowak and Behrens, 1995; 2001; Ihinger et al., 1999; Sowerby and Keppler, 1999; 2000; Ohlhorst et al., 2000; Behrens and Nowak, 2003; Liu et al., 2004; Schmidt, 2004; Botcharnikov et al., 2006; Behrens and Yamashita, 2008; Bauer et al., 2015; Behrens et al., 2018; Balzer et al., 2019a; 2019b; Balzer et al., 2020; Behrens et al., 2020). By substituting a set of measured

Table 2.2: Values of $\gamma_{H_2O_m}$, γ_{OH}, γ_O and $\gamma_{OH}^2/(\gamma_{H_2O_m} \cdot \gamma_O)$ at 5000 bars

T (°C)	$\gamma_{H_2O_m}$	γ_{OH}	γ_O	$\gamma_{OH}^2/(\gamma_{H_2O_m} \cdot \gamma_O)$
700	1.070	0.9939	0.9956	0.9272
800	1.086	0.9906	0.9936	0.9093
900	1.093	0.9879	0.9920	0.9004
1000	1.096	0.9856	0.9907	0.8945
1100	1.098	0.9836	0.9897	0.8902
1200	1.100	0.9819	0.9888	0.8868

The values of the activity coefficients of each component, H_2O_m, OH, and O, obtained by substituting the values of the seven interaction parameters calculated at 5000 bars (Table 2.1) into eq. (2.11), eq. (2.12), and eq. (2.13), and the values of the coefficient described by a combination of the activity coefficients that appear in the equilibrium constant of the second reaction of water dissolution K_{r2} (see eq. (7)). Note that $\gamma_{H_2O_m} = \gamma_A$ in eq. (2.11), $\gamma_{OH} = \gamma_B$ in eq. (2.12), and $\gamma_O = \gamma_C$ in eq. (2.13).

data at a given pressure and various temperatures into eq. (2.15) (the same as eq. (5)), $\Delta\overline{H}^\circ_{r2}$ and $\Delta\overline{S}^\circ_{r2}$ have been estimated from eq. (2.14), assumed as equivalent with eq. (2.15):

$$\begin{cases} K_{r2} \equiv \dfrac{a_{OH}^2}{a_{H_2O_m} \cdot a_O} \\ \qquad = \exp\left(-\dfrac{\Delta\overline{G}^\circ_{r2}}{RT}\right) = \exp\left(-\dfrac{\Delta\overline{H}^\circ_{r2}}{RT} + \dfrac{\Delta\overline{S}^\circ_{r2}}{R}\right), \end{cases} \tag{2.14}$$

$$Q_{r2} \equiv \frac{X_{OH}^2}{X_{H_2O_m} \cdot X_O}, \tag{2.15}$$

where $\Delta\overline{A}^\circ_{r2}$ (A = Gibbs free energy G, enthalpy H, and entropy S) are the changes of the partial molar thermodynamic quantities at the standard state through the second dissolution reaction r2 (eq. (2)), defined as $\equiv \overline{A}^{melt,\circ}_{2OH-O} - \overline{A}^{melt,\circ}_{H_2O_m}$, where $\overline{A}^{melt,\circ}_{2OH-O}$ and $\overline{A}^{melt,\circ}_{H_2O_m}$ are the partial molar value of water exists as OH in melt and the molar thermodynamic quantity of H_2O_m in melt, respectively. As a result, most studies have regarded both $\Delta\overline{H}^\circ_{r2}$ and $\Delta\overline{S}^\circ_{r2}$ as constants independent of temperature and pressure. However, the calculation results of this study show that $K_{r2} = \gamma_{OH}^2/(\gamma_{H_2O_m} \cdot \gamma_O) \cdot Q_{r2} < Q_{r2}$, and $\gamma_{OH}^2/(\gamma_{H_2O_m} \cdot \gamma_O)$ was found to be temperature-dependent. Therefore, a proper evaluation of the non-ideal behavior of mixing may reveal more accurate values of $\Delta\overline{H}^\circ_{r2}$ and $\Delta\overline{S}^\circ_{r2}$ and their temperature-dependence not yet discovered.

Then, since the values of $\gamma_{H_2O_m}(P)/\gamma_{H_2O_m}(5000)$ at each temperature can be calculated over a wide pressure range of 1-5000 bars (Fig. 2.1) by the same method as discussed in section 1.4, the values of $\gamma_{H_2O_m}(P)$ were successfully calculated from them and $\gamma_{H_2O_m}(5000)$ calculated using the steepest descent method. Although it is difficult at present, if the steepest descent method can be applied stably to much lower pressures than 5000 bars (e.g., 1 bar), it will be

possible to calculate γ_{OH} and γ_{O} in all pressure ranges. Experimental measurements on water speciation in rhyolitic melt at very high pressures (Hui et al., 2008) showed that K_{r2} was almost pressure-independent below about 20 kbar. If the behavior of γ_{OH} and γ_{O} over a wide pressure range is clarified, the knowledge on the pressure dependence of K_{r2} would be updated.

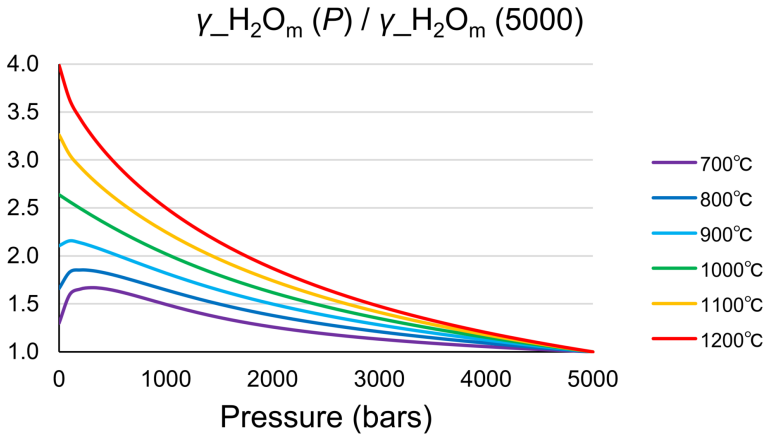

[Figure 2.1] The ratio of the activity coefficients of H_2O_m in melt, $\gamma_{H_2O_m}(P)/\gamma_{H_2O_m}(5000)$, calculated in the same way as in Fig. 1.3, when the reference pressure P_0 was set at 5000 bars.

Fig. 2.2 shows the ratio of $a_{H_2O_m}$ and $X_{H_2O_m}$ drawn based on $\gamma_{H_2O_m}$ calculated by the above method in the wide temperature and pressure range. The left end of each curve (approximately at the origin) corresponds to 1 bar and the right end to 5000 bars.

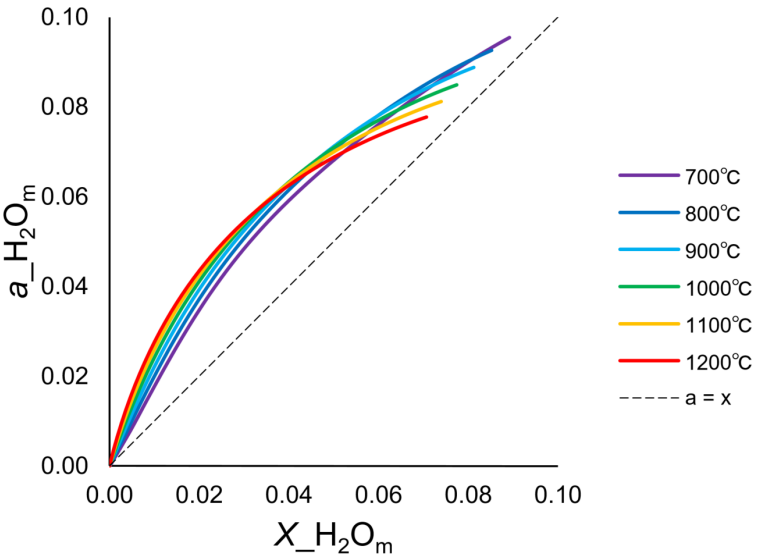

[Figure 2.2] The relation between $a_{H_2O_m}$ and $X_{H_2O_m}$. Based on the values of $\gamma_{H_2O_m}(5000)$ (Table 2.2) and $\gamma_{H_2O_m}(P)/\gamma_{H_2O_m}(5000)$ (Fig. 2.1) calculated in this study, the values of $\gamma_{H_2O_m}(P)$ for

a wide range of pressures 1-5000 bars were obtained. The left end of each curve (approximately at the origin) corresponds to 1 bar and the right end to 5000 bars.

. . . . . .

Part II

Temperature Dependence of Water Solubility in Silicate Melt

Chapter 3

Estimation of the heat of dissolution of water in rhyolitic melt

3.1 Previous studies

Sahagian and Proussevitch (1996) calculated the heat of exsolution of water from albite melt (equivalent to the opposite sign of the heat for the total dissolution reactions $\Delta\overline{H}_{\text{total}}$, later expained in eq. (3.1), in this study) based on the entropy change equation derived by Burnham and Davis (1974) over a very wide temperature and pressure range (700-1300°C and 0.1-1000 MPa, see Table 3 in their paper). The range 700-1200°C and 0.1-300 MPa of which is shown as the colored thick solid curves in Fig. 3 (a). They also estimated the temperature change of hydrous albite melt during equilibrium degassing by simple numerical calculations using the obtained values of the heat of exssolution. In this study, I significantly updated their numerical calculations and compared those in Chapter 4.

Zhang (1999b) pointed out that Sahagian and Proussevitch's (1996) method "Entropy method" had some non-negligible logical flaws. One of the critical points is that the speciation of water was not yet taken into account in Burnham and Davis's (1974) entropy change equation used, i.e., all water was assumed to dissolve as OH. Since the speciation of water in melt is sensitive to changes of temperature and pressure, the proportion of H_2O_m cannot be ignored especially at lower temperature or higher pressure. Then, Zhang (1999b) proposed a method for calculating the heat of exsolution of water from rhyolitic melt using the Gibbs-Helmholtz equation (later explained in section 3.2), which links the equilibrium constant to the enthalpy change in a chemical reaction under isobaric pressure, to calculate the heat of dissolution in the first and the second reactions of dissolution (r1 and r2, eq. (1) and eq. (2)), respectively. However, he was not able to obtain the concrete value of the heat of exsolution for r1 (equivalent to the opposite sign of the heat of dissolution for r1 $\Delta\overline{H}^{\circ}_{\text{r1}}$) because in those days the reliable experimental data of the equilibrium constant K_{r2} for r2 were not available for

Table 3.1: Compilation of water speciation data in rhyolite/haplogranite (AOQ) glasses/melts.

Source	Composition	$C_{\text{total } H_2O}$ (wt%)	T (°C)	$\Delta\overline{H}^{\circ}_{r2}$ (kJ/mol)	$\Delta\overline{S}^{\circ}_{r2}$ (J/mol)	Method
Ihi99	rhyolite	0.7 - 2.4	400 - 600	25.9 ± 0.4	15.7 ± 0.4	heat and quench
SK99	rhyolite	3.93	397 - 560	31.8 ± 2.5	24.9	in situ IR
NB01	haplogranite (AOQ)	1.3 - 5.2	500 - 800	35.0 ± 1.2	27.7 ± 1.3	in situ IR
BN03	haplogranite (AOQ)	1.0 - 7.9	332 - 634	29.9 ± 0.8	20.1	T_f by quench rate

· Source: Ihi99 - Ihinger et al. (1999). SK99 - Sowerby and Keppler (1999, 2000). NB01 - Nowak and Behrens (2001). BN03 - Behrens and Nowak (2003).
· $C_{\text{total } H_2O}$ (wt%) represents the range of total water content of the samples.
· T (°C) represents the temperature range of experimental determinations of $\Delta\overline{H}^{\circ}_{r2}$ and $\Delta\overline{S}^{\circ}_{r2}$ values.
· $\Delta\overline{H}^{\circ}_{r2}$ (kJ/mol) and $\Delta\overline{S}^{\circ}_{r2}$ (J/mol) represent the changes of the partial molar enthalpy and the partial molar entropy through the second reaction of water dissolution in melt r2 (eq. (2)), respectively.
· Method: heat and quench - After sufficient time for water species (H_2O_m and OH) to reach the equilibrium distribution, the glass/melt was quenched and IR spectroscopy was performed at room temperature. in situ IR - Water speciation was measured at high temperature and high pressure by in situ IR spectroscopy. T_f by quench rate - Hydrous melt was cooled from high temperature at a controlled rate and infrared spectroscopy was performed at room temperature. T_f is the fictive temperature at which water speciation is frozen.

higher total water content than 2.4 wt% and for higher temperature than 600°C (Zhang et al., 1991, 1995, 1997; Ihinger et al., 1999). Thus, he regarded $\Delta\overline{H}^{\circ}_{r1}$ as constant and only modeled the trend of how the heat of the total dissolution reactions $\Delta\overline{H}_{\text{total}}$ depends on pressure at very low pressure ($\leq$ 10 MPa). Note that he assumed ideal mixing for the mixture of silicate and water species.

Liu et al. (2005) performed experiments to determine water solubility in rhyolitic melt at very low pressures, including atmospheric pressure. Using the experimental data at 0.1, 6, and 11 MPa and the same theoretical method presented by Zhang (1999b), they obtained the heat of exsolution of water at (850°C, 0.1-12 MPa), shown as the black thick solid curve in Fig. 3 (a), which confirmed Zhang's (1999b) prediction.

As shown in Table 3.1, after Zhang's study, IR spectroscopic data on H_2O_m and OH species at higher water content or higher temperature have already been obtained (Sowerby and Keppler, 1999, 2000; Nowak and Behrens, 2001; Behrensand Nowak, 2003), which should make it possible to extend the application of the calculation method of Zhang (1999b) to a wider range of temperatures and pressures. Moreover, since I showed in Part I of this study that the ideal mixing model breaks down for the mixing of silicate and water, and calculated the

activity coefficient of H_2O_m when the regular solution model is applied, which is an indicator of non-ideality, these information can be used to update the value of the heat of dissolution of water calculated compared with Zhang (1999) and Liu et al. (2005) where ideal mixing was assumed.

In this chapter, those possibilities are explored in the case of rhyolitic melt. The reason why focusing on rhyolite-water (including haplogranite-water) system, not on albite-water system, is because its application to natural systems is relatively straightforward.

3.2 Calculation methods

While Part I focused on the pressure dependence of water solubility in melt with fixed temperature, by contrast, this chapter focuses on the temperature dependence of the equilibrium constants of the dissolution reactions, especially the first reaction r1 (eq. (1)) with fixed pressure. Therefore, in the following, pressure is assumed to be equal to the reference pressure ($P = P_1$), and pressure terms in equations are hereafter omitted. Note that the reference pressure P_1 is different from P_0 used in Part I. The goal of this Chapter is to obtain the partial molar dissolution heat of total water into rhyolitic melt $\Delta\overline{H}_{\mathrm{total}}(T)$, which is described as below:

$$\Delta\overline{H}_{\mathrm{total}}(T) = \Delta\overline{H}^{\circ}_{\mathrm{r1}}(T) + \left(1 - \frac{X_{\mathrm{H_2O_m}}(T)}{X_{\mathrm{total\ H_2O}}(T)}\right)\Delta\overline{H}^{\circ}_{\mathrm{r2}}, \tag{3.1}$$

where $\Delta\overline{H}^{\circ}_{\mathrm{r1}}(T)$ is the partial molar enthalpy change through r1, defined as $\equiv \overline{H}^{\mathrm{melt},\circ}_{\mathrm{H_2O_m}} - \overline{H}^{\mathrm{vapor},\circ}_{\mathrm{H_2O_m}}$, where $\overline{H}^{\mathrm{melt},\circ}_{\mathrm{H_2O_m}}$ and $\overline{H}^{\mathrm{vapor},\circ}_{\mathrm{H_2O_m}}$ are the partial molar enthalpy of $\mathrm{H_2O_m}$ in melt and the molar enthalpy of water vapor, respectively. The superscript $\circ$ means the standard state. The parentheses multiplied in the second term of the RHS means the proportion of $\mathrm{H_2O_m}$ dissolved in r1 of which proceeds to r2.

$\Delta\overline{H}^{\circ}_{\mathrm{r1}}(T)$ is acquired from the equilibrium constant of first reaction $K_{\mathrm{r1}}(T)$ by using the relation called the Gibbs-Helmholtz equation:

$$\frac{\partial \ln K(T)}{\partial(1/T)} = -\frac{\Delta\overline{H}^{\circ}(T)}{R}, \tag{3.2}$$

linking an equilibrium constant and a partial molar enthalpy change, which generally holds through an isobaric chemical reaction. Since $K_{\mathrm{r1}}(T)$ can be expressed as

$$K_{\mathrm{r1}}(T) = \frac{a_{\mathrm{H_2O_m}}(T)}{f_{\mathrm{H_2O}}(T)} = \frac{\gamma_{\mathrm{H_2O_m}}(T)\cdot X_{\mathrm{H_2O_m}}(T)}{f_{\mathrm{H_2O}}(T)}, \tag{3.3}$$

substituting eq. (3.3) into eq. (3.2), the following relation is obtained:

$$\Delta\overline{H}^{\circ}_{\mathrm{r1}}(T) = -R\frac{\partial \ln K_{\mathrm{r1}}(T)}{\partial(1/T)} = -R\frac{\partial \ln\left(\dfrac{\gamma_{\mathrm{H_2O_m}}(T)\cdot X_{\mathrm{H_2O_m}}(T)}{f_{\mathrm{H_2O}}(T)}\right)}{\partial(1/T)}. \tag{3.4}$$

For $\gamma_{\mathrm{H_2O_m}}(T)$, the values calculated by the assymetric regular solution model in section 2.3 are used. $X_{\mathrm{H_2O_m}}(T)$ and $f_{\mathrm{H_2O}}(T)$ can be calculated by the methods described in section 1.4.

$\Delta\overline{H}^{\circ}_{\mathrm{r2}}$ (and $\Delta\overline{S}^{\circ}_{\mathrm{r2}}$) in rhyolitic melt or haplogranite (AOQ) melt have been measured by mainly heat and quench and in situ IR spectroscopy over a wide range of temperatures and pressures (Ihinger et al., 1999; Sowerby and Keppler, 1999, 2000; Nowak and Behrens, 2001; Behrens and Nowak, 2003, see also Table 2 in Behrens, 2020). Reported data by them are recapitulated in Table 3.1. The positive value of $\Delta\overline{H}^{\circ}_{\mathrm{r2}}$ means that the forward reaction of r2 is

endothermic. These four speciation data were all investigated including the temperature region around the glass-melt transition point, and each suite of the values of $\Delta\overline{H}^{\circ}_{r2}$ and $\Delta\overline{S}^{\circ}_{r2}$ were reported as constant independent of temperature or pressure. Although the possibility that $\Delta\overline{H}^{\circ}_{r2}$ is not constant but depends on temperature, if taking the non-ideality of silicate-water mixing into account, was pointed out in section 2.3, for now it is treated as constant in Part II.

3.3 Calculation results

Fig. 3 (b)-(f) show the newly obtained calculation results in this study: $\Delta\overline{H}^{\circ}_{\mathrm{r1}}$ (the thin solid lines), $(1-X_{\mathrm{H_2O_m}}/X_{\mathrm{total\ H_2O}})\Delta\overline{H}^{\circ}_{\mathrm{r2}}$ (the thin dashed curves), and the sum of them (see eq. (3.1)), i.e., $\Delta\overline{H}_{\mathrm{total}}$ (the thick solid curves), plotted for the range of 700-1200°C in increments of 100°C at fixed pressures in the range of 0.1-300 MPa in increments of 0.1 MPa. $\Delta\overline{H}^{\circ}_{\mathrm{r1}}$ was calculated in two cases whether taking the non-ideality of silicate-water mixing into account or not. Fig. 3 (b)-(e) are "Regular solution model" in which the non-ideality was appropriately taken into account: for $\gamma_{\mathrm{H_2O_m}}(T)$ in eq. (3.4), the values calculated by the assymetric regular solution model in section 2.3 was used. In "Regular solution model," the values of $\Delta\overline{H}^{\circ}_{\mathrm{r2}}$ for four different speciation data: Ihinger et al. (1999), Behrens and Nowak (2003), Sowerby and Keppler (1999, 2000), and Nowak and Behrens (2001) were used, respectively (see Table 3.1). In contrast, for a comparison, Fig. 3 (f) is "Ideal solution model" in which the non-ideality was not taken into account: assuming $\gamma_{\mathrm{H_2O_m}}(T) = 1$ in eq. (3.4). In "Ideal solution model," Nowak and Behrens's (2001) $\Delta\overline{H}^{\circ}_{\mathrm{r2}}$ was also used for the comparison with Fig. 3 (e). I tried other speciation data than that of Nowak and Behrens (2001) and found that $\Delta\overline{H}^{\circ}_{\mathrm{r1}}$ depends on the choice of speciation data, while $\Delta\overline{H}_{\mathrm{total}}$ is almost independent of speciation data, as the same as reported in Liu et al. (2005).

In "Regular solution model," $\Delta\overline{H}^{\circ}_{\mathrm{r1}}$ behaved almost the same for all speciation data and was approximately -20 kJ/mol independent of temperature and pressure. The negative value means that the forward reaction of r1 is exothermic. Its absolute value $|\Delta\overline{H}^{\circ}_{\mathrm{r1}}|$ was slightly smaller at higher temperatures and decreased linearly with increasing pressure at the same rate independent of temperature. $(1 - X_{\mathrm{H_2O_m}}/X_{\mathrm{total\ H_2O}})\Delta\overline{H}^{\circ}_{\mathrm{r2}}$ decreased monotonically with pressure in all temperature ranges due to the temperature dependence of water speciation: the lower the temperature, the larger the fraction of $\mathrm{H_2O_m}$. As a result of the sum of these quantities, $\Delta\overline{H}_{\mathrm{total}}$ generally behaved taking over the characteristics of $(1 - X_{\mathrm{H_2O_m}}/X_{\mathrm{total\ H_2O}})\Delta\overline{H}^{\circ}_{\mathrm{r2}}$. The range of its possible values varied widely from negative to positive depending on the speciation data. For example, in Fig. 3 (b) the total dissolution reaction is exothermic over most of the temperature and pressure range, while in Fig. 3 (e) it is endothermic.

In "Ideal solution model," $\Delta\overline{H}^{\circ}_{\mathrm{r1}}$ showed a complicated behavior: at 700°C, it increased, decreased, and then increased again in response to increasing pressure, whereas it increased monotonically with pressure at 800°C and above. As a result of the sum of these quantities, $\Delta\overline{H}_{\mathrm{total}}$ showed a complex bending at low temperatures at 800°C and below, where r1 predominates, taking over the characteristics of $\Delta\overline{H}^{\circ}_{\mathrm{r1}}$, but increased monotonically at high temperatures at 900°C and above, where r2 predominates. Ryan et al. (2015) conducted ex-

periments to investigate the temperature dependence of water solubility in rhyolitic melt at (900-1100°C, 0.1 MPa) and obtained a value of $|\Delta\overline{H}_{\text{total}}| = 17.8$ kJ/mol assuming ideal mixing of silicate and water, which is almost the same as the theoretically estimated value at 0.1 MPa of 18.8-19.1 kJ/mol at 900°C and 22.5-22.6 kJ/mol at 1100°C in Fig. 3 (f). However, in any case, even though started from the ideal mixing assumption, the obtained values of $\Delta\overline{H}_{\text{total}}$ greatly deviate from 0, and it is clearly self-contradictory.

Both the values of $\Delta\overline{H}_{\text{total}}$ in "Regular solution model" and "Ideal solution model" showed completely different behaviors than that of Sahagian and Proussevitch (1996) in Fig. 3 (a). The low pressure part of $\Delta\overline{H}_{\text{total}}$ in "Regular solution model" and that of Liu et al. (2005) in Fig. 3 (a) appear to similarly behaves as its absolute value $|\Delta\overline{H}_{\text{total}}|$ increases with increasing pressure, which is later discussed in section 3.5.

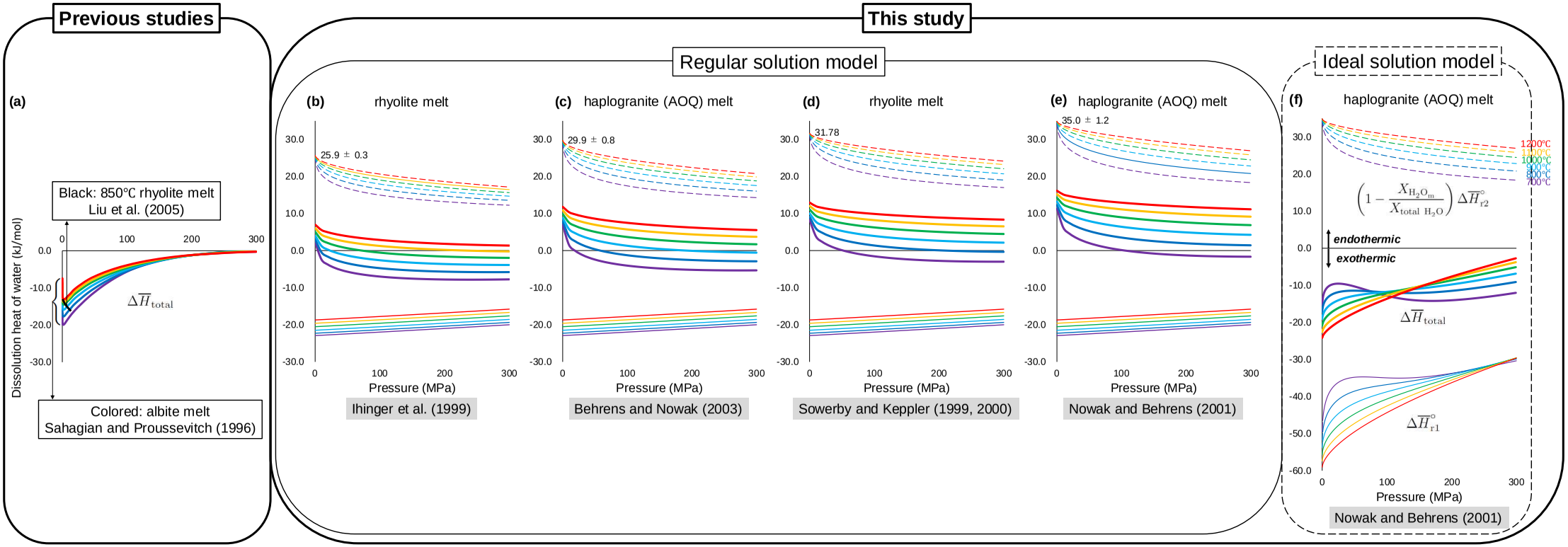
Previous studies
(a)
Black: 850°C rhyolite melt
Liu et al. (2005)
Dissolution heat of water (kJ/mol)
$\Delta\overline{H}_{\mathrm{total}}$
Colored: albite melt
Sahagian and Proussevitch (1996)
This study
Regular solution model
(b) rhyolite melt
25.9 ± 0.3
Ihinger et al. (1999)
(c) haplogranite (AOQ) melt
29.9 ± 0.8
Behrens and Nowak (2003)
(d) rhyolite melt
31.78
Sowerby and Keppler (1999, 2000)
(e) haplogranite (AOQ) melt
35.0 ± 1.2
Nowak and Behrens (2001)
Pressure (MPa)
Ideal solution model
(f) haplogranite (AOQ) melt
1200°C
1100°C
1000°C
900°C
800°C
700°C
$\left(1-\frac{X_{\mathrm{H_2O_m}}}{X_{\mathrm{total\ H_2O}}}\right)\Delta\overline{H}^{\circ}_{\mathrm{r2}}$
endothermic
exothermic
$\Delta\overline{H}_{\mathrm{total}}$
$\Delta\overline{H}^{\circ}_{\mathrm{r1}}$
Pressure (MPa)
Nowak and Behrens (2001)

[Figure 3] The enthalpy change, i.e., the heat of dissolution of water in silicate melts calculated by chemical-thermodynamic methods in the temperature and pressure range of 700-1200°C and 0.1-300 MPa.

(a) The calculation results from previous studies. The colored thick solid curves: $\Delta\overline{H}_{\rm total}$ for the total dissolution reaction in albite melt, calculated by "Entropy method" in Sahagian and Proussevitch (1996). The black thick solid curve: $\Delta\overline{H}_{\rm total}$ for rhyolitic melt at 850°C and 0.1-12 MPa in Liu et al. (2005), calculated through the Gibbs-Helmholtz equation, proposed in Zhang (1999b).

(b)-(f) The calculation results using the Gibbs-Helmholtz equation (see section 3.2) in this study in the cases of rhyolitic or haplogranite (AOQ) melt. (b)-(e) "Regular solution model" in which the non-ideality was appropriately taken into account. (f) "Ideal solution model" in which the non-ideality was not taken into account. The thin solid lines: $\Delta\overline{H}^{\circ}_{\rm r1}$ (<0, exothermic) for r1 (eq. (1)). The thin dashed curves: $(1-X_{\rm H_2O_m}/X_{\rm total\ H_2O})\Delta\overline{H}^{\circ}_{\rm r2}$ (>0, endothermic) for r2 (eq. (2)). The multiplied parentheses means the proportion of $\rm H_2O_m$ dissolved in r1 of which proceeds to r2. The thick solid curves: $\Delta\overline{H}_{\rm total} = \Delta\overline{H}^{\circ}_{\rm r1} + (1 - X_{\rm H_2O_m}/X_{\rm total\ H_2O})\Delta\overline{H}^{\circ}_{\rm r2}$ for the total dissolution reaction. Here four different speciation data were used: (b) Ihinger et al. (1999), (c) Behrens and Nowak (2003), (d) Sowerby and Keppler (1999, 2000) and (e) and (f) Nowak and Behrens (2001).

3.4 Comparison of "Regular solution model" with "Ideal solution model"

The values of $|\Delta\overline{H}^{\circ}_{\mathrm{r1}}|$ of Fig. 3 (b)-(e) "Regular solution model" are much smaller than that of (f) "Ideal solution model." In addition, the curves of $\Delta\overline{H}^{\circ}_{\mathrm{r1}}$ in (f) have a complex shape, whereas those in (b)-(e) are linearly aligned. This sharp contrast is due to the incorporation of the integrated partial molar volume by pressure in the process of determining the activity of H_2O_m in section 1.4.

Eq. (18) can be transformed as below:

$$\frac{a_{\mathrm{H_2O_m}}(T,P)}{f_{\mathrm{H_2O}}(T,P)} = \frac{a_{\mathrm{H_2O_m}}(T_0,P_0)}{f_{\mathrm{H_2O}}(T,P_0)} \exp\left(\frac{\displaystyle\int_{T_0}^{T} \Delta\overline{S}^{\circ}_{\mathrm{r1}}(T',P_0)dT'}{RT} - \frac{\displaystyle\int_{P_0}^{P} \overline{V}^{\mathrm{melt}}_{\mathrm{H_2O_m}}(T,P')dP'}{RT} \right). \tag{3.5}$$

Substituting this into eq. (3.4), expanded as follows:

$$\Delta\overline{H}^{\circ}_{\mathrm{r1}}|_{P=P_1} = -R \left.\frac{\partial \ln K_{\mathrm{r1}}(T)}{\partial(1/T)}\right|_{P=P_1} \tag{3.6}$$

$$= -R \left.\frac{\partial \ln\left(\dfrac{a_{\mathrm{H_2O_m}}(T,P)}{f_{\mathrm{H_2O}}(T,P)}\right)}{\partial(1/T)}\right|_{P=P_1} \tag{3.7}$$

$$= -R \left.\frac{\partial}{\partial(1/T)}\right|_{P=P_1} \left\{ \ln \frac{a_{\mathrm{H_2O_m}}(T_0,P_0)}{f_{\mathrm{H_2O}}(T,P_0)} + \left(\frac{\displaystyle\int_{T_0}^{T} \Delta\overline{S}^{\circ}_{\mathrm{r1}}(T',P_0)dT'}{RT} - \frac{\displaystyle\int_{P_0}^{P} \overline{V}^{\mathrm{melt}}_{\mathrm{H_2O_m}}(T,P')dP'}{RT} \right) \right\}. \tag{3.8}$$

As shown in eq. (1.10), since the pressure derivative of $\overline{V}^{\mathrm{melt}}_{\mathrm{total\ H_2O}}$ or even $\overline{V}^{\mathrm{melt}}_{\mathrm{H_2O_m}}$ is constant, the third term in the parentheses of eq. (3.8) is a linear function of pressuer P. This is the reason why $\Delta\overline{H}^{\circ}_{\mathrm{r1}}$ in Fig. 3 (b)-(e) is linearly aligned.

3.5 Comparison with Liu et al. (2005)

The behavior of $\Delta\overline{H}_{\rm total}$ (shown as the black thick solid curve in Fig. 3 (a)) reported by Liu et al. (2005) appears to be similar to that of $\Delta\overline{H}_{\rm total}$ of Fig. 3 (b)-(e) "Regular solution model" obtained in this study at low pressure. However, since ideal mixing was assumed in Liu et al. (2005), their results should be different from "Regular solution model" and should be the same as Fig. 3 (f) "Ideal solution model." It would make sense if Liu et al. (2005) had used $\Delta\overline{H}^{\circ}_{\rm r1}$ as constant in the same way as Zhang (1999b), but they did not clarify the specific value of $\Delta\overline{H}^{\circ}_{\rm r1}$ that they calculated. Therefore, it is difficult to pursue this discrepancy further here.

Supplement information on the definition of $\Delta\overline{H}^{\circ}_{\rm r1}$

The form of eq. (3.1) and the procedure of determining values of each term in this equation ($\Delta\overline{H}^{\circ}_{\rm r1}$, $X_{\rm H_2O_m}$, $X_{\rm total\ H_2O}$, and $\Delta\overline{H}^{\circ}_{\rm total}$) are similar to those considered in section 2.4 in Zhang (1999b), although there is an only one difference between Zhang's method and ours: the definition of $\Delta\overline{H}^{\circ}_{\rm r1}$. He defined "$\Delta H^{0}_{\rm r1} = \overline{H}^{\rm melt,0}_{\rm H_2O_m} - \overline{H}^{\rm vapor,0}_{\rm H_2O}(T, 1{\rm bar})$," where the reference pressures of vapor and $\rm H_2O_m$ in melt were taken at different pressures. In contrast, in this study both are assigned to an arbitrary pressure. Thus, the term in eq. (16) in his paper "$[\overline{H}^{\rm vapor}_{\rm H_2O} - \overline{H}^{\rm vapor,0}_{\rm H_2O}(T, 1\ {\rm bar})] - \Delta H^{0}_{\rm r1}$" (where [ ] is the correction term of the difference of enthalpies of water vapor between at 1 bar and an arbitrary pressure P) is equivalent to $-\Delta\overline{H}^{\circ}_{\rm r1}$ in this study. Since the Gibbs-Helmholtz equation used in the procedure for obtaining $\Delta\overline{H}^{\circ}_{\rm r1}$ is valid under constant pressure, that condition is incompatible with his definition of $\Delta\overline{H}^{\circ}_{\rm r1}$ and compatible with our definition of $\Delta\overline{H}^{\circ}_{\rm r1}$. Namely, the correction term [ ] added in his paper was extra and unnecessary. Note that the values of [ ] between 0.1-12 MPa discussed in Zhang (1999b) and Liu et al. (2005) are sufficiently small (0 kJ/mol at 0.1 MPa and about -0.9 kJ/mol at 12 MPa, by $\partial\overline{H}^{\rm vapor}_{\rm H_2O}/\partial P = -7.6$ J/(mol $\cdot$ bar) according to the steam table in Haar et al., 1984) to neglect compared to $\Delta H_{\rm ex,H_2O_t}$. Note that this does not help explain the difference of $\Delta\overline{H}_{\rm total}$ between Liu et al. (2005) and this study discussed above.

Chapter 4

Numerical calculations of temperature change of magma with decompression-induced vesiculation

4.1 Assumptions and formulation

When hydrous magmas ascend the volcanic conduit and decompress, water exsolution, i.e., vesiculation occurs. Using the newly obtained values of the heat of exsolution (the opposite sign of the heat of dissolution) of water in rhyolitic melt, here I estimate the temperature change of rhyolitic magma with decompression-induced vesiculation. The differential equations describing the temperature change due to the heat of exsolution and the mechanical work of vapor bubble expansion were numerically solved under the following physical conditions and assumptions. Out of applied conditions, those different from in Sahagian and Proussevitch's (1996) numerical calculations (including updates of referenced physical property data) are numbered as [**1**]-[**8**].

The system of interest is assumed as a closed system consisting of water-saturated rhyolitic melt and vapor exsolved from melt, and water dissolved in melt and vapor are in chemical equilibrium. Water exsolution is assumed as an adiabatic reversible process, i.e., decompression-induced vesiculation proceeds slowly along the water solubility curve. For the equation of water solubility in melts, Sahagian and Proussevitch (1996) used c (wt%) $= 0.424P'^{0.5}$ for albite melt (P' in MPa, eq. (34) in their paper), in which the temperature dependence is not taken into account, while this study uses $Liu(T, P')$ (eq. (1.12)) for rhyolitic melt [**1**]. Because of the very slow decompression and ascent of magma, the relative motion of vapor and melt does not need to be considered. The initial temperature and pressure ranges are 700°C $\leq T_{\rm i} \leq$ 1200°C and 1 MPa $\leq P_{\rm i} \leq$ 300 MPa, respectively.

In Sahagian and Proussevitch (1996), it was assumed that $\Delta\overline{H}_{\rm total}(T, P)$ retains its value at the initial temperature during decompression due to the small temperature dependence of $\Delta\overline{H}_{\rm total}(T, P)$ (see Fig. 3 (a)), so they simply integrated it by pressure to determine the effect

of the exsolution heat on the temperature change of magma. In contrast, in this study, I sequentially tracked the change of $\Delta\overline{H}_{\text{total}}(T,P)$ with the change of temperature and pressure [2]. When $x(T,P)$ represents the weight fraction of vapor in the system, the following differential equations can be formulated:

$$\begin{cases} dT = \dfrac{\partial T}{\partial x}dx + \dfrac{\partial T}{\partial P}dP = \dfrac{\Delta\overline{H}_{\text{total}}(T,P)dx + x(T,P)RT\dfrac{dP}{P}}{M_{\text{H}_2\text{O}}C'^{\text{magma}}_P(T,P)}, & (4.1) \\ dx = \dfrac{\partial x(T,P)}{\partial T}dT + \dfrac{\partial x(T,P)}{\partial P}dP = -\dfrac{1}{100}\left(\dfrac{\partial Liu(T,P)}{\partial T}dT + \dfrac{\partial Liu(T,P)}{\partial P}dP\right), & (4.2) \end{cases}$$

where $M_{\text{H}_2\text{O}}$ is the molar weight of water, $= 18.02 \times 10^{-3}$ (kg/mol). Eq. (4.1) expresses the temperature change of magma, modified from eq. (13) in Sahagian and Proussevitch (1996), where $\Delta\overline{H}_{\text{total}}(T,P)dx$ is the effect of the heat of exsolution of water, and $x(T,P)RTdP/P$ is the effect of mechanical work of vapor bubble expansion. C'_P (J/(kg · K)) is the specific heat capacity. In this study, I define the relation among the specific heat capacity C'_P, the molar heat capacity C_P (J/(mol · K)) and the molar weight M (kg/mol) as $C'_P \equiv C_P/M$. $C'^{\text{magma}}_P(T,P)$ in eq. (4.1) is written down as

$$C'^{\text{magma}}_P(T,P) = x(T,P)C'^{\text{vapor}}_P(T,P) + (1-x(T,P))C'^{\text{hydrous melt}}_P(T,P). \quad (4.3)$$

The term $x(T,P)C'^{\text{vapor}}_P(T,P)$, regarded as negligible in Sahagian and Proussevitch (1996), was taken into account in this study [3].

$C'^{\text{vapor}}_P(T,P)$ was obtained by interpolating the discrete values of the steam table, calculated by the equation of state of water as a real gas in Wagner and Pruß (2002). $C'^{\text{hydrous melt}}_P(T,P)$ is written as the sum of proportional distribution of those of total water in melt $C'^{\text{melt}}_{P,\text{total H}_2\text{O}}$ and of dry melt $C'^{\text{dry melt}}_P(T)$:

$$C'^{\text{hydrous melt}}_P(T,P) = \frac{\dfrac{Liu(T_\text{i},P_\text{i})}{100} - x(T,P)}{1-x(T,P)}C'^{\text{melt}}_{P,\text{total H}_2\text{O}} + \frac{1-\dfrac{Liu(T_\text{i},P_\text{i})}{100}}{1-x(T,P)}C'^{\text{dry melt}}_P(T), \quad (4.4)$$

where $C'^{\text{melt}}_{P,\text{total H}_2\text{O}} = 3144.0$ J/(kg · K) $(= C^{\text{melt}}_{P,\text{total H}_2\text{O}}/M_{\text{H}_2\text{O}} = 56.64$ J/(mol · K) / (18.02×10^{-3}) kg/mol) for pantellerite melt, closest to the rhyolitic composition, by Di Genova et al. (2014), which was not considered in Sahagian and Proussevitch (1996) [4]. $C'^{\text{dry melt}}_P(T)$ is expressed as $= C^{\text{dry melt}}_P(T)/M_{\text{dry melt}} = (80.69 + 7.615 \times 10^{-3}\ T + 9.990 \times 10^4\ T^{-2})$ J/(mol · K) / (64.67×10^{-3}) kg/mol, where $M_{\text{dry melt}}$ is the molar weight of dry rhyolitic melt. $C^{\text{dry melt}}_P(T)$ is calculated for the composition of dry rhyolitic melt from the C_P values of various oxides reported in Richet and Bottinga (1985).

Eq. (4.2) is based on the assumption that decompression proceeds along the solubility curve and no vapor exists at the start of decompression: $x(T_\mathrm{i}, P_\mathrm{i}) = 0$.

4.2 Calculation methods

The above two differential equations (4.1) and (4.2) were coupled and solved numerically using the Radau IIA family of order 5 (Wanner and Hairer, 1996), one of the implicit Runge-Kutta methods. The width of decompression step in the numerical calculation was set to 0.0001 MPa.

Calculation runs were performed substituting five different values of $\Delta\overline{H}_{\rm total}(T,P)$, newly obtained in this study, into (4.1) [5]. They are shown in Fig. 3 as (b)-(e) "Regular solution model" based on the four speciation data (Ihinger et al., 1999; Sowerby and Keppler, 1999, 2000; Nowak and Behrens, 2001; Behrens and Nowak, 2003) and (f) "Ideal solution model" based on Nowak and Behrens's (2001) speciation data. Here, newly introduced conditions in this study [1]-[8] were all applied. [6]-[8] related to the calculation-end conditions are explained later.

In addition, to evaluate the effect of the difference of numerical program on the calculation results with Sahagian and Proussevitch (1996), I calculated the temperature drop of albite melt using the water solubility equation for albite melt c (wt%) $= 0.424P'^{0.5}$ (eq. (34) in their paper) and $\Delta H_{\rm ev}$ (Table 3 in their paper, equivalent to the opposite sign of $\Delta\overline{H}_{\rm total}(T,P)$ in this study). For this run, to match their calculation conditions, $C'^{\rm vapor}_{P}(T,P)$ and $C'^{\rm melt}_{P,{\rm total}\ {\rm H_2O}}$ were not incorporated into the differential equations. Thus, in this case, exceptionally only [2], [6], and [8] were applied, but [1], [3], [4], ([5]), and [7] were not applied.

For the end of the calculation, following three conditions were applied.

[I] First, always applied, is that the calculation must end at atomospheric pressure 0.1 MPa.

[II] Second, the calculation is terminated when the magma temperature T falls below the glass transition point $T_{\rm g}$ (Dingwell, 1998) because the magma loses its viscous fluid properties:

$$T \le T_{\rm g} = 785.15 - 83.47 \ln c, \tag{4.5}$$

where c (wt%) is the water content in melt [6]. When the equilibrium degassing is assumed, melt is always water-saturated: $c = Liu(T,P)$.

[III] Third, the same as employed in Sahagian and Proussevitch (1996), the calculation is terminated when the volume fraction of vapor exceeds 80%, which is the limit of vesicularity in common scoria and pumice where bubbles are connected to each other and the melt films between them are fractured and isolated (Mangan et al., 1993):

$$x(T,P) \ge \frac{4\rho^{\rm vapor}(T,P)}{4\rho^{\rm vapor}(T,P) + \rho^{\rm melt}(T,P,c)}, \tag{4.6}$$

where $\rho^{\rm vapor}(T,P)$ and $\rho^{\rm melt}(T,P,c)$ (kg/m^3) are the densities of vapor and melt, respectively:

$$\rho^{\text{vapor}}(T,P) = \frac{M_{\text{H}_2\text{O}}}{\overline{V}^{\text{vapor}}(T,P)}, \tag{4.7}$$

$$\begin{aligned}
\rho^{\text{melt}}(T,P,c) = {} & 2341.211 \\
& - 0.25232(T - 973.15) \\
& + \Big[0.17985 - 1.1478 \times 10^{-5}(T - 973.15) + 1.5403 \times 10^{-3}\ c \\
& + \frac{c}{10}\left\{-1.9925 \times 10^{-6} + 1.7918 \times 10^{-3}\frac{(T - 973.15)}{50}\right\}\Big](P - 0.1) \\
& + \left\{-32.429 - 1.7441 \times 10^{-2}(T - 973.15) + 1.5403 \times 10^{-3}(P - 0.1)\right\} c,
\end{aligned} \tag{4.8}$$

where $\overline{V}^{\text{vapor}}(T,P)$ is the molar volume of vapor, obtained by interpolating the discrete values of the steam table, calculated by the equation of state of water as a real gas in Wagner and Pruß (2002), while calculated by the ideal gas law in Sahagian and Proussevitch (1996) [7]. Using the open source program DensityX (calculated in the Excel macro) provided by Iacovino and Till (2019), the density of hydrous rhyolitic melt was calculated for eight suites of different temperatures, pressures, and water contents: (700°C or 1200°C) × (0.1 MPa or 300 MPa) × (0 wt% or 10 wt%). Based on the obtained values, eq. (4.8) was derived by linear approximation, taking the reference point at (700°C, 0.1 MPa, 0 wt%). In Sahagian and Proussevitch (1996), the reference data used for ρ^{melt} was not clearly stated [8].

4.3 Calculation results

The calculation-end condition [II] ([6]) was satisfied at the initial temperature and pressure only in a very narrow region around 700°C and below 0.1 MPa. When decompression was started from higher pressure, i.e., higher water content, the calculation always ended by the calculation-end condition [III] ([7] and [8]) before entering that very narrow region.

Fig. 4.1 shows the calculation results of the temperature change of (a') albite melt and (b)-(f) rhyolitic or haplogranite (AOQ) melt on the $(T_\mathrm{i}, P_\mathrm{i})$ plane. The middle and the lower panels show the effects of exsolution ($\Delta T_\mathrm{exsolution}$) and expansion ($\Delta T_\mathrm{expansion}$), respectively, and the upper panels are the sum of them, i.e., the total temperature change (ΔT_total). (b)-(f) are the results when using the speciation-dependent values of $\Delta\overline{H}_\mathrm{total}$ corresponding to Fig. 3 (b)-(f), respectively. (a) is the original calculation result for albite melt (redrawn based on Fig. 9 in Sahagian and Proussevitch, 1996). Since the temperature dependence of $\Delta\overline{H}_\mathrm{total}(T, P)$ was not taken into account in Sahagian and Proussevitch (1996), the contour in (a) is parallel to the T_i axis.

Comparing (a) with (a'), calculated by the newly constructed numerical program in this study, $|\Delta T_\mathrm{expansion}|$ is almost the same, but $|\Delta T_\mathrm{exsolution}|$ is always smaller at any $(T_\mathrm{i}, P_\mathrm{i})$ in (a'), resulting about 10 K smaller $|\Delta T_\mathrm{total}|$ in (a').

In common with the newly calculated results in this study (a') and (b)-(f), $|\Delta T_\mathrm{expansion}|$ is almost the same and its T_i dependence is almost negligible at lower P_i, but it increases for higher T_i at higher P_i. In contrast, $\Delta T_\mathrm{exsolution}$ significantly varies depending on the speciation data and solution models. In comparison within "Regular solution model" (b)-(e), the negative region is dominant in (b), while the positive region is dominant in (e), and there is a difference of about 20 K between them at any $(T_\mathrm{i}, P_\mathrm{i})$. Comparing the results for different solution models using the same speciation data (Nowak and Behrens, 2001), "Regular solution model" (e) shows that the whole region is positive, whereas "Ideal solution model" (f) shows that the whole region is negative, which is extremely contrasting. Comparing ΔT_total, in (e) there is a small positive region at lower P_i, but in (f) the whole region is negative, and the difference between them reaches 50 K at $(T_\mathrm{i}, P_\mathrm{i}) = (1200°\mathrm{C}, 300\ \mathrm{MPa})$.

From the above, the choice of speciation data and solution models is very important because it greatly influences the calculation results in estimating temperature changes of magma during decompression-induced vesiculation.

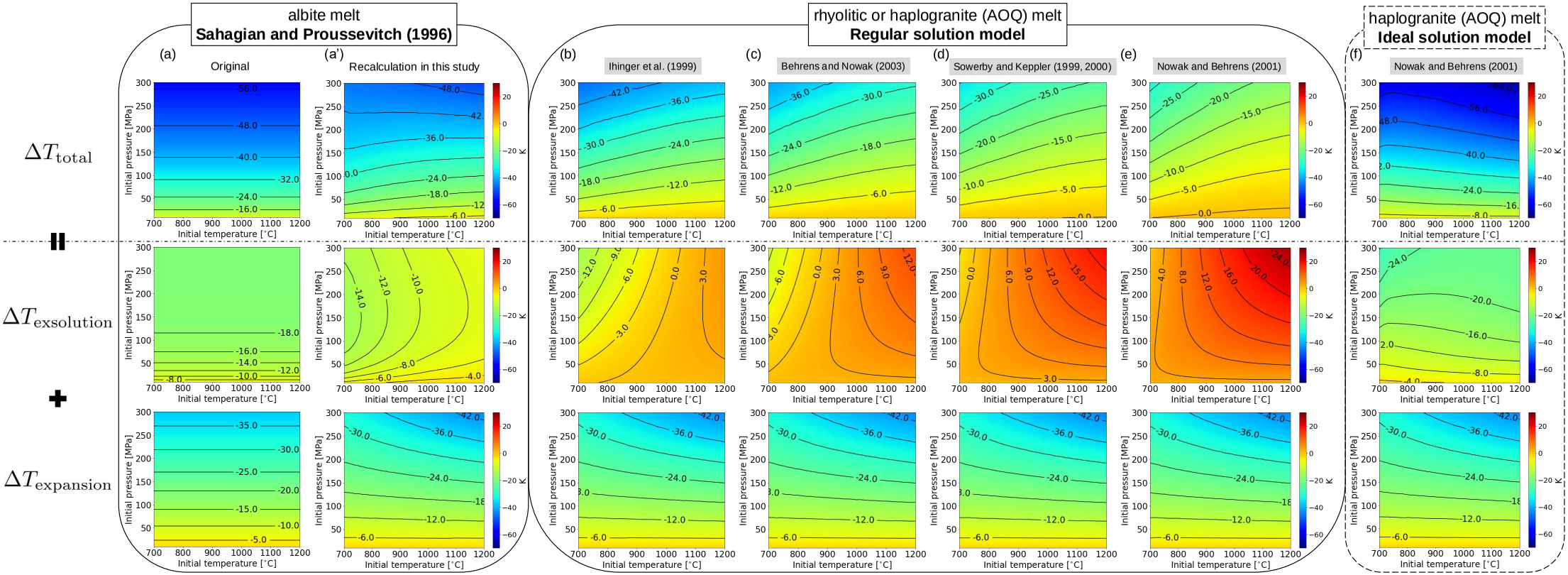
albite melt
Sahagian and Proussevitch (1996)
(a)
Original
(a')
Recalculation in this study
rhyolitic or haplogranite (AOQ) melt
Regular solution model
(b)
Ihinger et al. (1999)
(c)
Behrens and Nowak (2003)
(d)
Sowerby and Keppler (1999, 2000)
(e)
Nowak and Behrens (2001)
haplogranite (AOQ) melt
Ideal solution model
(f)
Nowak and Behrens (2001)
$\Delta T_{\mathrm{total}}$
=
$\Delta T_{\mathrm{exsolution}}$
+
$\Delta T_{\mathrm{expansion}}$
Initial pressure [MPa]
Initial temperature [°C]
K

[Figure 4.1] The numerical calculation results of the temperature change of hydours silicate melts during decompression-induced equilibrium water degassing. All panels are drawn on the plane of the initial temperature 700-1200°C and the initial pressure 0.1-300 MPa. Values on contours indicate the temperature change (K). The middle and lower panels show the effects of heat of exsolution ($\Delta T_{\mathrm{exsolution}}$) and expansion ($\Delta T_{\mathrm{expansion}}$), respectively, and the upper panels are the sum of them, i.e., the total temperature change ($\Delta T_{\mathrm{total}}$).

(a) The original calculation result for albite melt from Fig. 9 in Sahagian and Proussevitch (1996). (a') The recalculation result when substituting the values of the heat of exsolution from Table 3 in Sahagian and Proussevitch (1996) into the numerical program developed in this study.

(b)-(f) The results when using the speciation-dependent values of $\Delta\overline{H}_{\mathrm{total}}$ corresponding to Fig. 3 (b)-(f) in the cases of rhyolitic or haplogranite (AOQ) melt, respectively.

4.4 Comparison with Sahagian and Proussevitch (1996)

Comparing $|\Delta T_{\rm total}|$ in (b)-(e) of "Regular solution model" with that in (a), it is found that at $(T_{\rm i}, P_{\rm i})$ = (1200°C, 300 MPa) the former is about 20-40 K smaller than the latter. In other words, the calculations in this study, where various parameters are most appropriately taken into account, imply that Sahagian and Proussevitch's (1996) estimates of the temperature drop of the magma were overestimated.

Moreover, the very small positive region of $\Delta T_{\rm total}$ in (e) means that, regardless of $T_{\rm i}$, if decompression starts from lower $P_{\rm i}$ below a few 10 MPa, the temperature of magma can retain almost the same or even increase by a few K. This is in contrast to (a) the results of Sahagian and Proussevitch (1996), who stated that the temperature of magma drops regardless of which $(T_{\rm i}, P_{\rm i})$ the decompression starts from.

In the following, I discuss how each of the contributions of newly introduced conditions in this study [1]-[8] changed the numerical calculation results from (a) Sahagian and Proussevitch (1996).

[1]: water solubility equation - albite melt vs. rhyolitic melt
[2]: a set of differential equations to track the temperature and pressure dependence of $\Delta \overline{H}_{\rm total}$
[3]: specific heat capacity of vapor
[4]: specific heat capacity of water dissolved in melt
[5]: update of $\Delta \overline{H}_{\rm total}$
[6]: glass transition point
[7]: density of vapor calculated through the equation of state of a real gas
[8]: equation for estimating the density of hydrous melt

First, water solubility in albite melt is 7.34 wt% at (1200°C, 300 MPa), while that in rhyolitic melt is 7.23 wt% at (1200°C, 300 MPa) and is 7.62 wt% at (700°C, 300 MPa) calculated from eq. (1.12), so the latter is 0.985-1.04 times larger than the former, and the contribution of [1] is small.

As mentioned in section 4.2, since the reference data for $\rho^{\rm melt}$ was not stated in Sahagian and Proussevitch (1996), the contribution of [8] cannot be evaluated. Also, as mentioned at the beginning of section 4.3, [6] was only applied in the very narrow temperature and pressure range. In (a'), [2], [6], and [8] are applied, so the $\Delta T_{\rm exsolution}$ difference between (a) and (a') can be attributed to [2].

In the range of temperatures and pressures that can be taken in the calculations in this study, ($C'^{\rm dry\ melt}_{P}$ = 1355-1421 J/(kg · K), $C'^{\rm melt}_{P,{\rm total\ H_2O}}$ = 3144 J/(kg · K), and $C'^{\rm vapor}_{P} \simeq$ 2200-

4900 J/(kg · K)). From these, the value of C'^{magma}_P is larger than the value of $C'^{\text{dry melt}}_P$ used in Sahagian and Proussevitch (1996), but the range of possible values was at most 1.2 times larger. Although this should work to reduce the temperature change from eq. (4.1), since there is little difference when comparing the $\Delta T_{\text{expansion}}$ of (a) and the others (a')-(f), the contribution of [3] and [4] are small enough.

The ratio of the volume of vapor $\overline{V}^{\text{vapor}}(T, P)$ determined using the equation of state of a real gas to that determined by the ideal gas law can be regarded as unity in most temperature and pressure ranges. On the other hand, it is locally far from unity as shown in Fig. 4.2, e.g., 1.17 at (1200°C, 300 MPa) and 0.789 at (700°C, 100 MPa), thus the contribution of [7] cannot be ignored in such a temperature and pressure range.

The magnitude of $\Delta T_{\text{exsolution}}$ in (a') and (b)-(f) clearly reflects the magnitude of $\Delta \overline{H}_{\text{total}}$ in Fig. 3 (a)-(f) (vertical position of the curves), i.e. the contribution of [5].

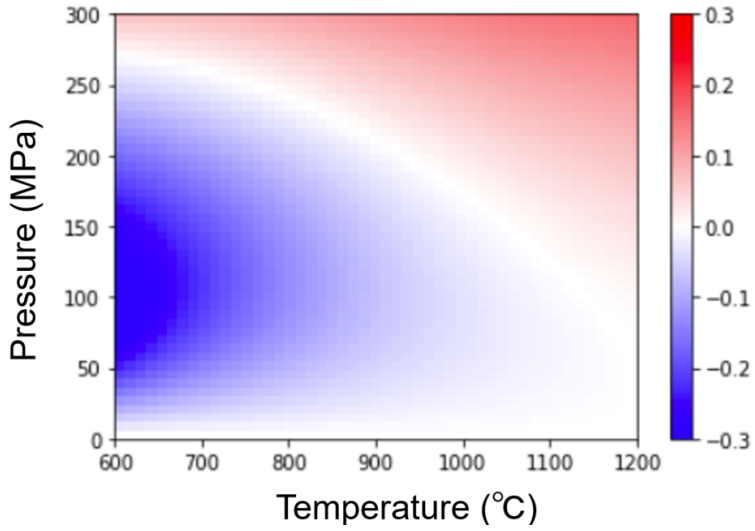

[Figure 4.2] The value subtracted 1 from the ratio of the volume of vapor $\overline{V}^{\text{vapor}}(T, P)$ determined using the equation of state of a real gas (Wagner and Pruß, 2002) to that determined by the ideal gas law.

4.5 Implications for natural systems

It was found that, assuming equilibrium degassing in a closed system, the temperature of rhyolitic magma does not change as much, or at most decreases by 45 K due to decompression-induced vesiculation. In real natural systems, vapor bubble exsolved from melt is partially coalesces into a permeable flow, i.e., it would be an open system, so that $|\Delta T_{\mathrm{expansion}}|$ would be smaller than the estimation in this study. Also, if a decompression rate is large enough, non-equilibrium degassing occurs before reaching thermal equilibrium, and $|\Delta T_{\mathrm{expansion}}|$ would be smaller (Sahagian and Proussevitch, 1996). Considering the above, the effect of expansion becomes smaller as the eruption intensity increases, and only the effect of exsolution becomes dominant, therefore the temperature of magma remains almost the same or even increases due to decompression-induced vesiculation.

In addition, in natural systems, crystallization proceeds simultaneously with decompression-induced vesiculation of magma. The fact that the heat of solidification released during crystallization is positive (exothermic) has been well confirmed by direct measurements by transposed-temperature-drop calorimetry and indirect measurements by solution calorimetry and differential scanning calorimetry (Lange et al., 1994; Kojitani and Akaogi, 1997; Sugawara and Akaogi, 2003; Sugawara, 2005; Whittington and Sehlke, 2011; Kolzenburg et al., 2016). Moreover, according to Blundy et al. (2006), a modeling based on microtextural observations of pyroclasts from two andesitic volcanic eruptions, Mount St. Helens and Shiveluch, indicates that the temperature of magma that starts decompression from 300 MPa may increase by about 100 K. Combining this with the numerical calculation results in this study, it is likely that crystallization tends to predominantly contribute to the temperature change of magma in the process of magma ascending the volcanic conduit, and even depending on the balance between the two, the temperature of magma will eventually increase in most cases.

Although not handled in this study, to obtain the specific temperature and pressure histories, it is necessary to simultaneously and sequentially solve the complicated transition of phase equilibrium relation among vapor bubbles, liquid melt and solid crystals in magma. In the future, it may be possible through such calculations to incorporate temperature changes due to vesiculation and crystallization of magma into conventional conduit flow models.

Conclusions

In this study, several problems related to the dissolution of water in silicate melts were theoretically treated using chemical thermodynamics, and the following new findings were obtained.

(1) Although the experimentally estimated partial molar volume of water in melts is approximately 20 cm^3/mol, it is known that the values estimated through theoretical equations for water solubility in melts vary widely, sometimes it can be negative. The cause of this paradox is that the conventional theoretical equation for water solubility assumed the ideal mixing of H_2O_m, OH, and O, even though their actual mixture clearly exhibits thermodynamic behavior different from that of ideal mixing. Therefore, the previously neglected non-ideal term (the ratio of the activity coefficients of H_2O_m at different pressures) in the theoretical equation was explicitly redescribed and its effect was quantitatively evaluated through simple calculations.

(2) By applying the asymmetric regular solution model to a three-component mixture of H_2O_m, OH, and O, values of interaction parameters between each component in the range 700-1200°C at 5000 bars were obtained. As a result, it was found that all parameters are temperature-dependent and that a particularly strong positive non-ideality appears when H_2O_m enters an O-rich environment. Besides, the behavior of activity coefficient of H_2O_m in a wide temperature and pressure range of 700-1200°C, 1-5000 bars, i.e., the relation between activity and mole fraction of H_2O_m, was clarified in detail.

(3) By applying the Gibbs-Helmholtz equation to the equilibrium constant of the first reaction of dissolution, the enthalpy change, i.e. the heat of dissolution, was determined over a wide range of temperature and pressure, and found to be approximately -20 kJ/mol (exothermic) regardless of temperature and pressure. By adding the heat of dissolution of the second reaction, the heat of dissolution of the overall reaction could also be calculated over a wide temperature and pressure range. It was found to shift towards endothermic at higher temperatures and towards exothermic at lower pressures, and the extent of the shift was highly dependent on the experimentally-estimated value of the heat of dissolution of the second reaction.

(4) The temperature change of magma during decompression-induced vesiculation was numerically calculated. It was found that the effect of the heat of exsolution worked to raise and the effect of the mechanical work of bubble expansion worked to lower the temperature of the

magma, but the latter effect was always greater, resulting in a slight cooling of magma. In natural systems, however, the temperature rise due to magma crystallization would predominate over the temperature drop due to vesiculation, thus the temperature of the magma would eventually increase.

Acknowledgments

I am especially thankful to the people in my laboratory: Group of Petrology and Volcanology, Department of Earth and Planetary Sciences, Faculty of Science, Kyushu University. I am grateful to my supervisor, Prof. Atsushi Toramaru, for his support throughout my undergraduate, master's, and doctoral studies. He has accompanied me in many long discussions and given me many comments on the manuscript of this thesis. The frequent discussions with Assoc. Prof. Takeshi Ikeda were extremely helpful in deepening my understanding of the fundamentals of rock thermodynamics, which is essential for this study. Asst. Prof. Tomoharu Miyamoto, Asst. Prof. Masatoshi Ohashi, and many students also helped me on a daily basis.

Discussions with Assoc. Prof. Shigeo Yoshida (Dynamics of the Earth's Interior Group) on the three-component asymmetric regular solution model were fruitful. I would like to thank the staff in the office of our department, especially Ms. Kanako Kimura, Ms. Kazuyo Matsumoto, Ms. Saori Tashiro, and the chief Ms. Yuki Yamaji, for their administrative support. The occasional interaction with students in other laboratories was always enjoyable.

The numerical program for calculation of the equation of state of water as a real gas created by Asst. Prof. Mitsuo Matsumoto (Laboratory of Geothermics, Department of Earth Resources Engineering, Faculty of Engineering, Kyushu University) was very useful in the calculation of fugacity and heat capacity of pure water vapor. The multiple numerical codes created by Mr. Kiichi Fukuya (already graduated from Graduate School of Science, The University of Tokyo, and currently works for IBM Japan, Ltd.) were very helpful in the estimation of the temperature change of magmas with decompression-induced vesiculation.

Discussion with Chief Researchers Isoji Miyagi and Akihiko Tomiya (Geological Survey of Japan, National Institute of Advanced Industrial Science and Technology, Tsukuba) contributed to improve the contents of Part II of this thesis and to obtain ideas on applying my numerical calculation results to natural systems. Comments in the viewpoint of chemistry and drawing structural formulas using ChemDraw by Prof. Nagatoshi Nishiwaki (School of Environmental Science and Engineering, Kochi University of Technology) inspired me to deeply consider the dissolution mechanism of water molecules into silicate melts.

My enjoyment of amateur orchestral activities and interaction with orchestral players was

a major motivational support for my life as a Ph.D. course student. It was especially fortunate for me given the opportunity to perform in the 206th through 209th subscription concerts and in the 2nd Special Concert in Tokyo held by Kyudai Philharmonic Orchestra. The experience of playing as a principal violist in Ropponmatsu Ensemble, one of the highest-level amateur ensembles, was extremely valuable. In addition, I have been invited as a guest performer many times by Fukuoka OB Philharmonic Orchestra and Ito Junior Orchestra, which improved my skills and experience as an orchestral player. The café "Manifold Ito," run by Fumiyo Sujita, leader of Ito Junior Orchestra, and her husband, Chef Toshiaki Sujita, provided me with excellent cuisine and an ideal environment to write this dissertation.

My family helped me in various aspects. I would like to thank many other people who have helped me at every turn, besides those mentioned above.

I also would like to thank the Ulatus translation service at Crimson Interactive Pvt. Ltd., Mumbai, India, for assistance with translation of the manuscript. This work was supported by JSPS KAKENHI grant 20J20188.

. . . . . .

Aside from the theoretical topics covered in this dissertation, I have conducted a variety of other research (experimenatl studies and mathematical studies) during my Ph.D. course, and I have been assisted by many people in each study.

Experimental studies

Under the generous guidance of Chief Researcher Takahiro Miwa, I have conducted a lot of experiments using cold-seal pressure vessels and various other equipments at National Research Institute for Earth Science and Disaster Resilience, Tsukuba. In introducing a quench system to the cold-seal pressure vessels, we received precise advice from Assoc. Prof. Satoshi Okumura and Ph.D. candidate Kazuhisa Matsumoto (Volcanology and Geofluids Research Group, Department of Earth Science, Tohoku University). For experiments at higher pressures, an internally heated pressure vessel (HIP) was used at Geological Survey of Japan, National Institute of Advanced Industrial Science and Technology, Tsukuba, with the help of Researcher Takayuki Nakatani and Technical Staff Toshihiro Suzuki.

For the measurements of water content in hydrous rhyolitic glasses prepared using above instruments, a micro FT-IR (Fourier Transform Infrared Spectroscopy) at the Earthquake Research Institute, University of Tokyo, was used with the support of Assoc. Prof. Atsushi Yasuda. The basic operation methods of a micro FT-IR was initially supported by Asst. Prof. Yumiko Tsubokawa and Prof. Tomoaki Kubo (Group of Deep Earth Materials Science, Department of Earth and Planetary Sciences, Faculty of Science, Kyushu University).

For the analyses using an FE-SEM and an FE-EPMA, I was helped by Technical Staff

Kazuhiko Shimada (Department of Earth and Planetary Sciences, Faculty of Science, Kyushu University). For the analyses using a micro focus X-ray CT scanner, I was helped by Technical Staff Takuya Matsuzaki (Center for Advanced Marine Core Research, Kochi University).

Mathematical studies

Ph.D. candidate Shota Shigetomi (Graduate School of Mathematics, Kyushu University) played a central role in a challenging joint research project to apply the elliptic theta functions to classical nucleation theory. The co-authored paper with him was already published as Shigetomi and Nishiwaki (2022) in a peer-reviewed journal.

In an exploratory study that gives a topological interpretation of the laws of thermodynamics for multi-component and multi-phase systems, I was able to expand my world thanks to the deep mathematical insight of Prof. Shizuo Kaji (Institute of Mathematics for Industry, Kyushu University) and Ph.D. candidate Tomoki Yuji (Research Institute for Mathematical Sciences, Kyoto University).

References

Bagdassarov, N., Dorfman, A., and Dingwell, D. B., 2000. Effect of alkalis, phosphorus, and water on the surface tension of haplogranite melt. Am. Mineral. 85 (1), 33-40. https://doi.org/10.2138/am-2000-0105

Balzer, R., Behrens, H., Reinsch, S., and Fechtelkord, M., 2019a. Structural investigation of hydrous phosphate glasses. Phys. Chem. Glasses - Eur. J. Glass. Sci. Technol. B 60 (2), 49-61. https://doi.org/10.13036/17533562.60.2.041

Balzer, R., Behrens, H., Schuth, S., Waurischk, T., Reinsch, S., Müller, R., Fechtelkord, M., and Deubener, J., 2019b. The influence of H_2O and SiO_2 on the structure of silicoborate glasses. J. Non-Cryst. Solids 519 (1), 38-51. https://doi.org/10.1016/j.jnoncrysol.2019.05.030

Balzer, R., Behrens, H., Waurischk, T., Reinsch, S., Müller, R., Kiefer, P., Deubener, J., and Fechtelkord, M., 2020. Water in alkali aluminosilicate glasses. Front. Mater. 7, 85. https://doi.org/10.3389/fmats.2020.00085

Bartholomew, R. F., Bulter, B. L., Hoover, H. L. and Wu, C. K., 1980. Infrared spectra of a water-containing glass. J. Am. Ceram. Soc. 63 (9-10), 481-485. https://doi.org/10.1111/j.1151-2916.1980.tb10748.x

Bauer, U., Behrens, H., Fechtelkord, M., Reinsch, S., and Deubener, J., 2015. Water- and boron speciation in hydrous soda-lime-borate glasses. J. Non-Cryst. Solids 423-424 (1), 58-67. https://doi.org/10.1016/j.jnoncrysol.2015.05.004

Behrens, H., 2020. Water speciation in oxide glasses and melts. Chem. Geol. 558, 119850. https://doi.org/10.1016/j.chemgeo.2020.119850

Behrens, H., and Nowak, M., 2003. Quantification of H_2O speciation in silicate glasses and melts by IR spectroscopy-in situ versus quench techniques. Phase Transit. 76 (1-2), 45-61. https://doi.org/10.1080/0141159031000076048

Behrens, H., and Yamashita, S., 2008. Water speciation in hydrous sodium tetrasilicate and hexasilicate melts: Constraint from high temperature NIR spectroscopy. Chem. Geol. 256 (3-4), 306-315. https://doi.org/10.1016/j.chemgeo.2008.06.053

Behrens, H., Bauer, U., Reinsch, R., Kiefer, P., Müller, R., and Deubener, J., 2018. Structural relaxation mechanisms in hydrous sodium borosilicate glasses. J. Non-Cryst. Solids 497

(1), 30-39. https://doi.org/10.1016/j.jnoncrysol.2018.05.025

Blander, M., and Katz, J. L., 1975. Bubble nucleation in liquids. AIChE J. 21 (5), 833-848. https://doi.org/10.1002/aic.690210502

Blank, J. G., Stolper, E. M., and Carroll, M. R., 1993. Solubilities of carbon dioxide and water in rhyolitic melt at 850°C and 750 bars. Earth Planet. Sci. Lett. 119 (1-2), 27-36. https://doi.org/10.1016/0012-821X(93)90004-S

Blundy, J., Cashman, K., and Humphreys, M., 2006. Magma heating by decompression-driven crystallization beneath andesite volcanoes. Nature, 443 (7107), 76-80. https://doi.org/10.1038/nature05100

Botcharnikov, R. E., Behrens, H., and Holtz, F., 2006. Solubility and speciation of C-O-H fluids in andesitic melt at T = 1100-1300°C and P = 200 and 500 MPa. Chem. Geol. 229 (1-3), 125-143. https://doi.org/10.1016/j.chemgeo.2006.01.016

Bouhifd, A. M., Whittington, A., and Richet, P., 2001. Partial molar volume of water in phonolitic glasses and liquids. Contrib. Mineral. Petrol. 142 (2), 235-243. https://doi.org/10.1007/s004100100286

Bureau, H., and Keppler, H., 1999. Complete miscibility between silicate melts and hydrous fluids in the upper mantle: experimental evidence and geochemical implications. Earth Planet. Sci. Lett. 165 (2), 187-196. https://doi.org/10.1016/S0012-821X(98)00266-0

Buresti, G., and Casarosa, C., 1989. One-dimensional adiabatic flow of equilibrium gas-particle mixtures in long vertical ducts with friction. J. Fluid Mech. 203, 251-272. https://doi.org/10.1017/S002211208900145X

Burnham, C. W., 1975. Water and magmas; a mixing model. Geochim. Cosmochim. Acta 39 (8), 1077-1084. https://doi.org/10.1016/0016-7037(75)90050-2

Burnham, C. W., 1979. The importance of volatile constituents., in: Yoder, H. S., The evolution of the igneous rocks. Princeton University Press, pp. 439-482.

Burnham, C. W., and Davis, N. F., 1971. The role of H_2O in silicate melts: I. P-V-T relations in the system $NaAlSi_3O_8$-H_2O to 10 kilobars and 1000°C. Am. J. Sci. 270 (1), 54-79. https://doi.org/10.2475/ajs.270.1.54

Burnham, C. W., and Davis, N. F., 1974. The role of H_2O in silicate melts: II. Thermodynamic and phase relations in the system $NaAlSi_3O_8$-H_2O to 10 kilobars, 700° to 1100 °C. Am. J. Sci. 274 (8), 902-940. https://doi.org/10.2475/ajs.274.8.902

Burnham, C. W., and Jahns, R. H., 1962. A method for determining the solubility of water in silicate melts. Am. J. Sci. 260 (10), 721-745. https://doi.org/10.2475/ajs.260.10.721

Burnham, C. W., Holloway, J. R., and Davis, N. F., 1969. Thermodynamic properties of water to 1,000°C and 10,000 bars. Geol. Soc. Am. 132, 1-96. https://doi.org/10.1130/

SPE132-p1

Cashman, K. V., and Sparks, R. S. J., 2013. How volcanoes work: A 25 year perspective. Geol. Soc. Am. Bull. 125 (5-6), 664-690. https://doi.org/10.1130/B30720.1

Cassidy, M., Manga, M., Cashman, K., and Bachmann, O., 2018. Controls on explosive-effusive volcanic eruption styles. Nature communications, 9 (1), 1-16.
https://doi.org/10.1038/s41467-018-05293-3

Cluzel, N., Laporte, D., Provost, A., and Kannewischer, I., 2008. Kinetics of heterogeneous bubble nucleation in rhyolitic melts: implications for the number density of bubbles in volcanic conduits and for pumice textures. Contrib. Mineral. Petrol. 156 (6), 745-763. https://doi.org/10.1007/s00410-008-0313-1

Costa, A., Melnik, O., and Sparks, R. S. J., 2007a. Controls of conduit geometry and wallrock elasticity on lava dome eruptions. Earth Planet. Sci. Lett. 260 (1-2), 137-151. https://doi.org/10.1016/j.epsl.2007.05.024

Costa, A., Melnik, O., and Vedeneeva, E., 2007b. Thermal effects during magma ascent in conduits. J. Geophys. Res. Solid Earth, 112, B12205. https://doi.org/10.1029/2007JB004985

Di Genova, D., Romano, C., Giordano, D., and Alletti, M., 2014. Heat capacity, configurational heat capacity and fragility of hydrous magmas. Geochim. Cosmochim. Acta 142, 314-333. https://doi.org/10.1016/j.gca.2014.07.012

Dingwell, D. B., 1998. The glass transition in hydrous granitic melts. Phys. Earth Planet. Inter. 107 (1-3), 1-8. https://doi.org/10.1016/S0031-9201(97)00119-2

Dixon, J. E., Stolper, E. M., and Holloway, J. R., 1995. An experimental study of water and carbon dioxide solubilities in mid-ocean ridge basaltic liquids. Part I: calibration and solubility models. J. Petrol. 36 (6), 1607-1631. https://doi.org/10.1093/oxfordjournals.petrology.a037267

Dobran, F., 1992. Nonequilibrium flow in volcanic conduits and application to the eruptions of Mt. St. Helens on May 18, 1980, and Vesuvius in AD 79. J. Volcanol. Geotherm. Res. 49 (3-4), 285-311. https://doi.org/10.1016/0377-0273(92)90019-A

Duan, X., 2014. A general model for predicting the solubility behavior of H_2O-CO_2 fluids in silicate melts over a wide range of pressure, temperature and compositions. Geochim. Cosmochim. Acta 125, 582-609. https://doi.org/10.1016/j.gca.2013.10.018

Eichelberger, J. C., 1995. Silicic volcanism: ascent of viscous magmas from crustal reservoirs. Annu. Rev. Earth Planet. Sci. 23 (1), 41-63.
https://doi.org/10.1146/annurev.ea.23.050195.000353

Epel'baum, M. B., 1973. Surface tension of felsic magmatic melts at high temperatures and

pressure. Geochem. Int. 10, 343-345.

Ernsberger, F., 1977. Molecular water in glass. J. Am. Ceram. Soc., 60 (1-2), 91-92.

Gardner, J. E., 2012. Surface tension and bubble nucleation in phonolite magmas. Geochim. Cosmochim. Acta 76, 93-102. https://doi.org/10.1016/j.gca.2011.10.017

Gardner, J. E., and Ketcham, R. A., 2011. Bubble nucleation in rhyolite and dacite melts: temperature dependence of surface tension. Contrib. Mineral. Petrol. 162 (5), 929-943. https://doi.org/10.1007/s00410-011-0632-5

Gardner, J. E., Ketcham, R. A., and Moore, G., 2013. Surface tension of hydrous silicate melts: Constraints on the impact of melt composition. J. Volcanol. Geotherm. Res. 267, 68-74. https://doi.org/10.1016/j.jvolgeores.2013.09.007

Gardner, J. E., Hajimirza, S., Webster, J. D., and Gonnermann, H. M., 2018. The impact of dissolved fluorine on bubble nucleation in hydrous rhyolite melts. Geochim. Cosmochim. Acta 226, 174-181. https://doi.org/10.1016/j.gca.2018.02.013

Gerya, T. V., Maresch, W. V., Burchard, M., Zakhartchouk, V., Doltsinis, N. L., and Fockenberg, T., 2005. Thermodynamic modeling of solubility and speciation of silica in H_2O–SiO_2 fluid up to 1300°C and 20 kbar based on the chain reaction formalism. Eur. J. Mineral. 17 (2), 269-283. https://doi.org/10.1127/0935-1221/2005/0017-0269

Ghiorso, M. S., and Gualda, G. A., 2015. An H_2O-CO_2 mixed fluid saturation model compatible with rhyolite-MELTS. Contrib. Mineral. Petrol. 169 (6), 1-30. https://doi.org/10.1007/s00410-015-1141-8

Giberti, G., and Wilson, L., 1990. The influence of geometry on the ascent of magma in open fissures. Bull. Volcanol. 52, 515-521. https://doi.org/10.1007/BF00301532

Gonnermann, H. M., 2015. Magma fragmentation. Annu. Rev. Earth Planet. Sci. 43 (1), 431-458. https://doi.org/10.1146/annurev-earth-060614-105206

Gonnermann, H. M., and Gardner, J. E., 2013. Homogeneous bubble nucleation in rhyolitic melt: Experiments and nonclassical theory. Geochem. Geophys. 14 (11), 4758-4773. https://doi.org/10.1002/ggge.20281

Gonnermann, H. M., and Manga, M., 2007. The fluid mechanics inside a volcano. Annu. Rev. Fluid Mech., 39, 321-356. https://doi.org/10.1146/annurev.fluid.39.050905.110207

Goranson, R. W., 1931. The solubility of water in granite magmas. Am. J. Sci. Ser. 5, 22 (132), 481-502. https://doi.org/10.2475/ajs.s5-22.132.481

Goranson, R. W., 1938. Silicate-water systems: phase equilibria in the $NaAlSi_3O_8$-H_2O and $KAlSi_3O_8$-H_2O systems at high temperatures and pressures. Am. J. Sci. 35, 71-91. https://earth.geology.yale.edu/~ajs/1938-A/71.pdf

Guggenheim E. A., 1952. Mixtures. Oxford University Press. 270 pp.

Haar, L., Gallagher, J. S., and Kell, G. S., 1984. NBS/NRC steam tables: Thermodynamic and transport properties and computer programs for vapor and liquid states of water in SI units. Hemisphere, Washington, DC, 320 pp.

Hamada, M., Laporte, D., Cluzel, N., Koga, K. T., and Kawamoto, T., 2010. Simulating bubble number density of rhyolitic pumices from Plinian eruptions: constraints from fast decompression experiments. Bull. Volcanol. 72 (6), 735-746. https://doi.org/10.1007/s00445-010-0353-z

Hirth, J. P., Pound, G. M., and St Pierre, G. R., 1970. Bubble nucleation. Metall. Trans. 1 (4), 939-945. https://doi.org/10.1007/BF02811776

Holloway, J. R., 1977. Fugacity and activity of molecular species in supercritical fluids. In: Fraser, D. G. (Ed.), Thermodynamics in geology. NATO Advanced Study Institutes Series 30. Springer, Dordrecht. https://doi.org/10.1007/978-94-010-1252-2_9

Holloway, J. R. and Blank, J. G., 1994. Application of experimental results to C−O−H species in natural melts. In: Carroll, M. R. and Holloway, J. R. (Eds.), Volatiles in Magmas. Mineral. Soc. Am. Rev. Mineral., 30, 187-230.
https://doi.org/10.1515/9781501509674-012

Holtz, F., Behrens, H., Dingwell, D. B., and Johannes, W., 1995. H_2O solubility in haplogranitic melts: compositional, pressure, and temperature dependence. Am. Mineral. 80 (1-2), 94-108. https://doi.org/10.2138/am-1995-1-210

Holtz, F., Behrens, H., Dingwell, D. B., and Taylor, R. P., 1992. Water solubility in aluminosilicate melts of haplogranite composition at 2 kbar. Chem. Geol. 96 (3-4), 289-302. https://doi.org/10.1016/0009-2541(92)90060-I

Hui, H., Zhang, Y., Xu, Z., and Behrens, H., 2008. Pressure dependence of the speciation of dissolved water in rhyolitic melts. Geochim. Cosmochim. Acta 72 (13), 3229-3240. https://doi.org/10.1016/j.gca.2008.03.025

Iacono-Marziano, G., Morizet, Y., Le Trong, E., and Gaillard, F., 2012. New experimental data and semi-empirical parameterization of H_2O-CO_2 solubility in mafic melts. Geochim. Cosmochim. Acta 97, 1-23. https://doi.org/10.1016/j.gca.2012.08.035

Iacovino, K., and Till, C. B., 2019. DensityX: A program for calculating the densities of magmatic liquids up to 1,627°C and 30 kbar. Volcanica 2 (1), 1-10.
https://doi.org/10.30909/vol.02.01.0110

Iacovino, K., Matthews, S., Wieser, P. E., Moore, G. M., and Bégué, F., 2021. VESIcal Part I: An open- source thermodynamic model engine for mixed volatile (H_2O-CO_2) solubility in silicate melts. Earth Space Sci. 8 (11), e2020EA001584. https://doi.org/10.1029/

2020EA001584

Ihinger, P. D., Zhang, Y., and Stolper, E. M., 1999. The speciation of dissolved water in rhyolitic melt. Geochim. Cosmochim. Acta 63 (21), 3567-3578. https://doi.org/10.1016/S0016-7037(99)00277-X

Jaupart, C., 1996. Physical models of volcanic eruptions. Chem. Geol. 128 (1-4), 217-227. https://doi.org/10.1016/0009-2541(95)00175-1

Kakuda, Y., Uchida, E., and Imai, N., 1991. A new thermodynamic model for ternary solid solutions (in Japanese). J. Mineral. Soc. Jpn. 20 (1-2), 25-32. https://doi.org/10.2465/gkk1952.20.25

Kakuda, Y., Uchida, E., and Imai, N., 1994. A new model of the excess Gibbs energy of mixing for a regular solution. Proc. Jpn. Acad., Ser. B, Phys. Biol. Sci. 70 (10), 163-168. https://doi.org/10.2183/pjab.70.163

Kennedy, G. C., Wasserburg, G. J., Heard, H. C., and Newton, R. C., 1962. The upper three-phase region in the system SiO_2-H_2O. Am. J. Sci. 260 (7), 501-521. https://doi.org/10.2475/ajs.260.7.501

Khitarov, N. I., Kadik, A. A., and Lebedev, E. B., 1963. Estimate of the thermal effect of the separation of water from felsic melts based on data for the system albite-water. Geokhimiya 7, 637-649.

Khitarov, N. I., Lebedev, Y. B., Dorfman, A. M., and Bagdasarov, N., 1979. Effects of temperature, pressure, and volatiles on the surface tension of molten basalt. Geochem. Int. 16 (5), 78-86.

Klug, C., and Cashman, K. V., 1996. Permeability development in vesiculating magmas: implications for fragmentation. Bull. Volcanol. 58 (2), 87-100. https://doi.org/10.1007/s004450050128

Kojitani, H., and Akaogi, M., 1997. Melting enthalpies of mantle peridotite: calorimetric determinations in the system CaO-MgO-Al_2O_3-SiO_2 and application to magma generation. Earth Planet. Sci. Lett. 153 (3-4), 209-222. https://doi.org/10.1016/S0012-821X(97)00186-6

Kolzenburg, S., Giordano, D., Cimarelli, C., and Dingwell, D. B., 2016. In situ thermal characterization of cooling/crystallizing lavas during rheology measurements and implications for lava flow emplacement. Geochim. Cosmochim. Acta 195, 244-258. https://doi.org/10.1016/j.gca.2016.09.022

Kozono, T., 2021. The dynamics of dual-magma-chamber system during volcanic eruptions inferred from physical modeling. Earth Planets Space 73 (1), 1-11. https://doi.org/10.1186/s40623-021-01421-4

Kuritani, T., 2007. Water and magma (in Japanese). J. Geog. (Chigaku Zasshi) 116 (1), 133-153. https://doi.org/10.5026/jgeography.116.133

Lange, R. A., 1994. The effects of H_2O, CO_2 and F on the density and viscosity of silicate melts. Rev. Mineral. 30, 331-369. https://doi.org/10.1515/9781501509674-015

Lange, R. A., Cashman, K. V., and Navrotsky, A., 1994. Direct measurements of latent heat during crystallization and melting of a ugandite and an olivine basalt. Contrib. Mineral. Petrol., 118 (2), 169-181. https://doi.org/10.1007/BF01052867

Legros, F., and Kelfoun, F., 2000. Sustained blasts during large volcanic eruptions. Geology 28 (10), 895-898. https://doi.org/10.1130/0091-7613(2000)28<895:SBDLVE>2.0.CO;2

Lesne, P., Scaillet, B., Pichavant, M., Iacono-Marziano, G., and Beny, J. M., 2011. The H_2O solubility of alkali basaltic melts: an experimental study. Contrib. Mineral. Petrol. 162 (1), 133-151. https://doi.org/10.1007/s00410-010-0588-x

Liu, Y., Behrens, H., and Zhang, Y., 2004. The speciation of dissolved H_2O in dacitic melt. Am. Mineral. 89 (2-3), 277-284. https://doi.org/10.2138/am-2004-2-304

Liu, Y., Zhang, Y., and Behrens, H., 2005. Solubility of H_2O in rhyolitic melts at low pressures and a new empirical model for mixed H_2O−CO_2 solubility in rhyolitic melts. J. Volcanol. Geotherm. Res. 143 (1-3), 219-235. https://doi.org/10.1016/j.jvolgeores.2004.09.019

Makhluf, A. R., Newton, R. C. and Manning, C. E., 2020. Experimental investigation of phase relations in the system $NaAlSi_3O_8$-H_2O at high temperatures and pressures: liquidus relations, liquid-vapor mixing, and critical phenomena at deep crust-upper mantle conditions. Contrib. Mineral. Petrol. 175 (8), 76. https://doi.org/10.1007/s00410-020-01711-2

Mangan, M. T., Cashman, K. V., and Newman, S., 1993. Vesiculation of basaltic magma during eruption. Geology, 21 (2), 157-160.
https://doi.org/10.1130/0091-7613(1993)021<0157:VOBMDE>2.3.CO;2

Mangan, M., and Sisson, T., 2000. Delayed, disequilibrium degassing in rhyolite magma: decompression experiments and implications for explosive volcanism. Earth Planet. Sci. Lett. 183 (3-4), 441-455. https://doi.org/10.1016/S0012-821X(00)00299-5

Mangan, M., and Sisson, T., 2005. Evolution of melt- vapor surface tension in silicic volcanic systems: Experiments with hydrous melts. J. Geophy. Res. Solid Earth 110 (B1). https://doi.org/10.1029/2004JB003215

Mangan, M. T., Sisson, T. W., and Hankins, W. B., 2004. Decompression experiments identify kinetic controls on explosive silicic eruptions. Geophys. Res. Lett. 31 (8).
https://doi.org/10.1029/2004GL019509

Massol, H., Jaupart, C., and Pepper, D. W., 2001. Ascent and decompression of viscous

vesicular magma in a volcanic conduit. J. Geophys. Res. Solid Earth 106 (B8), 16223-16240. https://doi.org/10.1029/2001JB000385

Mastin, L. G., 2002. Insights into volcanic conduit flow from an open- source numerical model. Geochem. Geophys. 3 (7), 1-18. https://doi.org/10.1029/2001GC000192

Mastin, L. G., and Ghiorso, M. S., 2001. Adiabatic temperature changes of magma-gas mixtures during ascent and eruption. Contrib. Mineral. Petrol., 141 (3), 307-321. https://link.springer.com/content/pdf/10.1007/s004100000210

Melnik, O., and Sparks, R., 1999. Nonlinear dynamics of lava dome extrusion. Nature 402, 37-41. https://doi.org/10.1038/46950

Mitchell, K. L., 2005. Coupled conduit flow and shape in explosive volcanic eruptions. J. Volcanol. Geotherm. Res. 143 (1-3), 187-203. https://doi.org/10.1016/j.jvolgeores.2004.09.017

Moore, G., 2008. Interpreting H_2O and CO_2 contents in melt inclusions: constraints from solubility experiments and modeling. Rev. Mineral. Geochem. 69 (1), 333-362. https://doi.org/10.2138/rmg.2008.69.9

Moore, G., Vennemann, T., and Carmichael, I. S. E., 1998. An empirical model for the solubility of H_2O in magmas to 3 kilobars. Am. Mineral. 83 (1-2), 36-42. https://doi.org/10.2138/am-1998-1-203

Mourtada-Bonnefoi, C. C., and Laporte, D., 2002. Homogeneous bubble nucleation in rhyolitic magmas: an experimental study of the effect of H_2O and CO_2. J. Geophys. Res. Solid Earth 107 (B4), ECV-2. https://doi.org/10.1029/2001JB000290

Mourtada-Bonnefoi, C. C., and Laporte, D., 2004. Kinetics of bubble nucleation in a rhyolitic melt: an experimental study of the effect of ascent rate. Earth Planet. Sci. Lett. 218 (3-4), 521-537. https://doi.org/10.1016/S0012-821X(03)00684-8

Mysen, B. O., 2007. The solution behavior of H_2O in peralkaline aluminosilicate melts at high pressure with implications for properties of hydrous melts. Geochim. Cosmochim. Acta 71 (7), 1820-1834. https://doi.org/10.1016/j.gca.2007.01.007

Mysen, B. O., and Acton, M., 1999. Water in H_2O-saturated magma-fluid systems: solubility behavior in K_2O-Al_2O_3-SiO_2-H_2O to 2.0 GPa and 1300°C. Geochim. Cosmochim. Acta, 63 (22), 3799-3815. https://doi.org/10.1016/S0016-7037(99)00216-1

Mysen, B. O., and Cody, G. D., 2004. Solubility and solution mechanism of H_2O in alkali silicate melts and glasses at high pressure and temperature. Geochim. Cosmochim. Acta 68 (24), 5113-5126. https://doi.org/10.1016/j.gca.2004.07.021

Mysen, B. O., and Wheeler, K., 2000. Solubility behavior of water in haploandesitic melts at high pressure and high temperature. Am. Mineral. 85 (9), 1128-1142.

https://doi.org/10.2138/am-2000-8-903

Navon, O., and Lyakhovsky, V., 1998. Vesiculation processes in silicic magmas. Geol. Soc. Spec. Publ. 145 (1), 27-50. https://doi.org/10.1144/GSL.SP.1996.145.01.03

Newman, S., and Lowenstern, J. B., 2002. VolatileCalc: a silicate melt-H_2O-CO_2 solution model written in Visual Basic for excel. Comput. Geosci. 28 (5), 597-604. https://doi.org/10.1016/S0098-304(01)00081-4

Nishiwaki, M., and Toramaru, A., 2019. Inclusion of viscosity into classical homogeneous nucleation theory for water bubbles in silicate melts: Reexamination of bubble number density in ascending magmas. J. Geophys. Res. Solid Earth 124 (8), 8250-8266. https://doi.org/10.1029/2019JB017796

Nowak, M., and Behrens, H., 1995. The speciation of water in haplogranitic glasses and melts determined by in situ near-infrared spectroscopy. Geochim. Cosmochim. Acta 59 (16), 3445-3450. https://doi.org/10.1016/0016-7037(95)00237-T

Nowak, M., and Behrens, H., 2001. Water in rhyolitic magmas: getting a grip on a slippery problem. Earth Planet. Sci. Lett. 184 (2), 515-522. https://doi.org/10.1016/S0012-821X(00)00343-5

Ochs III, F. A., and Lange, R. A., 1997. The partial molar volume, thermal expansivity, and compressibility of H_2O in $NaAlSi_3O_8$ liquid: new measurements and an internally consistent model. Contrib. Mineral. Petrol. 129 (2), 155-165. https://doi.org/10.1007/s004100050329

Ochs III, F. A., and Lange, R. A., 1999. The density of hydrous magmatic liquids. Science 283 (5406), 1314-1317. https://doi.org/10.1126/science.283.5406.1314

Ohlhorst, S., Behrens, H., Holtz, F., and Schmidt, B. C., 2000. Water speciation in aluminosilicate glasses and melts. In: Rammlmair, D., Mederer, J., Oberthür, Th., Heimann, R. B., Pentinghaus, H. (Eds.), Applied Mineralogy in Research, Economy, Technology and Culture. Proc. 6th Int. Conf. Appl. Mineral, Vol. 1. Balkema, Rotterdam, pp. 193-196.

Orlova, G. P., 1962. Solubility of water in albite melts -under pressure. Int. Geol. Rev. 6 (2), 254-258. https://doi.org/10.1080/00206816409474616

Ostrovsky, I. A., 1966. PT-diagram of the system SiO_2-H_2O. Geol. J. 5 (1), 127-134. https://doi.org/10.1002/gj.3350050110

Ostrovskii, I. A. and Orlova, G. P., 1966. On the partial molar volume of water in albite melt. Akad. Nauk SSSR Izv., Ser. Geol. 12, 118-122.

Ostrovskiy I. A., Orlova G. P., and Rudnitskaya, Y. S., 1964. Stoichiometry in the solution of water in alkali-aluminosilicate melts. Doklady Akad Nauk SSR 157,149-151.

Paillat, O., Elphick, S. C., and Brown, W. L., 1992. The solubility of water in $NaAlSi_3O_8$

melts: a re-examination of Ab-H_2O phase relationships and critical behaviour at high pressures. Contrib. Mineral. Petrol. 112, 490-500. https://doi.org/10.1007/BF00310780

Papale, P., 1997. Modeling of the solubility of a one-component H_2O or CO_2 fluid in silicate liquids. Contrib. Mineral. Petrol. 126 (3), 237-251. https://doi.org/10.1007/s004100050247

Papale, P., 1999. Modeling of the solubility of a two-component H_2O + CO_2 fluid in silicate liquids. Am. Mineral. 84 (4), 477-492. https://doi.org/10.2138/am-1999-0402

Papale, P., 2001. Dynamics of magma flow in volcanic conduits with variable fragmentation efficiency and nonequilibrium pumice degassing. J. Geophys. Res. Solid Earth 106 (B6), 11043-11065. https://doi.org/10.1029/2000JB900428

Papale, P., Moretti, R., and Barbato, D., 2006. The compositional dependence of the saturation surface of H_2O + CO_2 fluids in silicate melts. Chem. Geol. 229 (1-3), 78-95. https://doi.org/10.1016/j.chemgeo.2006.01.013

Papale, P., Moretti, R., and Paonita, A., 2022. Thermodynamics of multi-component gas-melt equilibrium in magmas: Theory, models, and applications. Rev. Mineral. Geochem. 87 (1), 431-556. https://doi.org/10.2138/rmg.2022.87.10

Proussevitch, A. A., and Sahagian, D. L., 1998. Dynamics and energetics of bubble growth in magmas: analytical formulation and numerical modeling. J. Geophys. Res. Solid Earth 103 (B8), 18223-18251. https://doi.org/10.1029/98JB00906

Richet, P., and Bottinga, Y., 1985. Heat capacity of aluminum-free liquid silicates. Geochim. Cosmochim. Acta, 49 (2), 471-486. https://doi.org/10.1016/0016-7037(85)90039-0

Richet, P., Hovis, G., and Whittington, A., 2006. Water and magmas: Thermal effects of exsolution. Earth Planet. Sci. Lett. 241 (3-4), 972-977. https://doi.org/10.1016/j.epsl.2005.10.015

Ryan, A. G., Russell, J. K., Nichols, A. R., Hess, K. U., and Porritt, L. A., 2015. Experiments and models on H_2O retrograde solubility in volcanic systems. Am. Mineral. 100 (4), 774-786. https://doi.org/10.2138/am-2015-5030

Sahagian, D. L., and Proussevitch, A. A., 1996. Thermal effects of magma degassing. J. Volcanol. Geotherm. Res. 74 (1-2), 19-38. https://doi.org/10.1016/S0377-0273(96)00047-9

Sahagian, D., and Proussevitch, A., 2005. Standardized model runs and sensitivity analysis using the "Bubbledrive-1" volcanic conduit flow model. J. Volcanol. Geotherm. Res, 143 (1-3), 173-185. https://doi.org/10.1016/j.jvolgeores.2004.09.016

Schaller, T., and Sebald, A., 1995. One- and two-dimensional ^{1}H magic-angle spinning experiments on hydrous silicate glasses. Solid State Nucl. Magn. Reson. 5 (1), 89-102.

https://doi.org/10.1016/0926-2040(95)00028-0

Schmidt, B. C., 2004. Effect of boron on the water speciation in (alumino)silicate melts and glasses. Geochim. Cosmochim. Acta 68 (24), 5013-5025. https://doi.org/10.1016/j.gca.2004.06.036

Shaw, H. R., 1964. Theoretical solubility of H_2O in silicate melts: Quasi-crystalline models. J. Geol. 72 (5), 601-617. https://doi.org/10.1086/627016

Shaw, H. R., 1974. Diffusion of H_2O in granitic liquids: Part I. Experimental data; Part II. Mass transfer in magma chambers. in Geochemical transport and kinetics 634, 139-170. Carnegie Inst. Washington Publ.

Shea, T., 2017. Bubble nucleation in magmas: a dominantly heterogeneous process?. J. Volcanol. Geotherm. Res. 343, 155-170. https://doi.org/10.1016/j.jvolgeores.2017.06.025

Shen, A., and Keppler, H., 1995. Infrared spectroscopy of hydrous silicate melts to 1000° and 10 kbar: Direct observation of H_2O speciation in a diamond-anvil cell. Am. Mineral. 80 (11-12), 1335-1338. https://doi.org/10.2138/am-1995-11-1223

Shen, A., and Keppler, H., 1997. Direct observation of complete miscibility in the albite-H_2O system. Nature 385 (6618), 710-712. https://doi.org/10.1038/385710a0

Shigetomi, S., and Nishiwaki, M., 2022. Exploration of non-trivial relations for the non-steady state nucleation rate: usefulness of the elliptic theta functions for its experimental estimations. SN Appl. Sci. 4, 301. https://doi.org/10.1007/s42452-022-05189-4

Shishkina, T. A., Botcharnikov, R. E., Holtz, F., Almeev, R. R., Jazwa, A. M., and Jakubiak, A. A., 2014. Compositional and pressure effects on the solubility of H_2O and CO_2 in mafic melts. Chem. Geol. 388, 112-129. https://doi.org/10.1016/j.chemgeo.2014.09.001

Silver, L. A., and Stolper, E., 1985. A thermodynamic model for hydrous silicate melts. J. Geol. 93 (2), 161-178. https://doi.org/10.1086/628938

Silver, L., and Stolper, E., 1989. Water in albitic glasses. J. Petrol. 30 (3), 667-709. https://doi.org/10.1093/petrology/30.3.667

Silver, L. A., Ihinger, P. D., and Stolper, E., 1990. The influence of bulk composition on the speciation of water in silicate glasses. Contrib. Mineral. Petrol. 104 (2), 142-162. https://doi.org/10.1007/BF00306439

Sowerby, J. R., and Keppler, H., 1999. Water speciation in rhyolitic melt determined by in-situ infrared spectroscopy. Am. Mineral. 84 (11-12), 1843-1849. https://doi.org/10.2138/am-1999-11-1211

Sowerby, J. R., and Keppler, H., 2000. Water speciation in rhyolitic melt determined by in-situ infrared spectroscopy. Am. Mineral. 85 (5-6), 880 (erratum).

Sparks, R. S. J., 1978. The dynamics of bubble formation and growth in magmas: A review and analysis. J. Volcanol. Geotherm. Res. 3 (1-2), 1-37. https://doi.org/10.1016/0377-0273(78)90002-1

Stalder, R., Ulmer, P., Thompson, A. B., and G'unther, D., 2000. Experimental approach to constrain second critical end points in fluid/silicate systems: Near-solidus fluids and melts in the system albite-H_2O. Am. Mineral. 85 (1), 68-77. https://doi.org/10.2138/am-2000-0108

Stolper, E., 1982a. Water in silicate glasses: an infrared spectroscopic study. Contrib. Mineral. Petrol. 81 (1), 1-7. https://doi.org/10.1007/BF00371154

Stolper, E., 1982b. The speciation of water in silicate melts. Geochim. Cosmochim. Acta 46 (12), 2609-2620. https://doi.org/10.1016/0016-7037(82)90381-7

Sugawara, T., 2005. Thermodynamic properties of magmatic liquid: Review and future directions (in Japanese). Bull. Volcanol, Soc. Japan 50 (2), 103-142.
https://doi.org/10.18940/kazan.50.2_103

Sugawara, T., and Akaogi, M., 2003. Heats of mixing of silicate liquid in the systems diopside-anorthite-akermanite, diopside-anorthite-forsterite, and diopside-silica. Am. Mineral. 88 (7), 1020-1024. https://doi.org/10.2138/am-2003-0710

Sun, K. H., 1947. Fundamental condition of glass formation. J. Am. Ceram. Soc. 30 (9), 277-281. https://doi.org/10.1111/j.1151-2916.1947.tb19654.x

Takata, M., Acocella, J., Tomozawa, M., and Watson, E. B., 1981. Effect of water content on the electrical conductivity of Na_2O-$3SiO_2$ glass. J. Am. Ceram. Soc. 64 (12), 719-724. https://doi.org/10.1111/j.1151-2916.1981.tb15894.x

Tanaka, R., and Hashimoto, T., 2013. Transition in eruption style during the 2011 eruption of Shinmoe-dake, in the Kirishima volcanic group: Implications from a steady conduit flow model. Earth Planets Space 65 (6), 645-655. https://doi.org/10.5047/eps.2013.05.002

Taniguchi, H., 2001. Invitation to magma science (in Japanese). Shokabo, Chiyoda, Tokyo, 179 pp.

Toramaru, A., 1989. Vesiculation process and bubble size distributions in ascending magmas with constant velocities. J. Geophys. Res. Solid Earth 94 (B12), 17523-17542.
https://doi.org/10.1029/JB094iB12p17523

Toramaru, A., 1995. Numerical study of nucleation and growth of bubbles in viscous magmas. J. Geophys. Res. Solid Earth 100 (B2), 1913-1931. https://doi.org/10.1029/94JB02775

Toramaru, A., 2006. BND (bubble number density) decompression rate meter for explosive volcanic eruptions. J. Volcanol. Geotherm. Res. 154 (3-4), 303-316.
https://doi.org/10.1016/j.jvolgeores.2006.03.027

Toramaru, A., 2022. Vesiculation and crystallization of magma: Fundamentals of volcanic eruption process, conditions for magma vesiculation. Springer Nature, Basingstoke, Hampshire. https://doi.org/10.1007/978-981-16-4209-8

Uchida, E., 2012. Thermodynamics in Mineralogy and Petrology (in Japanese). Kyoritsu Shuppan, Bunkyo, Tokyo, 151 pp.

Wagner, W., and Kretzschmar, H. J., 2007. International steam tables - properties of water and steam based on the industrial formulation IAPWS-IF97. Springer Science+Business Media, Berlin. https://doi.org/10.1007/978-3-540-74234-0

Wagner, W., and Pruß, A., 2002. The IAPWS formulation 1995 for the thermodynamic properties of ordinary water substance for general and scientific use. J. Phys Chem. Ref. Data, 31 (2), 387-535. https://doi.org/10.1063/1.1461829

Wanner, G., and Hairer, E., 1996. Solving ordinary differential equations II. Springer Berlin Heidelberg. https://doi.org/10.1007/978-3-642-05221-7

Wasserburg, G., 1957. The effects of H_2O in silicate systems. J. Geol. 65 (1), 15-23. https://doi.org/10.1086/626402

Whittington, A. G., and Sehlke, A., 2021. Spontaneous reheating of crystallizing lava. Geology, 49 (12), 1457-1461. https://doi.org/10.1130/G49148.1

Wilke, M., Behrens, H., Burkhard, D. J., and Rossano, S., 2002. The oxidation state of iron in silicic melt at 500 MPa water pressure. Chem. Geol. 189 (1-2), 55-67. https://doi.org/10.1016/S0009-2541(02)00042-6

Wilson, L., Sparks, R. S. J., and Walker, G. P., 1980. Explosive volcanic eruptions-IV. The control of magma properties and conduit geometry on eruption column behaviour. Geophys. J. Int. 63 (1), 117-148. https://doi.org/10.1111/j.1365-246X.1980.tb02613.x

Woods, A. W., and Koyaguchi, T., 1994. Transitions between explosive and effusive eruptions of silicic magmas. Nature 370 (6491), 641-644. https://doi.org/10.1038/370641a0

Wu, C. K., 1980. Nature of incorporated water in hydrated silicate glasses. J. Am. Ceram. Soc. 63 (7- 8), 453-457. https://doi.org/10.1111/j.1151-2916.1980.tb10211.x

Yamashita, S., 1999. Experimental study of the effect of temperature on water solubility in natural rhyolite melt to 100 MPa. J. Petrol. 40 (10), 1497-1507. https://doi.org/10.1093/petroj/40.10.1497

Yoshida, S., and Koyaguchi, T., 1999. A new regime of volcanic eruption due to the relative motion between liquid and gas. J. Volcanol. Geotherm. Res. 89 (1-4), 303-315. https://doi.org/10.1016/S0377-0273(99)00005-0

Yoshimura, S., and Nakamura, M., 2010. Chemically driven growth and resorption of bubbles in a multivolatile magmatic system. Chem. Geol. 276 (1-2), 18-28.

https://doi.org/10.1016/j.chemgeo.2010.05.010

Zhang, Y., Stolper, E. M., and Ihinger, P. D., 1995. Kinetics of the reaction H_2O + O = 2OH in rhyolitic and albitic glasses: Preliminary results. Am. Mineral. 80 (5-6), 593-612. https://doi.org/10.2138/am-1995-5-619

Zhang Y., Stolper E. M. and Wasserburg G. J., 1991. Diffusion of water in rhyolitic glasses. Geochim. Cosmochim. Acta 55 (2) 441-456. https://doi.org/10.1016/0016-7037(91)90003-N

Zhang, Y., 1999a. H_2O in rhyolitic glasses and melts: measurement, speciation, solubility, and diffusion. Rev. Geophys., 37 (4), 493-516. https://doi.org/10.1029/1999RG900012

Zhang, Y., 1999b. Exsolution enthalpy of water from silicate liquids. J. Volcanol. Geotherm. Res. 88 (3), 201-207. https://doi.org/10.1016/S0377-0273(98)00115-2

Zhang, Y., Belcher, R., Ihinger, P. D., Wang, L., Xu, Z., and Newman, S., 1997. New calibration of infrared measurement of dissolved water in rhyolitic glasses. Geochim. Cosmochim. Acta 61 (15), 3089-3100. https://doi.org/10.1016/S0016-7037(97)00151-8